ELECTRON PARAMAGNETIC RESONANCE OF Mn^{2+} AND VO^{2+} IN SINGLE CRYSTALS

A Thesis Submitted

In Partial Fulfilment of the Requirements

for the Degree of

DOCTOR OF PHILOSOPHY

by

ADIBHATLA VENKATA JAGANNADHAM

to the

DEPARTMENT OF PHYSICS

INDIAN INSTITUTE OF TECHNOLOGY KANPUR

AUGUST 1969

This is to certify that the work presented in this thesis has been performed by Mr. A. V. Jagannadham under my supervision.

Putcha Venkateswarlu

Putcha Venkateswarlu
Professor of Physics

ACKNOWLEDGEMENTS

I wish to place on record my deep sense of gratitude to Professor Putcha Venkateswarlu who initiated me to the study of applications of Electron Paramagnetic Resonance to the solution of various problems in Solid State Physics. His words of encouragement in times of stress, his ideal approach to problems and his valuable guidance make him a 'friend, philosopher and guide'. My special thanks are due to him for the financial help he has given.

I am thankful to Dr P.K.Kelkar, Director, Indian Institute of Technology, Kanpur who took deep interest in giving all facilities to help the cause of training a teacher of Physics in an affiliated college.

My special thanks are due to Professor J. Mahanty who had never failed to extend a helpful hand in times of need.

Thanks are due to Dr N.A.Narasimham, Spectroscopy Division, Bhabha Atomic Research Centre, Bombay for the spectrographic analysis of the doped crystals.

Thanks are due to Dr G.C.Uprethi who went through the manuscript as it was taking shape, Dr M.Yusoof for discussions in perturbation theory, Dr T.M.Srinivasan for providing liquid nitrogen facilities even at a short notice, Dr D.R.Rao for the use of Cary-14 Spectrophotometer, Dr B.D.N.Rao for inspiration and the Faculty Members of the Physics Department and Professor V.Subbarao of the Department of Chemical Engineering Department for unfailing courtesy in rendering sundry help.

It is a pleasure to thank my young friends Dr M.D.Sastry, Shri K.V.Subbarao, Shri S.D.Pande, Dr K.N.Shrivastava, Dr.B.V.R.Chowdury and Shri Aswadha Narayana for helpful discussions, Shri S.N.Dwivedi for help in taking x-ray diffraction photographs, Messrs B.L.Arora and O.P.Saxena for neat draughtsmanship and photographic reproduction of line diagrams, Messrs Adhikari, Ravi Kumar and Natarajan of Computer Centre for help rendered in Programming.

Financial assistance from the National Bureau of Standards, Washington and the Indian Institute of Technology, Kanpur is gratefully acknowledged. Thanks are due to the Government of Rajasthan for granting me five years leave at a stretch to complete my research program.

In the end I thank my wife Devabala whose cooperation and constant encouragement enabled me to complete my work according to time schedule.

A V Jagannadham

(A.V.Jagannadham)

TABLE OF CONTENTS

Preface Page vii

Chapter

1. Introduction to Electron Spin Resonance 1
2. Theory of EPR spectra of Transition Metal Ions with particular reference to Mn^{2+} and VO^{2+} 17
3. Electron Paramagnetic Resonance of Mn^{2+} doped in single crystals of caesium sulphate, Cs_2SO_4 46
4. Electron Paramagnetic Resonance of VO^{2+} doped in single crystals of caesium sulphate, Cs_2SO_4 88
5. Electron Paramagnetic Resonance of Mn^{2+} in sodium fluoride single crystals 112
6. Electron Paramagnetic Resonance of VO^{2+} in the Alkali Chlorides 132

Appendices 150

(A) Spin Hamiltonian Parameters of Mn^{2+} and VO^{2+} in various lattices

(B) Computer Programs

PREFACE

Electron spin resonance offers a wide variety of applications. The symmetry of crystalline field influences the resonance spectrum in a predetermined fashion and as such resonance phenomena can supplement x-ray diffraction techniques. In suitable cases a small percentage of metal ions can be replaced by any suitable paramagnetic ion and the paramagnetic resonance spectrum of the ion will enable the position of the metal ion in the structure to be determined to an accuracy of about 1° to 3°. Similarly the bond direction of a molecular ion consisting of a paramagnetic metal and oxygen atoms with reference to the direction of metal-oxygen bond in the crystal can be determined by studying the resonance spectrum. Changes in phase which are temperature dependent can be detected more readily as compared to x-ray and dielectric measurements and the transition temperature can be determined to an accuracy of about 1 $^{\circ}C$. In addition, some information as to the sites becoming magnetically inequivalent can be obtained automatically. The defects occuring in the crystalline solids, the position and the behaviour of vacancies formed therein can be studied with the help of a resonance spectrum. The degree of covalency can also be determined with its help.

Figs. (3.2), (3.3) and (3.4) show the three spectra related to the z, y and x axes respectively of the complex.

Angular variation studies and spin-Hamiltonian analysis of these spectra lead to the identification of the complex. In this complex Mn^{2+} is found to substitute a β-Cs^{+} position and get associated in the ab-plane with the nearest neighbour β-Cs^{+} vacancy, the direction of association being the z-axis of the complex. The y-axis of this complex is in the same ab plane at an angle of 90° to the z-axis while its x-axis is along the c-axis of the crystal and is perpendicular to the plane containing y and z axes of the complex.

The angle which this complex is expected to make with a known direction in the crystal, say, b-axis, is calculated from the structural parameters as obtained from x-ray studies[9]; this agrees fairly well with that obtained from resonance data. Fig.(3.5) gives the proposed model for the observed vacancy complex. For this complex which is in the ab-plane the z-axis makes an angle of 25° with the crystallographic b-axis the calculated angle being $24^{\circ}51'$. The associated vacancy can occur in any one of the directions Mn^{2+}—β Cs^{+} (Fig.3.5) and one expects two identical spectra when the static magnetic field is making equal angles of $24^{\circ}51'$ each on either side of b axis.

In this thesis the author has used the phenomenon of spin resonance to study these varied aspects in some detail. All spectra have been recorded for the first time except two of the vacancy spectra in Mn^{2+}-doped sodium fluoride.

Chapter I is divided into two parts. Part one serves as an introduction to the phenomenon of Electron Paramagnetic Resonance, (EPR). In part two is described the work reported in this thesis broadly.

Chapter II gives the necessary theoretical background in interpreting EPR spectra reported in this thesis. Crystal field parameters necessary to describe crystalline fields of lower symmetry and the energy levels one expects when the spin of anion influences the paramagnetic ion are discussed in detail for transition metal ions in general with particular reference to the ions studied.

Chapter III describes the EPR spectrum of divalent manganese ion in single crystals of caesium sulphate at 9.5 Gc/sec. It has been found that in the ab- plane the divalent manganese ion Mn^{2+} takes the place of a monovalent site of caesium ion Cs^{+}. The line joining Mn^{2+} ion and the associated vacancy at Cs^{+} site makes an angle of 25° with the crystallographic b-axis in the ab-plane. Correlation with the known x-ray diffraction

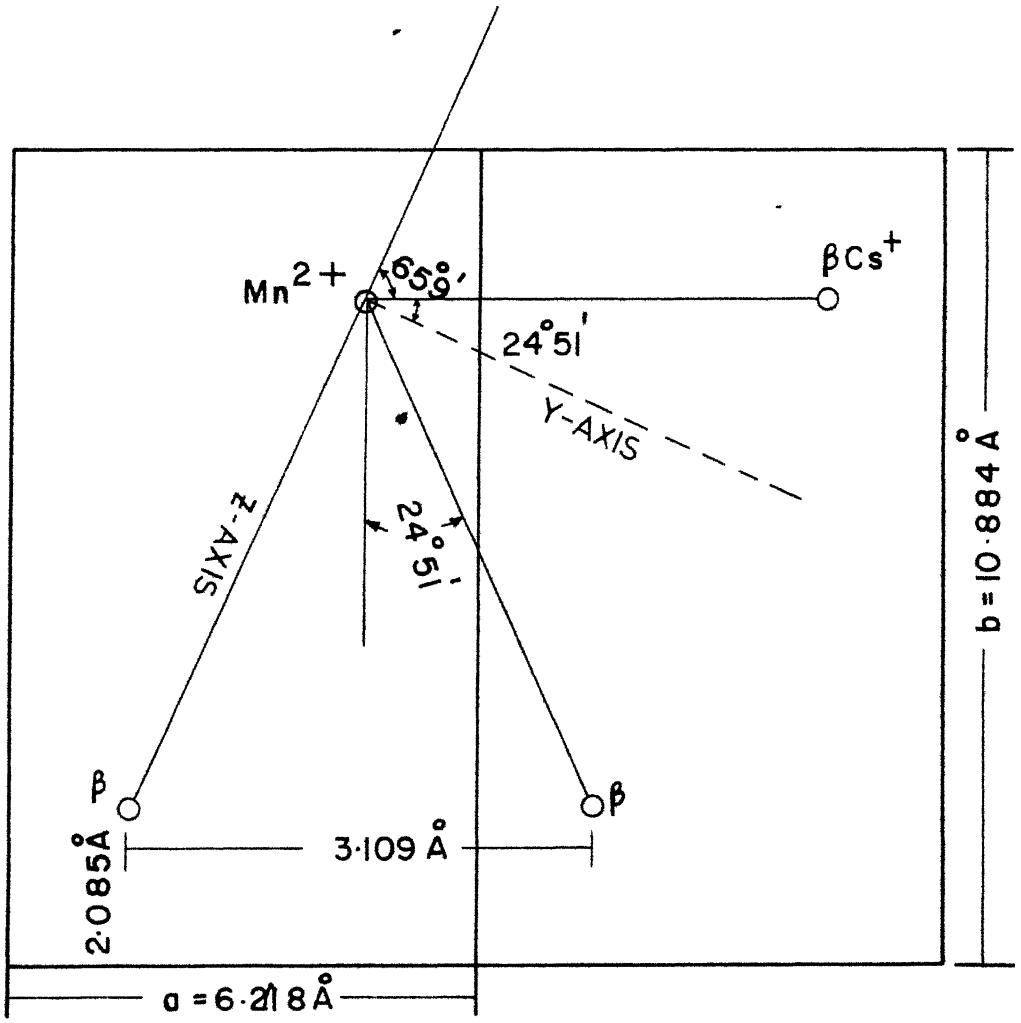

3·5. MODEL OF $\beta\beta$ - COMPLEX IN THE ab PLANE OF Cs_2SO_4 : Mn^{2+} CRYSTAL - Mn^{2+} SUBSTITUTED IN THE β - Cs^+ POSITION AND THE NEAREST NEIGHBOUR β's ARE THE ASSOCIATED VACANCIES.

TABLE 3.6

The Lines of $Mn^{2+}:Cs_2SO_4$ at Room Temperature 20 °C

H || x-axis of the complex
(All values in Oersted)

DPPH[a] 3376

Line	-3/2 ↔ -5/2		-½ ↔ -3/2		-½ ↔ +½		½ ↔ +3/2		+5/2 ↔ +3/2	
	Ob-served	cal-culated	Ob-served	cal-culated	Ob-served	cal-culated	Ob-served	cal-culated	Ob-served	cal-culated
	1844	1821	2192	2207	2724	2724	3383	3411	5020	5004
	1927	1902	2283	2290	2814	2810	3486	3499	5098	5095
	2009	1985	2361	2376	2903	2899	3571	3590	5184	5189
	2098	2071	2449	2465	3002	2990	3667	3684	5284	5285
	2192	2160	2537	2556	3096	3083	3758	3780	5389	5383
	2283	2251	2630	2649	3192	3179	3837	3879	5496	5484

Standard deviation 19; [a]Diphenylpicrylhydrazyl

Input parameters (for second order perturbation equations 3.2(a)):

$A_x(=B)=-91$; $A_z(=A)=-93$; $A_y(=C)=-91$

$H_{ox}=3357$ ($g_x=2.0149$); $D_x=452$; $E_x=475$; $(b_4^0)_x=-8$; $(b_4^2)_x=-45$

studies on crystal structure indicate that the ions responsible are β-Cs^+ ions. This complex gives rise to three spectra which have been analysed using an electron spin S=5/2 and nuclear spin I=5/2 in the orthorhombic spin Hamiltonian. The values of the crystal field parameters are refined by diagonalising the relevent 36x36 energy matrix. In this chapter are also included temperature variation studies from room temperature to liquid nitrogen temperature. Throughout this temperature range the nature of the spectrum does not change and the crystalline field parameters varied smoothly indicating there is no detectable phase transition in this temperature range.

While the position of metal ion studies in caesium sulphate are described in chapter III, in chapter IV are described the spin resonance spectra of VO^{2+} molecular ion under the influence of highly asymmetric crystalline field of caesium sulphate. The spectrum obtained is somewhat complicated. A tentative analysis of the spectrum suggests that the VO^{2+} ion probably substitutes the α-Cs^+ ions. The V-O bond appears to have three preferential directions: one along the c-axis of the crystal, one in a direction making an angle of 30^o with the c-axis in the bc plane and yet another nearly along the a-axis. These directions are the directions of nearest approach from the position of α-Cs^+ to the neighbouring oxygens. The possibility of the existence

4.1 INTRODUCTION

The electron paramagnetic resonance (EPR) of VO^{2+} in single crystals of alkali halides[1], NH_4Cl[2] and KNO_3 and $CsNO_3$[3] is known to be independent of the orientation of the crystal with respect to the magnetic field direction indicating that there is no preferred orientation of the V-O bond axis in these crystals. On the other hand, it is strongly angular dependent in crystals of Tutton salts[4] and alkali alums[5,6,7] doped with VO^{2+} showing the existence of preferred orientation of V-O bond. The EPR studies on Mn^{2+} ion in caesium sulphate have given interesting information about the associated lattice defects. The present work on caesium sulphate doped with VO^{2+} ion has been taken up to get information about the structure of vanadyl complex in the crystal and also about the associated lattice defects.

4.2 THEORY

A tetravalent vanadium ion with outer electronic configuration $3d^1$ exists in the most stable form as VO^{2+} the binding with the oxygen being highly covalent. The LCAO-MO description of this molecular ion in the complex $VO(H_2O)_5^{2+}$ had shown[8,9] that the unpaired "d" electron occupies a non-bonding b_2 type vanadium orbital ($3d_{xy}$) the lowest state thus being an orbital singlet. Due to the magnetic interaction with the vanadium nucleus

of canted axes is investigated by a harmonic analysis of g^2-θ curves studied in the three principal crystallographic planes. The g^2-matrix has been obtained from the appropriate second order equations by the method of least squares and it is diagonalised to give the three principal g-values and nine direction cosines of the principal axes of the g-tensor with reference to the known crystallographic axes. The crystallographic axes themselves are identified from an analysis of x-ray rotation photographs.

In chapter V the EPR spectrum of divalent manganese in sodium fluoride has been presented. In addition to the determination of the parameters in the ... spectra found by other workers, a new isotropic spectrum consisting of six lines and a broad line resonance have been found and analysed. Superhyperfine structure, SHFS, due to surrounding fluorine ions has been analysed in all spectra. Determination of SHFS parameters in the isotropic spectrum and in the spectrum designated 'weak' by earlier workers is new to this work. A number of weak lines at very low fields have been observed which are due to half-field transitions. Temperature variation studies have been made from 300 ^{o}C down to liquid nitrogen temperature and a vacancy model has been proposed.

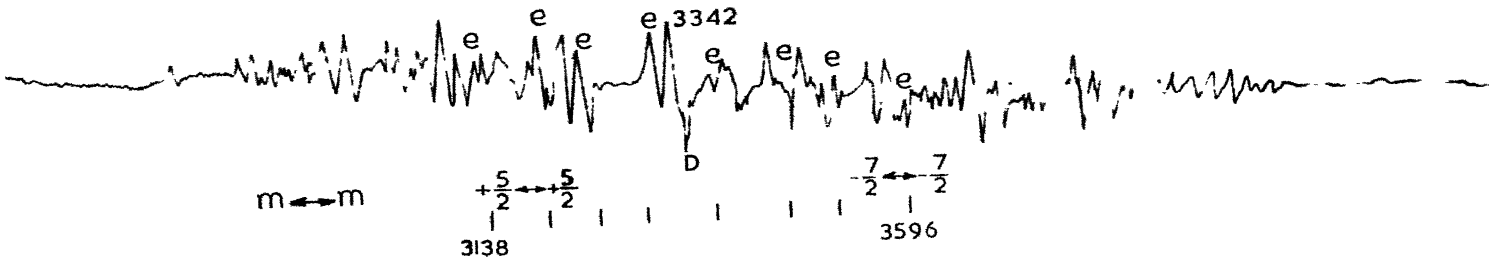

FIG. 4.6 EPR SPECTRUM OF VO^{++} IN CS_2SO_4 SINGLE CRYSTAL AT ROOM TEMPERATURE. H IS AT AN ANGLE OF 120° TO AXIS (a-AXIS VERTICAL) e's DENOTE $\perp x$. D IS THE FIELD MARKER. FIELD VALUES ARE IN OERSTED

In chapter VI electron spin resonance studies of vanadyl molecular ion in single crystals of sodium, potassium and rubidium chloride have been described in a temperature range 77 ^{o}K to 330 ^{o}K. At liquid nitrogen temperature anisotropic spectra are recorded in each case while at room temperature only isotropic spectra are observed suggesting there is a fast readjustment of VO^{2+} molecular ion in these crystals at high temperatures while this tumbling motion has been hindered at very low temperatures. Spin-Hamiltonian constants are calculated from isotropic and anisotropic spectra recorded in each case. The line widths in each case are found to obey a law originally put forward by Kivelson. The haphazard orientation of VO^{2+} bond in these alkali chloride crystals which do not contain oxygen is in contrast with oriented VO-bond studies described in chapter IV in the case of vanadyl-doped caesium sulphate. They are explained on the assumption that the medium behaves as a liquid for VO^{2+} molecular ion as far as the paramagnetic resonance behaviour is concerned.

be a highly distorted coordination with practically all the metal ion oxygen distances being different from one another (Fig. 4.1a). It is, however, very easy to visualise a $C_{\infty v}$ local symmetry for the VO^{2+} ion in all the three complexes discussed in this chapter. Though the present experiments cannot unambiguously describe the type of coordination involved, the optical absorption studies and the EPR studies definitely show the formation and existence of the VO^{2+} ion in the Cs_2SO_4 crystal.

It is interesting and in a way puzzling to note that while the present work indicates that VO^{2+} substitutes $-Cs^+$ ions in Cs_2SO_4 crystal, the work of Pande[20] in our laboratory shows that VO^{2+} substitutes $\beta-NH_4^+$ ions in $(NH_4)_2SO_4$ single crystal. However, such type of differences in substitution have been found earlier in the $(NH_4)_2SO_4$ and alkali sulphate crystals. Mn^{2+} is found [21] to substitute one of the two possible types (α or β) of NH_4^+ ions in $(NH_4)_2SO_4$ and get associated with the second type of NH_4^+ vacancy. On the other hand in K_2SO_4[22] and Cs_2SO_4 (chapter III) crystals, Mn^{2+} substitutes $\beta-K^+$ (or Cs^+) ion and gets associated with a β-alkali ion vacancy.

It is to be pointed out that there are a number of unmarked lines in the Figures 4.2 — 4.6. It is possible that they are due to some additional complexes of VO^{2+} which are as yet unidentified.

These chapters are followed by appendices giving up-to-date information on g-values of the ions studied in various lattices and computer programs used in the calculation. The diagonalisation program is a standard one using Jacobi's method adopted for the particular needs of the problem while the leasr square programs in other cases are especially written. A bibligraphy of the work done on manganese and vanadyl ions in various lattices is included here.

If the crystalline field has a higher symmetry, say, cubic, D=0 and it splits $^6S_{5/2}$ into a doublet and a quartet. In moderate crystalline fields, the zero field splittings will be so small that the fine structure cannot be resolved, and the spectrum contains only isotropic sextet at g = 2.

5.4 RESULTS AND DISCUSSION

Four different kinds of spectra have been observed and are designated as spectra I, II, III_2 and III_4 for a convenient comparison with the corresponding spectra[6] in Mn^{2+}:NaCl. The spectrum I represents a broad overlapping absorption which is more prominent at low temperature. This is due to Mn^{2+} ions which occur in aggregates or clusters. Spectrum II shows a hyperfine sextet and is due to Mn^{2+} ions at the alkali sites having a cubic site symmetry with no nearby alkali vacancies. Spectra III_2 and III_4 are due to Mn^{2+} ions at the alkali sites with tetragonal site symmetries, the $\langle 100 \rangle$ axis being the tetragonal axis. These two spectra have been observed and analysed by the earlier workers though no specific models have been proposed. Hall et al[13] identified these spectra as due to Mn^{2+} ions associated with vacancies. Spectrum III_2 has a large spread compared to spectrum III_4 showing that the Mn^{2+} ions responsible for spectrum III_2 experience a larger crystalline field compared to those responsible for spectrum III_4. These observations indicate that the complex responsible for the spectrum III_2 is a Mn^{2+} ion

CHAPTER I
INTRODUCTION

1.1 Electron Paramagnetic Resonance

The seeds of magnetic resonance phenomena were laid in 1936 when Gorter[1] demonstrated that a paramagnetic salt placed in a high frequency alternating magnetic field absorbed energy and that this was influenced by the application of a static magnetic field either parallel or perpendicular to the alternating magnetic field. The development of electronics during the second world war placed high frequency oscillators at the disposal of experimentalists. Zaviosky[2] in Russia and Cummerow and Halliday[3] in U.S.A obtained the first paramagnetic resonance absorption spectra. Since then the phenomena of paramagnetic resonance has become quite useful in fundamental research.

Historical

The principle of the method is as follows. Consider a paramagnetic ion. It has a magnetic moment and therefore its ground state is degenerate. If this ion is placed in a strong static magnetic field the degeneracy is lifted and the energy levels undergo a Zeeman splitting. Application of an oscillating magnetic field of appropriate frequency will be able to induce transitions between the Zeeman levels and energy is absorbed from the electromagnetic field. If the static magnetic field is slowly varied the absorption shows a series of maxima. The plot between the absorbed energy and the magnetic field is called the electron paramagnetic resonance spectrum or electron

Principle

The corresponding spectra are shown in Figs.(5.2),(5.3) and (5.4) respectively in which the calculated SHFS patterns are also drawn to scale. The values obtained for the constants A_s and A_σ for all the three spectra are given in Table (5.4) where the data available from the earlier work on spectrum III_4 are also included.

Watkins[5] has shown that the halogen ion nearer to the charge compensating vacancy undergoes a slight displacement towards the divalent impurity ion. The effect of such a displacement of F^- ions is not detected in the present SHFS and also in the study of $Mn^{2+}:KF$[17].

spin resonance spectrum. The phenomenon itself is called electron paramagnetic resonance, EPR, or electron spin resonance, ESR.

Paramagnetic species

A system of charges exhibits paramagnetism whenever it has a resultant angular momentum. Among the paramagnetic substances may be mentioned the transition group of elements containing 3d, 4f and 5f electrons, monoatomic gases such as atomic hydrogen with its ground state $^2S_{1/2}$, oxygen gas with the molecule in the ground state $^3\Sigma_g^-$, or organic free radicals such as diphenylpicrylhydrazyl, (DPPH), having an unpaired electron. Fig. 1.1 shows the structure of DPPH which is often used for calibration in EPR spectra. If a substance is not paramagnetic, it can be exposed to high energy radiation[4] or subjected to mechanical stresses[5] so that the normal bonds are disrupted and paramagnetic species are formed.

All the work reported in this thesis was conducted at x-band with spectrometer operating at nearly 0.3 cm^{-1}. Fig. 1.2 shows the block diagram of the essentials of the equipment.

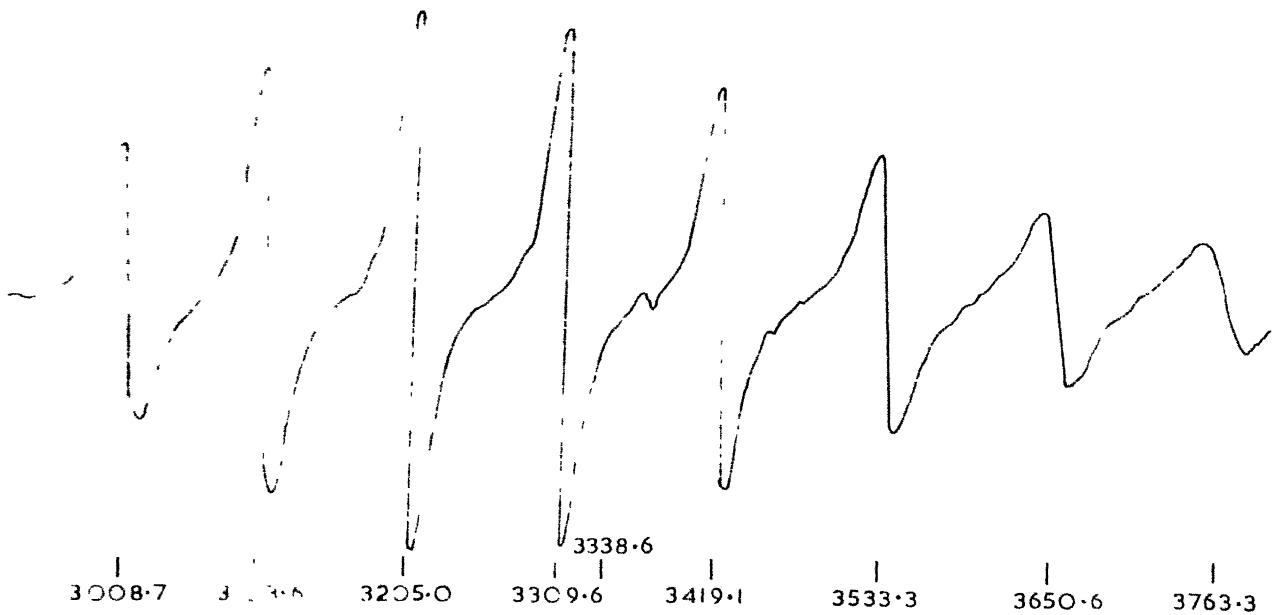

FIG·6·1 SPECTRUM I ELECTRON PARAMAGNETIC RESONANCE SPECTRUM OF VO^{2+} IN NaCl AT ROOM TEMPERATURE. THE X-COORDINATE REPRESENTS MAGNETIC FIELD VALUES IN GAUSS.

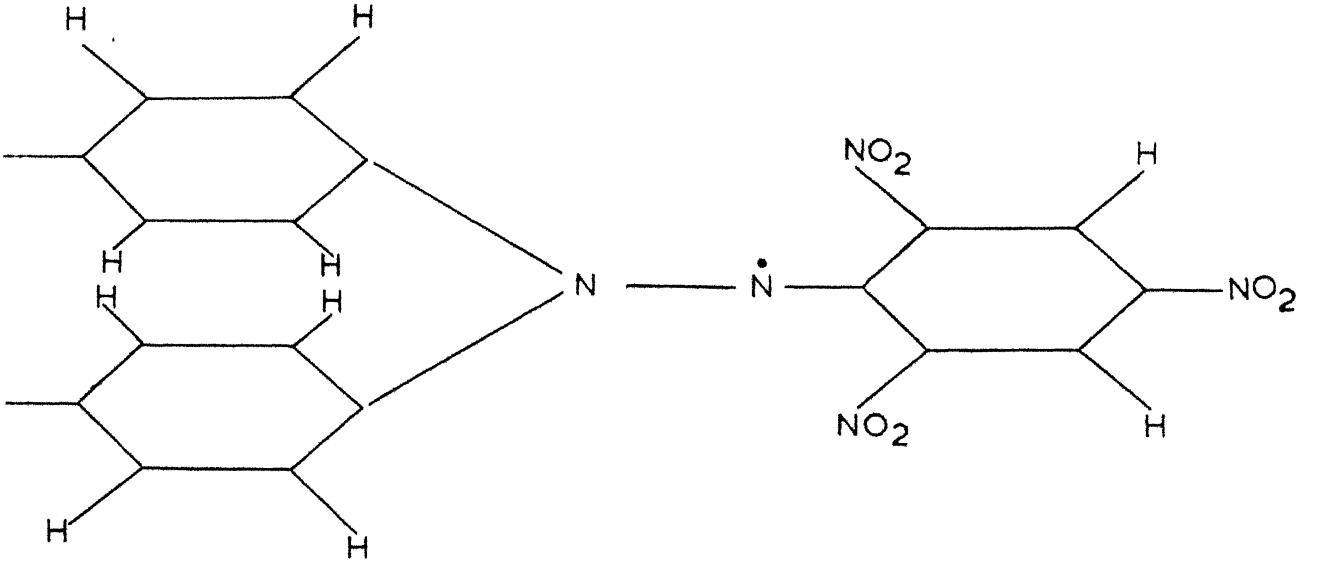

OLECULAR STRUCTURE OF D.P.P.H

E DOT OVER N SHOWS THE UNPAIRED ELECTRON THE MAGNETIC

WHICH INTERACTS WITH EITHER OF THE NITROGEN NUCLEI

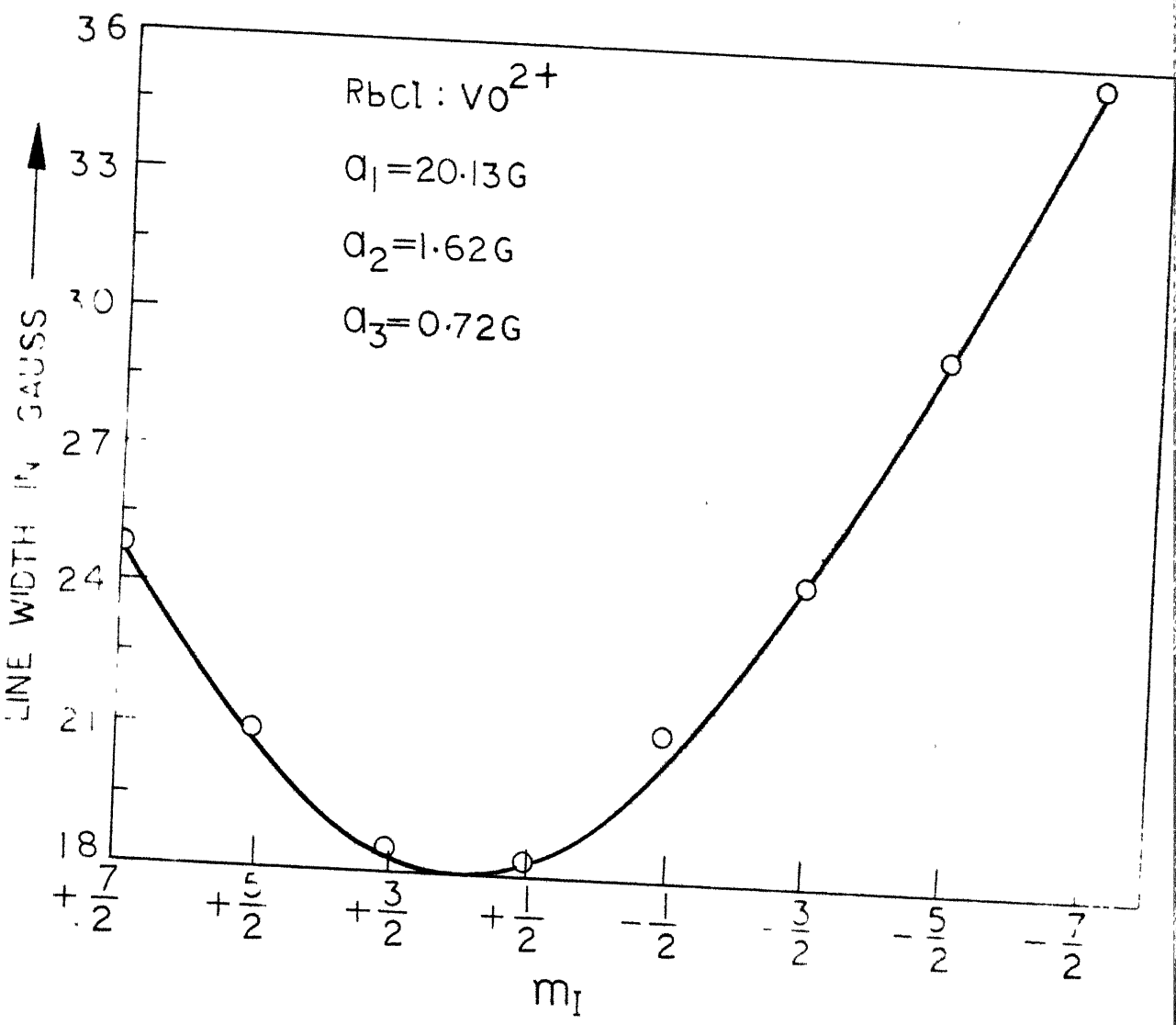

FIG. 5 PLOT OF LINE WIDTH VERSUS m_I IN THE EPR OF RbCl : VO^{2+} SYSTEM. THE SOLID CURVE REPRESENTS PREDICTED VARIATION OF THE LINE WIDTH WHILE CIRCLES INDICATE ACTUAL EXPERIMENTAL VALUES AT ROOM TEMPERATURE.

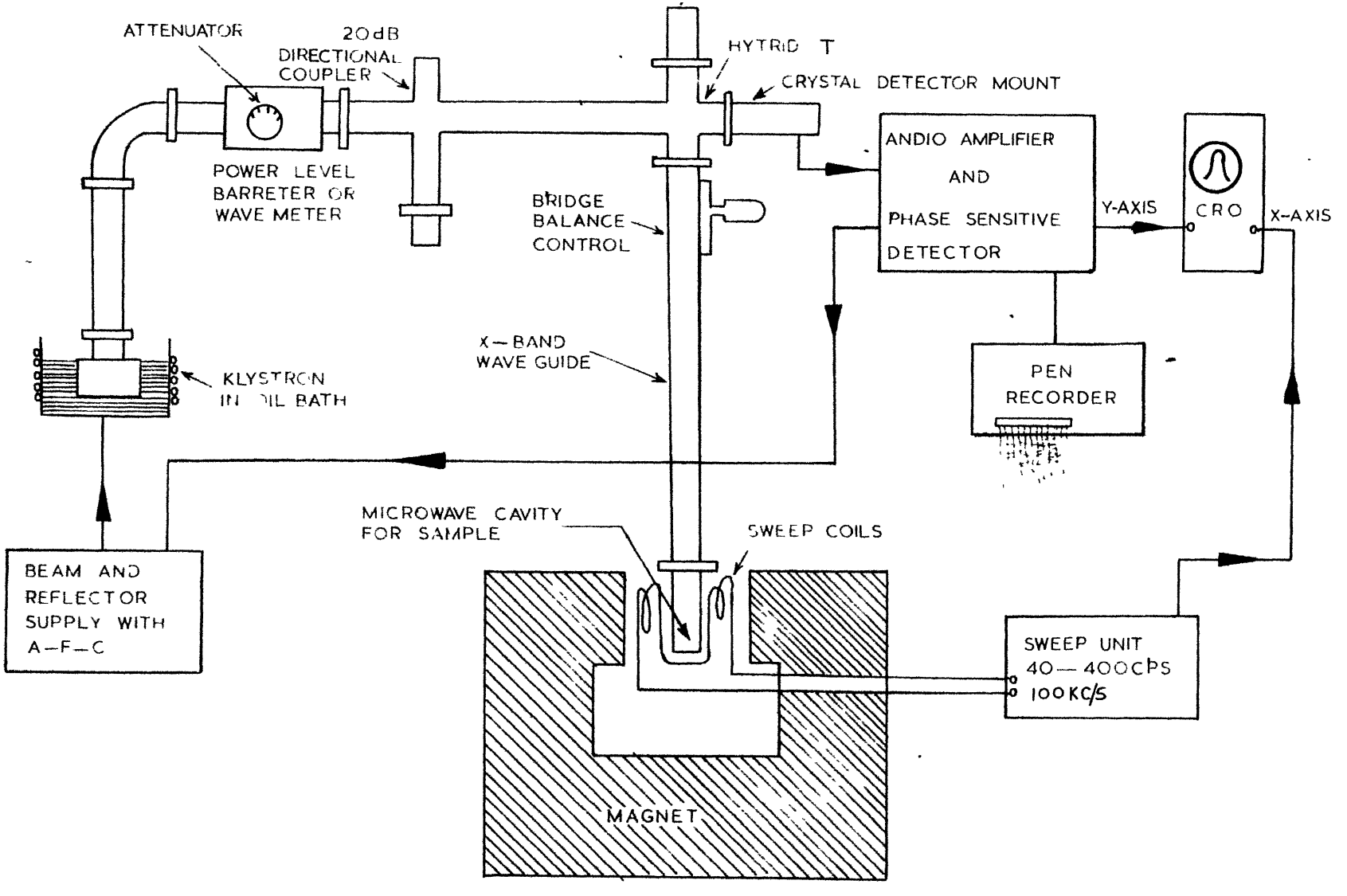

FIG12 BLOCK DIAGRAM OF X—BAND EPR SPECTROMETER (VARIAN MODEL)

(p) Work was done at x-band
Room temperature parameters 300 °K
Error in g's 0.003; error in D is 7 Oe;
error in E is 3 Oe; error in A's 1 Oe
b_4^0=0±1 Oe; b_4^2=13 Oe ; b_4^4=-77 Oe

The complex is in the ab plane; Mn^{2+} ion substitutes -Cs^+ ion and gets associated itself with a vacancy at a nearest neighbour -Cs^+ site.
The angle between the direction of the complex taken as z axis and the crystallographic c-axis is $25^0 \pm 1^0$.

(q) Work was done at x-band
Room temperature parameters 300 °K
Error in g's 0.0001; error in A's 0.5 Oe
Three orientations of V-O bond giving rise to three complexes have been reported.
Complex I is in the direction of crystallographic c-axis
Complex II makes an angle of 30^0 to the c-axis in the bc plane
Complex III is nearly along the crystallographic a-axis.

Let us consider a system of ions in a magnetic field H_o. Assuming the ion obeys Russel-Saunders or LS-coupling, the situation would be that the total orbital magnetic moment L and the total spin moment S combine to give a resultant J. This precesses round the field with a frequency $2\pi\nu_o$. Corresponding to M_J values, $J \geq M \geq -J$, there will be 2J+1 energy levels which are equally spaced.

$$E_{M_J} = g_o \beta H_o M_J \qquad .. \quad (1.1)$$

Application of a periodic magnetic field $H \cos 2\pi\nu t$ perpendicular to the direction of static magnetic field H_o results in magnetic dipole transitions between adjacent levels such that $\Delta M = \pm 1$. When the resonance condition is satisfied on has $\nu = \nu_o$ and

The resonance condition

$$E_M - E_{M'} = g_o \beta H_o = h\nu \qquad .. \quad (1.2)$$

This is the quantum mechanical picture of resonance; the corresponding classical frequency is ν.

The quantity g in equation (1.2) is called the 'spectroscopic splitting factor'[6] as this determines the magnitude of the splitting of energy levels in a magnetic field. This is an important quantity which is obtained even in those cases where the resonance spectrum consists of even a single line. For a free ion the value of g is very nearly 2. Fidone and Stevens[7] pointed out that the effects of

The spectroscopic splitting factor

VITAE

A.V.Jagannadham was born on 15th February, 1924 in Gudivada Agraharam, Andhra Pradesh. He received his Education from the Secondary to Degree stage at Maharajah's College, Vizianagram. After taking B.Sc degree with Physics Main and Mathematics and Chemistry as subsidiary subjects from Andhra University in 1944 he studied at Benares Hindu University and took his M.Sc degree in Physics in 1946. Since then he was teaching Physics to Degree and Post-graduate students at Birla College, Pilani (affiliated to the Agra Universit Government College, Ajmer (Affiliated to the University of Rajasthan) and Trichandra College, Nepal, Kathmandu (Affiliated to the Tribhuwan University). He took his early training in x-ray crystallography under Prof. K. Banerji in Allahabad University, Allahabad and Indian Association for the Cultivation of Science, Calcutta. He is on Study Leave from the Government of Rajasthan since July 1964 and is a graduate student in the Physic Department of the Indian Institute of Technology, Kanpu

covalent bonding can give positive contribution to g while the departure from the free ion value of 2.002322 in either direction gives an idea of the effective covalent bonding when the ion is subjected to a crystalline field[7,8]. In crystals the value of g may vary with the direction of the applied field. This anisotropy in g-value is related to spin-orbit coupling which mixes the ground state of the free ion with the excited states. Thus the electronic moment gets a definite contribution from the otherwise quenched orbital angular momentum.

When once the resonance condition is achieved there are other factors which control the continuous absorption of energy of the electromagnetic field by the spin system. At any temperature and frequency, the lower state is more populated than the upper one. To make this population difference significant the paramagnetic substance is cooled to liquid nitrogen or liquid helium temperatures and higher frequencies are employed. With the absorption of microwave power the population difference tends to equalise itself and unless there is a mechanism which establishes the population difference continuously, paramagnetic resonance absorption ceases to be significant. Such mechanisms are called relaxation processess. The lattice itself plays an important role in this respect. It acts like a huge reservoir with which the spin system exchanges energy.

Relaxation processess

The rate of this process is characterised by the spin-lattice relaxation time and is intimately related to the line width of the paramagnetic resonance spectrum.

Role of electronics in detecting EPR

Microwave electronics play a large part in proper detection of the EPR signal. The paramagnetic sample is placed in a cavity resonator in the region of maximum radio frequency magnetic field. The form of microwave magnetic field as existing in a typical rectangular cavity operating in TE_{012} mode is shown in Fig. 1.3[9]. The effect on losses and resulting frequency shifts in the microwave cavity follow the general equation for electrically resonant systems[10]. The changes in quantities involved are detected using an impedance bridge.(Fig.1.2).

EPR and magnetic susceptibility

The power absorbed by a paramagnetic specimen in a resonant cavity is proportional to the static magnetic susceptibility χ_o. In the dynamic phenomena it is usual to consider susceptibility as a complex quantity: $\chi = \chi' - i\chi''$. Here χ' is the dynamic susceptibility and represents the magnetisation which changes in phase with the field while χ'' determines the absorption of energy from the periodic magnetic field. The general relation between these two quantities is given by Kramers-Kronig equations[11].

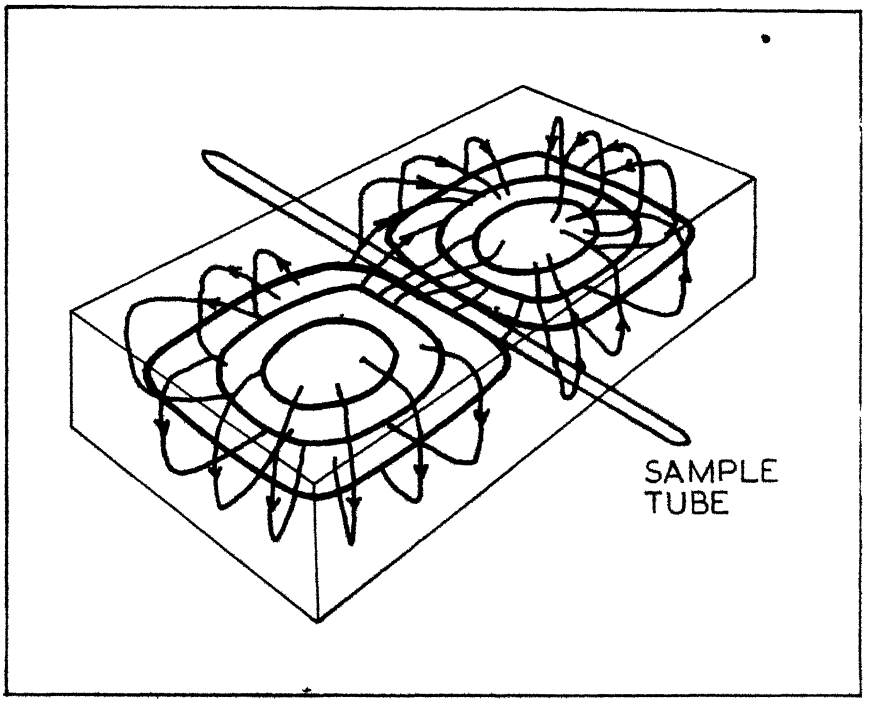

FIG.1.3 MICROWAVE MAGNETIC FIELDS IN TE_{012} MODE

An oscillating magnetic field can be thought of as a superposition of two rotating magnetic fields. Any precessing magnetic moment induced by a rotating magnetic field can be described in terms of frequency sensitive susceptibility. The susceptibility is maximum at resonance.

Paramagnetic dispersion and absorption

At resonance the Kramers-Kronig relations insure that the radio frequency susceptibility is a complex quantity and there will be both dispersion and energy dissipation from the rotating field. Fig. 1.4[12] shows the form of curves of paramagnetic resonance absorption and dispersion of susceptibility as the field is varied.

EPR would be of academic interest only if the magnetic states of the electron were independent of its surroundings. But it so happens that the interaction between the electron and its surroundings perturb the magnetic states of the system giving rise to additional transitions. This means EPR can be used with advantage and serves as a powerful tool in various applications in solid state physics. Low and Offenbacher[13] reviewed the success of paramagnetic resonance as an important structural tool in perovskites, spinels, and garnets as it often determines the site preference of a particular magnetic ion, the point symmetry, distortion of cubic symmetry and the number of inequivalent magnetic sites so that it has been possible to find the 'single ion' contribution to the magnetic anisotropy.

Scope of EPR

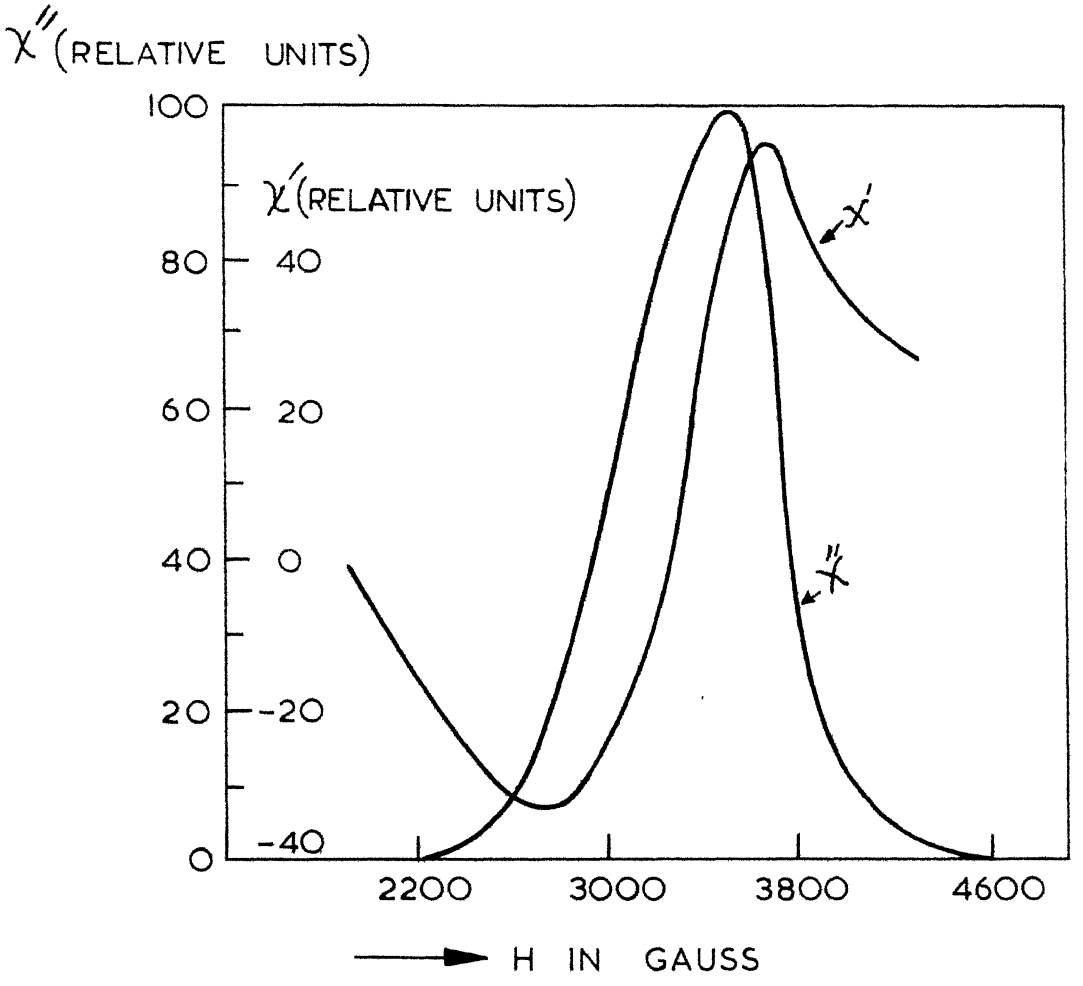

FIG.4 PARAMAGNETIC RESONANCE ABSORPTION (χ'') AND DISPERSION (χ') OF SUSCEPTIBILITY VERSUS MAGNETIC FIELD (TYPICAL VARIATION) AT X—BAND.

A survey of the Physical and Solid State applications is given by Ingram[14]. Bennet and Blackmore[15] recently used electron spin resonance spectroscopy to determine the absolute concentrations of hydrogen atoms in a gas-flow system at room temperature at total pressures between one and ten torr.

1.2 Present Investigation

In this thesis Mn^{2+} and VO^{2+} are studied after doping any one of them in minute concentrations in single crystals of caesium sulphate (Cs_2SO_4), sodium fluoride (NaF) and chlorides of sodium, potassium and rubidium. The object of these studies is three-fold. It is proposed to utilise the EPR techniques firstly to determine the site preference of the doubly charged Mn^{2+} magnetic ion doped in alkali sulphates. In the general study of doped alkali sulphates which has been taken in our laboratory a few years ago[16,17], caesium sulphate (Cs_2SO_4) doped with divalent manganese in concentrations of the order of three hundred parts per million has been taken for complete analysis. The site preference of Mn^{2+} ion to various Cs^+ ions is studied and the magnetic axial directions are correlated with the positions of Cs^+ ions as known from x-ray studies. Spin-Hamiltonian parameters of various magnetic complexes are determined first by using second order perturbation theory to the spectra obtained in three mutually perpendicular directions. Later the parameters so obtained

have been refined by using the fine structure and the hyperfine structure matrix for the ion placed in a field of rhombic symmetry and determining the eigenvalues by diagonalising it. The parameters have been varied slightly to reproduce the observed eigenvalues by a least square fit. Temperature variation studies of these parameters in the range 300 ^{o}K to 77 ^{o}K indicated that there is no detectable phase transformation in the case of Cs_2SO_4 single crystal doped with Mn^{2+} in this temperature interval.

The vanadyl ion is also doped in the single crystals of caesium sulphate to investigate the direction of VO bond in these crystals. Whereas Mn^{2+} entered the host lattice substitutionally in the Cs^{+} positions, the charge compensation occuring due to the formation of vacancies in appropriate positions, VO^{2+} enters substitutionally at a Cs^{+} position in giving highly angular dependent spectra. The variation of g-tensor and A-tensor has been investigated in the three planes and the direction cosines of these tensors and their principal values have been determined by forming the appropriate matrix and diagonalising it. These studies form an attempt to investigate the relative VO direction with respective oxygens in the sulphate group in this crystal by using a magnetic probe of a vanadyl complex. All the spectra obtained by doping divalent manganese ion and molecular vanadyl ion in caesium sulphate have been analysed for the first time.

The second type of studies are undertaken to estimate the effects of ligands of the host lattice of the doped ion. For this purpose EPR spectra of divalent manganese doped in single crystal of sodium fluoride (NaF) are studied in a temperature range of 573 ^{o}K to 77 ^{o}K. A complicated spectrum of more than 540 lines has been analysed. Three distinct complexes have been isolated one of which has been analysed for the first time. The interaction of d-electron of the doped manganese with the fluorine ligands of the host gave an extensive superhyperfine structure which has been analysed completely in all spectra. High temperature studies have been done and a model for the doped crystal has been suggested.

The third type of studies concern with the line widths of EPR spectra. For this purpose the vanadyl ion has been chosen. This molecular ion has been doped in oxygen-free host lattices of sodium, potassium and rubidium chlorides. Unlike the studies of VO^{2+} doped caesium sulphate single crystals, the EPR of vanadyl ion in these host lattices is interesting in that the ion enters the lattices without forming oriented magnetic complexes. Such studies are important in two ways: firstly, the EPR spectrum can be used for a rapid quantitative determination of the vanadium present in the matrix and this has important economic bearing in oil and glass technology; secondly, the relaxation processes in solids can be studied. In this thesis EPR studies of vanadyl ion doped in single crystals

of sodium chloride, potassium chloride and rubidium chloride are described and the line widths are found to have an m_I dependence as originally suggested by Kivelson[18] who developed a theory of line widths in liquids. Temperature variation studies have indicated that at very low temperatures there is a very fast readjustment of vanadyl ion and the 'Brownian tumbling motion'[19] is partly arrested. This purely temperature effect has been detected in the anisotropic spectrum which is obtained at liquid nitrogen temperature.

REFERENCES

1. C.J.Gorter, Physica 3,503(1936); Physica 3,1006(1936).
2. E.Zavoisky, J.Phys.U.S.S.R.,9,211(1945); J.Phys.U.S.S.R.,10,197(1946).
3. R.L.Cummerow and D.Halliday, Phys.Rev.70,433(1946).
4. D.J.E.Ingram, SPECTROSCOPY AT RADIO AND MICROWAVE FREQUENCIES, Butterworths Scientific Publications, London, (1955).
5. T.Kushida, G.B.Benedek and N.Bloembergen, Phys.Rev., 104, 1364(1956); G.B.Benedek and E.M.Purcell, J.Chem.Phys.,22,2003(1954); W.M.Walsh, Phys.Rev., 114,1485(1959); 122,762(1961).
6. C.Kittel, Phys.Rev.76,743,(1949).
7. I.Fidone and K.W.H.Stevens, Proc.Phys.Soc.73,116(1959)
8. G.B.Watkins,Phys.Rev.110,986(1958).
9. EPR Operating Manual, Varian Associates, Palo Alto, California,U.S.A.
10. J.C.Slater, MICROWAVE ELECTRONICS, D.Van Nostrand, (1950).
11. H.A.Kramers, Atti Congr.Fis.,Como,545,(1927); R.J.Kronig, Opt.Soc.Amer.12,547(1926).
12. B.M.Kozyrev, S.G.Salikhov, Yu. Ya. Shamonin, Zh.Exp. i Teor.Fiz.22,56,(1952).
13. W.Low and E.L.Offenbacher, Solid State Physics,17, 135, Academic Press (1965).
14. D.J.E.Ingram, J.Brit.I.R.E.,19,357(1959).
15. J.E.Bennet and D.R.Blackmore, Proc.Roy.Soc.A.,305, 575(1968).
16. B.V.R.Chowdari and Putcha Venkateswarlu, J.Chem.Phys. 48,318(1968).
17. B.V.R.Chowdari and Putcha Venkateswarlu, Proc.Ind. Acad.Sc.,67,130(1968).
18. D.Kivelson, J.Chem.Phys.33,1094(1960).
19. M. McConnell, J.Chem.Phys.25,709(1956).

CHAPTER II

THEORY AND INTERPRETATION OF EPR SPECTRA

ABSTRACT The general theory of EPR of transition metal ions and complexes is outlined with a special reference to the spectra of the ions V^{4+} and Mn^{2+}. The energy levels of the d-electrons in crystalline fields of various symmetries are briefly described. Basic features of the spin Hamiltonian formalism as a guide to interpreting EPR spectra are mentioned. The g-tensor in ions with $S=\frac{1}{2}$ has been described. General features concerning hyperfine splitting from the metal nucleus, covalent bonding and ligand hyperfine structure are also discussed. Theory of EPR spectra in liquids with a special reference to vanadyl molecular ion is given.

2.1 Introduction

The unpaired d-electrons in the ions of iron group transition metals render them paramagnetic. Table 2.1 gives the number of electrons, spin-orbit constant, spin arrangement of free ion and the total spin in the case of tetravalent vanadium and divalent manganese.

TABLE 2.1

Characteristics of some free ions of the Iron-group Transition Metals

Ions	Configuration	Spin-orbit constant λ in cm^{-1}	Spin arrangement of free ion	Total spin S	Ground state	Nuclear spin I and abundance
V^{4+}	$3d^1$	154	↑——	½	$^2D_{3/2}$	7/2(V^{51})99.8%
Mn^{2+}	$3d^5$	347	↑↑↑↑↑	5/2	$^6S_{5/2}$	5/2(Mn^{55})100%

2.2 The d-orbitals of a free-ion:

For a d-electron the ℓ-value is 2 and the total orbital degeneracy is 5. The degeneracy is partly lifted when the d electron is placed in a crystalline field of octahedral or tetrahedral symmetry. The three-fold degenerate orbitals are designated as t and the two-fold degenerate ones as e.

t →

$$d_{xy} = \frac{1}{\sqrt{2}}(\phi_{22} - \phi_{2-2})$$

$$= R_{3d}(r).\frac{\sqrt{15}}{2}.\sqrt{\pi}\,xy$$

$$d_{xz} = \frac{1}{\sqrt{2}}(\phi_{21} + \phi_{2-1}) \qquad .. \quad (2.1)$$

$$= R_{3d}(r).\frac{\sqrt{15}}{2}.\sqrt{\pi}\,xz$$

$$d_{yz} = \frac{1}{\sqrt{2}}(\phi_{21} - \phi_{2-1})$$

$$= R_{3d}(r).\frac{\sqrt{15}}{2}.\sqrt{\pi}\,yz$$

e →

$$d_{x^2-y^2} = \frac{1}{\sqrt{2}}(\phi_{22} + \phi_{2-2})$$

$$= R_{3d}(r).\frac{\sqrt{15}}{4}.\sqrt{\pi}(x^2-y^2) \qquad .. \quad (2.2)$$

$$d_{z^2} = \phi_{20}$$

$$= R_{3d}(r).\frac{\sqrt{15}}{4}.\sqrt{\pi}(2z^2-x^2-y^2)$$

where x,y and z are taken as the coordinates of a point at unit distance from the origin, $R_{3d}(r)$ is the radial wave function for a 3d electron; and the ϕ_{22} et cetera are the $\phi_{(\ell m_\ell)}$. These are illustrated graphically in Fig2.1When the crystal field symmetry is lower than cubic the orbital degeneracy of both t and e orbitals could be further partly or completely lifted.

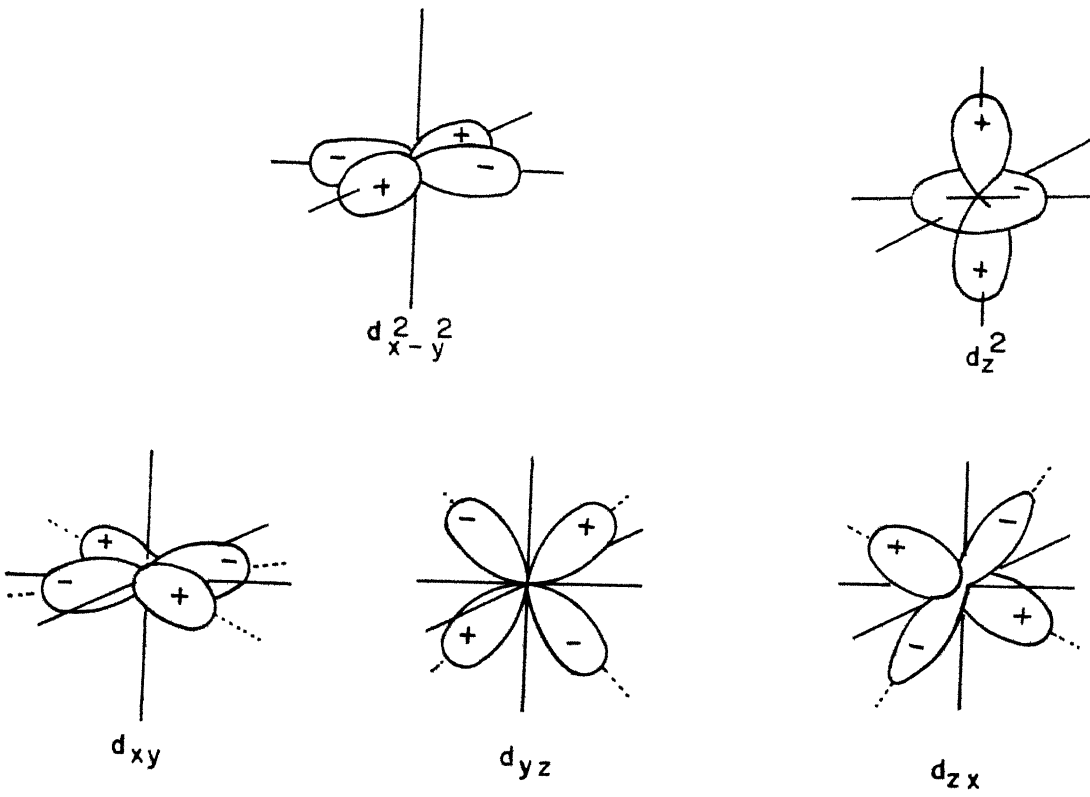

FIG. 2·1 REAL FORMS OF THE d – ORBITALS

2.3 Effect of ligand field on energy levels

If a paramagnetic ion such as Mn^{2+} is placed substitutionally at a cation site in a crystal of NaF or Cs_2SO_4, it is surrounded by F^- ions or $SO_4^=$ ions respectively. These are called "ligands". The number of ligands surrounding the central ion is called the coordination number. These ligands which may be negative ions or neutral molecules with a permanant lone pair of electrons change the energy level scheme with the result we have "ligand-field splitting" of the d-orbitals of the embedded paramagnetic ion. Usually, the orbital degeneracy of the d-orbitals is partly or fully removed by the crystal field. In NaF the F^- ligands form nearly octahedral coordination about the Mn^{2+} ion. The electrostatic field of the negative charges and the covalent bonding with the ligand orbitals affect the d-electrons of the metal ion. This causes the energy levels corresponding to d_{z^2} and $d_{x^2-y^2}$ to be raised and those corresponding to d_{xy}, d_{yz} and d_{xz} to be lowered. The energy gap between these two types of orbitals is the ligand-field splitting and is called Δ or $10Dq$ by convention.[1] Fig.(2.2)b shows the energy level scheme for this type of symmetry.

The ligands often cause distortion of the atomic orbitals of the paramagnetic ion so that very few complexes in the solid state actually possess regular symmetry. Thus the classification of regular symmetries

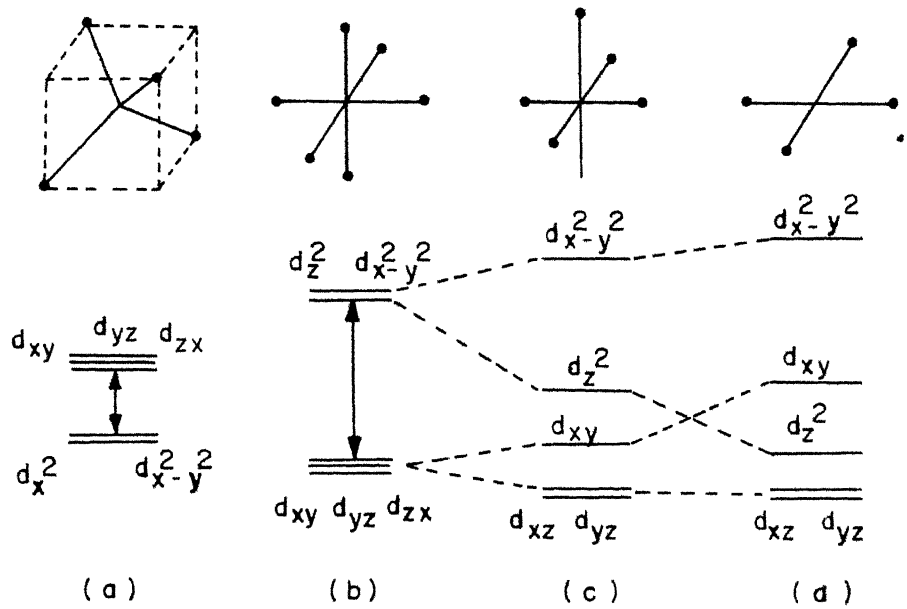

FIG·2·2 SPLITTING OF THE d-ORBITALS UNDER THE INFLUENCE OF LIGANDS WITH DIFFERENT SYMMETRY

(a) TETRAHEDRAL
(b) OCTAHEDRAL
(c) OCTAHEDRON WITH TETRAGONAL DISTORTION
(d) SQUARE PLANAR

referred to in Fig.(2.2) are only ideal. Table(2.2) gives the notation and transformation properties of atomic orbitals under crystalline fields of different symmetries. Paramagnetic resonance experiments reveal easily tetragonal or trigonal distortions in cubic systems. The tetragonal distortion in tetrahedral complexes corresponds to a flattening of the tetrahedron, Fig. 2.3(a), while the trigonal distortion in octohedral complexes correspond to a slight compression or elongation along a three-fold axis, Fig. 2.3(c). The effect of these distortions is a further removal of degeneracy of d-orbitals, Fig. 2.3(b), (d). However, the splitting of energy levels in the absence of a magnetic field is governed by Kramers' Theorem: in a system containing an odd number of electrons, at least twofold degeneracy must remain in the absence of a magnetic field. The pairs of states, (Kramers' doublets"), involved are time-conjugate, one being obtained from the other by time-reversal and are thus not split by an electrostatic perturbation, which is even under time reversal.

2.4 Spin-orbit interaction

In the first transition group elements the outermost 3d electrons are exposed to the surroundings, and therefore the interaction with the crystalline field is quite strong and in many cases stronger than the spin-orbit interaction. On the other hand, in the case of

TABLE 2.2

Notation and transformation properties of atomic orbitals under crystalline fields of different symmetries

Atomic Orbital	Octahedral O_h	Tetrahedral T_d	Square planar D_{4h}	Low symmetry $D_{2h}=D_2$ xi
s	a_{1g}	a_1	a_{1g}	
p_x	t_{1u}	t_2	e_u	
p_y				
p_z			a_{2u}	
d_{xy}	t_{2g}		b_{2g}	B_1
d_{xz}			e_g	B_2
d_{yz}				B_3
d_{z^2}	e_g	e	a_{1g}	A
$d_{x^2-y^2}$			b_{1g}	

rare earth ions, the 4s electrons are shielded from the surroundings by $5s^2 5p^6$ electrons and therefore are less affected by the crystal field. In this case spin-orbit interaction is stronger than crystalline field interaction. Therefore there are two interactions which vie with each other, one the spin-orbit coupling and the other the interaction of crystalline field with the orbital motion. The spatial degeneracy is partly lifted when the latter interaction is stronger than the former. In the iron group of transition elements this is of the order of 20,000 cm^{-1}. Depending upon its strength, the spin-orbit coupling causes a little of the orbital magnetic moment to be admixed with the spin so that the behaviour in a magnetic field is modified.

2.5 Spin-Hamiltonian

The magnetic properties of an ionic complex in a crystal field are intimately connected with the energy levels of the ion. For complexes of the first transition group the magnitude of the potential V provided by the ligands[2] is such as to make

$$\lambda(r)\, \underline{\ell}.\underline{s} < V < e^2/r_{ij}$$

The potential V provided by the ligands can be expressed as[2]

$$V = V(R) + V_o$$

where V_R spans the a_{1g} representation in the group O_h.

V_o expanded in Cartesian coordinates is

$$x^4 + y^4 + z^4 - \frac{3}{5} r^4$$

The results of electron paramagnetic resonance experiments are interpreted on the basis of a model of several magnetic complexes related to each other through a specific point group symmetry elements of the local sublattice. To study the problem one has to consider the dominant terms in the Hamiltonian. In the order of decreasing magnitude these are given in Table 2.3 for the salts containing iron group elements as impurities.[1-5]

Levels more than 10^3 cm^{-1} above the ground level can be neglected at room temperatures as they are insufficiently populated to give an absorption spectrum. Thus we are left with the lowest group of levels of the free-ion Hamiltonian which is characterised by orbital and spin angular quantum numbers L and S and is described by Russell-Saunder's coupling.

The 3d-ion configuration $1s^2 2s^2 2p^6 3s^2 3p^6 3d^n$ where n varies from 1 to 9 is taken for granted to classify $^{2S+1}L_J$ energy level (Table 2.3). To explain certain features such as hyperfine structure, configurational mixing is taken into consideration. This enables one to treat $1s^2 2s^2 2p^6 3s^2 3p^6$ closed shell with L=S=0 as diamagnetic. For paramagnetic ions of iron group n is non-zero. For Mn^{2+} n=5, L=0, S=5/2 while for V^{4+} n=1, L=2, S=½ and we have

TABLE 2.3

Dominant Terms in the Hamiltonian
for salts of Iron Group Transition Metals

Sub-Hamiltonian H_{sub}	Magnitude of the Energy (cm^{-1})	Symbol
Free Ion Energy (spin-independent)	10^5	$(\mathcal{H}_1)$ $W_F = \sum_k \left(\frac{p_k^2}{2m} - \frac{Ze^2}{r_k}\right) + \sum_{j<k} e^2/r_{jk}$
Crystal Field	10^4	$(\mathcal{H}_2)$ V
Spin-orbit Interaction	10^2	$(\mathcal{H}_3)$ W_{LS}
Zeeman Term	1	$(\mathcal{H}_4)\beta\, \underline{H}.(\hat{\underline{L}} + 2\hat{\underline{S}})$
Spin-spin Interaction	1	$(\mathcal{H}_5)$ W_{SS}
Interaction with the nuclear field	10^{-2}	$(\mathcal{H}_6)$ W_{NN}
Interaction with the external field	10^{-3}	$(\mathcal{H}_7)\gamma\beta_N.\underline{H}.\underline{I}$

$(2L+1).(2S+1)$ energy levels which are degenerate. This degeneracy is partly lifted by a crystalline potential described already.

One interesting fact about the magnetic properties of the iron-group transition elements is that the leading contribution to the magnetic moment arises from the spin magnetic moment only. This allows us to introduce a fictitious spin S', whose components are

$$S'_x = \tfrac{1}{2}\begin{pmatrix} 0 & 1 \\ 1 & 0 \end{pmatrix}$$

$$S'_y = \tfrac{1}{2}\begin{pmatrix} 0 & -i \\ i & 0 \end{pmatrix}$$

$$S'_z = \tfrac{1}{2}\begin{pmatrix} 1 & 0 \\ 0 & -1 \end{pmatrix}$$

and the concept of spin Hamiltonian

$$\mathcal{H} = g\beta\, \underline{H}.\underline{S} \qquad .. \qquad (2.3)$$

To determine the energy perturbation in a magnetic field the eigen values of the spin Hamiltonian equation 2.3 are to be found. This concept of the spin Hamiltonian is due to Abragam and Pryce[2]. The lowest orbital $|0\rangle$ contains a single electron in the ground state of the complex. Neglecting the spin-orbit coupling this may be represented by $|0\ ,\ \tfrac{1}{2}\rangle$, $|0\ ,\ -\tfrac{1}{2}\rangle$. The perturbation $\lambda\, \hat{\underline{L}}.\hat{\underline{S}}$ changes these states. The perturbed forms are:

$$|0\ ,\ \tfrac{1}{2}\rangle + c|\ 1\ ,\ -\tfrac{1}{2}\rangle = |\ "\tfrac{1}{2}"\ \rangle$$

$$|0\ ,\ -\tfrac{1}{2}\rangle + c|-1\ ,\ \tfrac{1}{2}\rangle = |"-\tfrac{1}{2}"\rangle$$

In the absence of a magnetic field these two states are degenerate and form a Kramers' doublet. Application of a magnetic field H_z in the direction of z-axis produces a perturbation $\beta H_z(\hat{\underline{L}}_z + 2\hat{\underline{S}}_z)$. The matrix elements of this perturbation and the states $|\ "\pm\tfrac{1}{2}"\ \rangle$ determine the energy separation between the resulting pair of levels. The result is that the observable splitting is just what one would expect if we can completely ignore the orbital angular momentum and replace its effect by an anisotropic coupling between the electron spin and the magnetic field. As the g-tensor is derived by constructing the matrix of $(\underline{L} + g_e \underline{S})$ for the states $|+\rangle$ and $|-\rangle$, the spin-Hamiltonian is

$$\begin{aligned} \mathcal{H} &= \beta\, \underline{H}.\underline{g}.\underline{S} \\ &= \beta\{g_{\parallel} H_z \hat{S}_z + g_{\perp}(H_x \hat{S}_x + H_y \hat{S}_y)\} \quad .. \quad (2.4) \end{aligned}$$

where $\hat{S}_x$, $\hat{S}_y$ and $\hat{S}_z$ are components of the fictitious spin $\underline{S}$. The states $|+\rangle$ and $|-\rangle$ are the eigenfunctions of $\hat{S}_z$ with eigen values $+\tfrac{1}{2}$ and $-\tfrac{1}{2}$, respectively. The z-axis of the g-tensor coincides with the symmetry axis of the system. It follows that the spin-Hamiltonian is so-called since it operates on wave functions expressed in terms of spin variables only.

2.6 Applications of Spin Hamiltonian

The above considerations will now be applied to the specific case of an ion with a single 3d electron. The ground state of such an ion, (eg. Ti^{3+}, V^{4+}), is a D state. By spin-orbit coupling this splits into $^2D_{3/2}$ and $^2D_{5/2}$, the former being lower. This is a valid classification in the crystalline complex as $\mathcal{H}_2$ (=V) is stronger than $\mathcal{H}_3$ (spin-orbit) and the free-ion spin-orbit coupling is completely broken. The spin-orbit interaction is represented by

$$\mathcal{H}_3 = \lambda \hat{\underline{L}} . \hat{\underline{S}}$$

For a d^1 system the shell is less than half-filled and, therefore, λ is positive. In the absence of an applied magnetic field, the lower t level of a d^1 system is split into three Kramers' doublets because of either a crystalline field or spin-orbit coupling or both. Application of magnetic field at this stage amounts to introducing a perturbation $\mathcal{H}_4$:

$$\mathcal{H}_4 = \underline{H} . (\hat{\underline{L}} + 2\hat{\underline{S}})$$

This interaction which is linear in magnetic field lifts the Kramers' degeneracy completely. In a paramagnetic resonance experiment only the lowest doublet is effective at the magnetic fields available in the laboratory and one absorption line results. This situation is shown in Fig. 2.4 for a crystalline field of rhombic

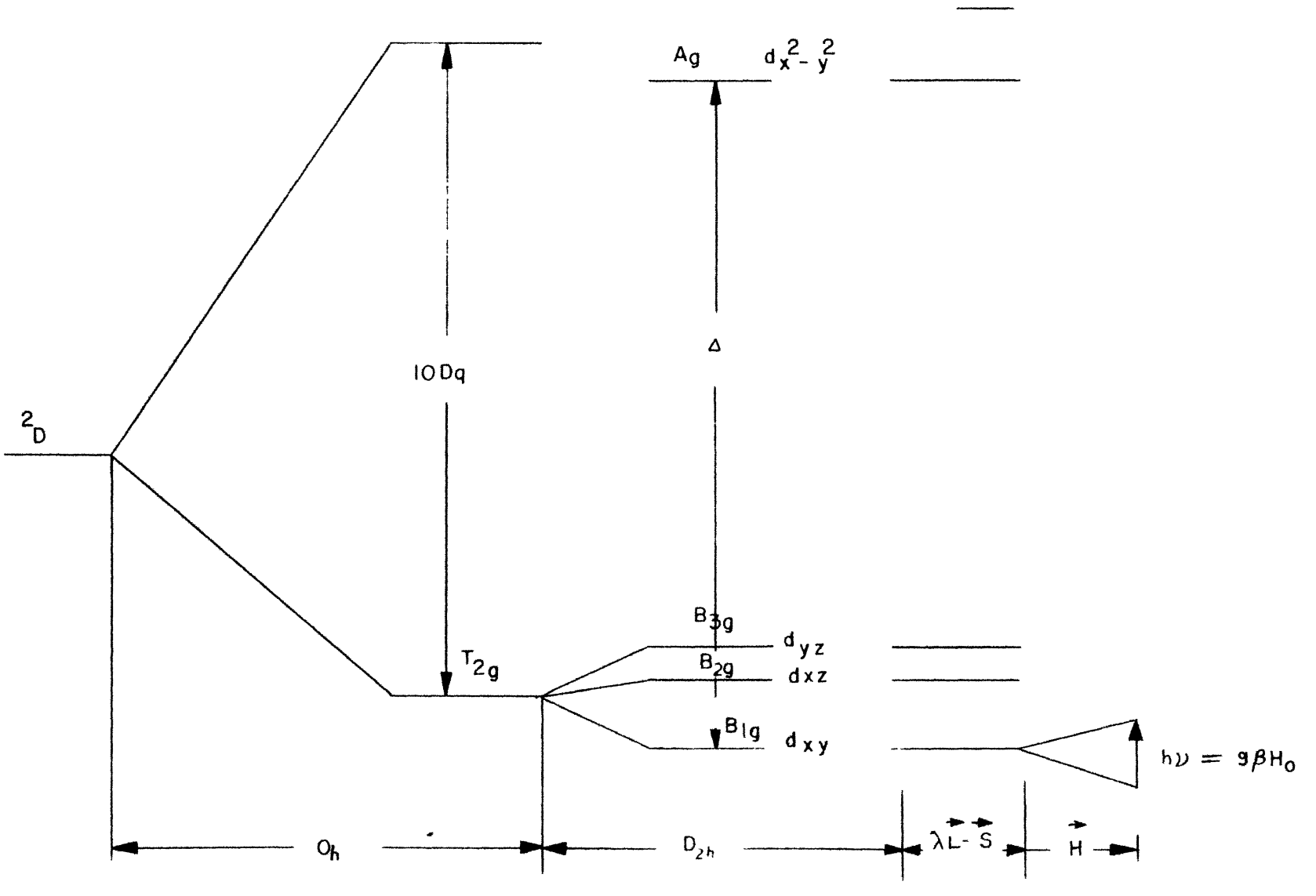

FIG·2·4 REMOVAL OF DEGENERACY IN THE ^2D STATE ($3d^1$ CONFIGURATION) OF VO^{++} ION BY VARIOUS PERTURBATIONS (HYPERFINE COUPLING $\vec{I} \cdot \vec{S}$ OF THE ELECTRON AND V^{51} NUCLEAR SPINS IS NOT SHOWN)

symmetry. However, due to the hyperfine interaction with the nucleus each of the two levels is further split into (2I+1) levels where I is the spin of metal ion nucleus. For example in the case of V^{4+}, I=7/2 and this results in an eight line hyperfine spectrum, (Fig.6.1).

2.7 S-State Ions

The paramagnetic spectrum of divalent manganese ion in crystalline media is more complicated and theoretically more interesting. The ground state of the free ion Mn^{2+} is six-fold degenerate, the spectroscopic classification being $(d^5)^6S_{5/2}$. It is important to note that a pure $^6S_{5/2}$ manifold is not split by the perturbation $\mathcal{H}_2$ since an electric field is spin-independent and $^6S_{5/2}$ is an orbital singlet. However, if a divalent manganese ion is placed in a crystal environment of cubic symmetry, the electron paramagnetic resonance spectrum shows[3] that the octohedral cubic field splits the free-ion ground-state manifold into two levels: the upper four-fold degenerate state Γ_8, the lower two-fold degenerate state Γ_7. This ground state splitting $(\Gamma_8 - \Gamma_7)$ can be accounted for qualitatively by observing that because of the presence of spin-orbit interaction the ground state is not a pure $^6S_{5/2}$. If the cubic field environment is regarded as equivalent to an electric field with cubic symmetry, it follows from symmetry arguments[4] that such a manifold

is split by a cubic perturbation into sub-manifolds of 2 and 4. Thus the splitting in $Mn^{2+}(^6S_{5/2})$ arises as the free ion spin-orbit coupling mixes together states with the same J-value. For instance, $^6S_{5/2}$ can mix with $^4P_{5/2}$ and $^4P_{5/2}$ with $^2D_{5/2}$. If the crystalline field has a symmetry lower than the cubic, further distortions split the quartet into two more doublets and in all one has three doublets with Kramers' degeneracy. An external magnetic field removes this degeneracy and six levels result. Magnetic dipole transitions among these six levels give rise to five absorption lines, which is the so-called fine structure of EPR spectrum, (Fig. 2.5). The nucleus of Mn^{55} has a spin of 5/2 and the hyperfine interaction causes each of the six fine structure levels split into six levels giving rise to a total of 36 levels. This results, using the selection rules $\Delta M_s = \pm 1$ and $\Delta m_I = 0$, in a 5x6 (=30) lines in the EPR spectrum of Mn^{2+} placed in a crystal field of symmetry lower than cubic.

2.8 Hyperfine Structure

Hyperfine interactions are mainly magnetic dipole interactions between the electronic magnetic moment and the nuclear magnetic moment of the paramagnetic ion, neglecting the nuclear moments of neighbouring ions. In the case of s-electrons it is the Fermi contact interaction which is important. The octet in

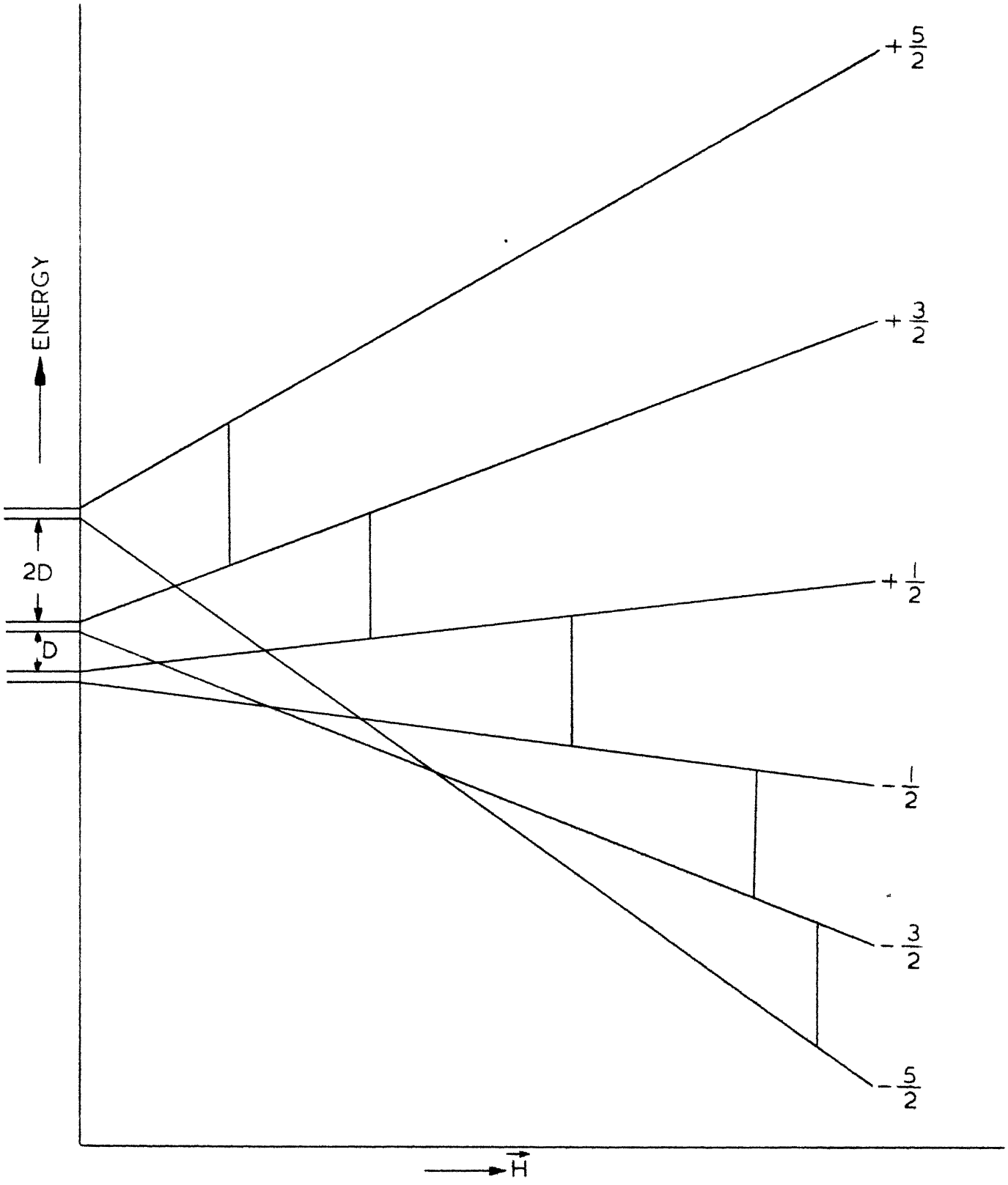

FIG·2·5 ZERO-FIELD SPLITTING BETWEEN THE THREE KRAMERS' DOUBLETS OF A SEXTET STATE IN THE Mn^{2+} ION LEADING TO FINE STRUCTURE IN EPR SPECTRUM. (HYPERFINE INTERACTION DUE TO Mn^{55} NUCLEUS NOT SHOWN)

the EPR of vanadyl ion and the sextets in the EPR of divalent manganese are the result of hyperfine interactions. The classical expression for the potential energy V_{ij} of magnetic interaction between two magnetic dipoles of moments $\vec{\mu}_i$ and $\vec{\mu}_j$ a distance $\vec{r}_{ij}$ apart, is:

$$V_{ij} = \frac{\vec{\mu}_i \cdot \vec{\mu}_j}{\vec{r}_i^{\,3}} - \frac{3(\vec{\mu}_i \cdot \vec{r}_{ij}).(\vec{\mu}_j \cdot \vec{r}_{ij})}{\vec{r}_{ij}^{\,5}} \quad .. \quad (2.5)$$

Expression (2.5), treated as an operator, and summed over all neighbours, is the dipole-dipole interaction term in the Hamiltonian. In our effective spin-Hamiltonian we attempt to relate the electronic moment to the spin vector $\underline{S}$. Abragam et al[2] described the nuclear hyperfine structure by the following Hamiltonian:

$$\mathcal{H} = \gamma_e \gamma_n \left[\frac{3(\underline{I}.\underline{r}).(\underline{r}.\underline{s})}{r^5} - \frac{\underline{s}.\underline{I}}{r^3} + \frac{\underline{L}.\underline{I}}{r^3} + \frac{8\pi}{3} \delta(r).(\underline{s}.\underline{I}) \right] \quad .. \quad (2.6)$$

The first two terms in this expression correspond to the dipolar interaction between the electronic and nuclear magnetic moments. The third term gives the contribution resulting from the orbital motion of the electron while the last term describes the Fermi contact interaction[5]. Interactions in Equation (2.6) depend mainly on that part of the wave function which is near to the nucleus.

Introducing a tensor operator $\hat{\underline{A}}$ analogous to $\hat{\underline{g}}$ tensor, (2.6) can also be written as

$$\mathcal{H}_{\text{hyperfine}} = A_x I_x S_x + A_y I_y S_y + A_z I_z S_z$$

in a principal axis system. In general, the electron-nucleus hyperfine interaction is represented by $\hat{\underline{S}}.\hat{\underline{T}}.\hat{\underline{I}}$ where T is the hyperfine tersor. This can be written as the sum

$$a\,\hat{\underline{S}}.\hat{\underline{I}} + \hat{\underline{S}}.\underline{T}'.\hat{\underline{I}} \qquad .. (2.7)$$

where a is the isotropic part and T' is the magnetic dipolar tensor. In the system $VO^{2+}:Cs_2SO_4$ described in chapter 4 of this thesis the anisotropic splittings which are due to T' are investigated in some detail.

2.9 Ligand Hyperfine Structure:

The spectrum of Mn^{2+} in the substitutional sites in NaF single crystal which has been studied in detail in this thesis in chapter 5 provides an extensive super-hyperfine structure (SHFS) in addition to the usually observed fine and hyperfine structure. This additional structure has been ascribed to the interaction of F^{19} nuclei with the localised spin magnetization of the Mn^{2+} ion and is described by the addition of the following sub-Hamiltonian:

$$\mathcal{H}^{19} = \sum_i \underline{S}.A^i.I_i \qquad .. \quad (2.8)$$

where the summation is to be taken over the six neighbouring F^{19} nuclei each of spin ½. This interaction splits each level into a number of sublevels to provide as many as fifteen new lines for each hyperfine line. Tinkham[6] ascribed this effect to covalent bonding between the metal ions and the fluorine ions. Stevens[7] and Griffiths and Owen[8] adopted this covalent bond theory while discussing the SHFS of Ir^{4+} ion in chloroplatinates. For octohedral complexes of MX_6 type Owen suggested that the unpaired electrons responsible for the paramagnetism might be partially transferred from M to X_6 in molecular orbitals which are usually of anti-bonding type. Shulman and Jaccarino[10] favoured the superexchange mechanisms discussed by Anderson[11]. Clogston et al[12] adopted the covalent bonding theory in their phenomenological description of the fluorinehyperfine interaction where the entire burden of the interaction rests upon the augmented d-wave functions. Fig. 2.6 shows schematic representation of bonding orbitals in an octohedral complex as described by Hall et al[13].

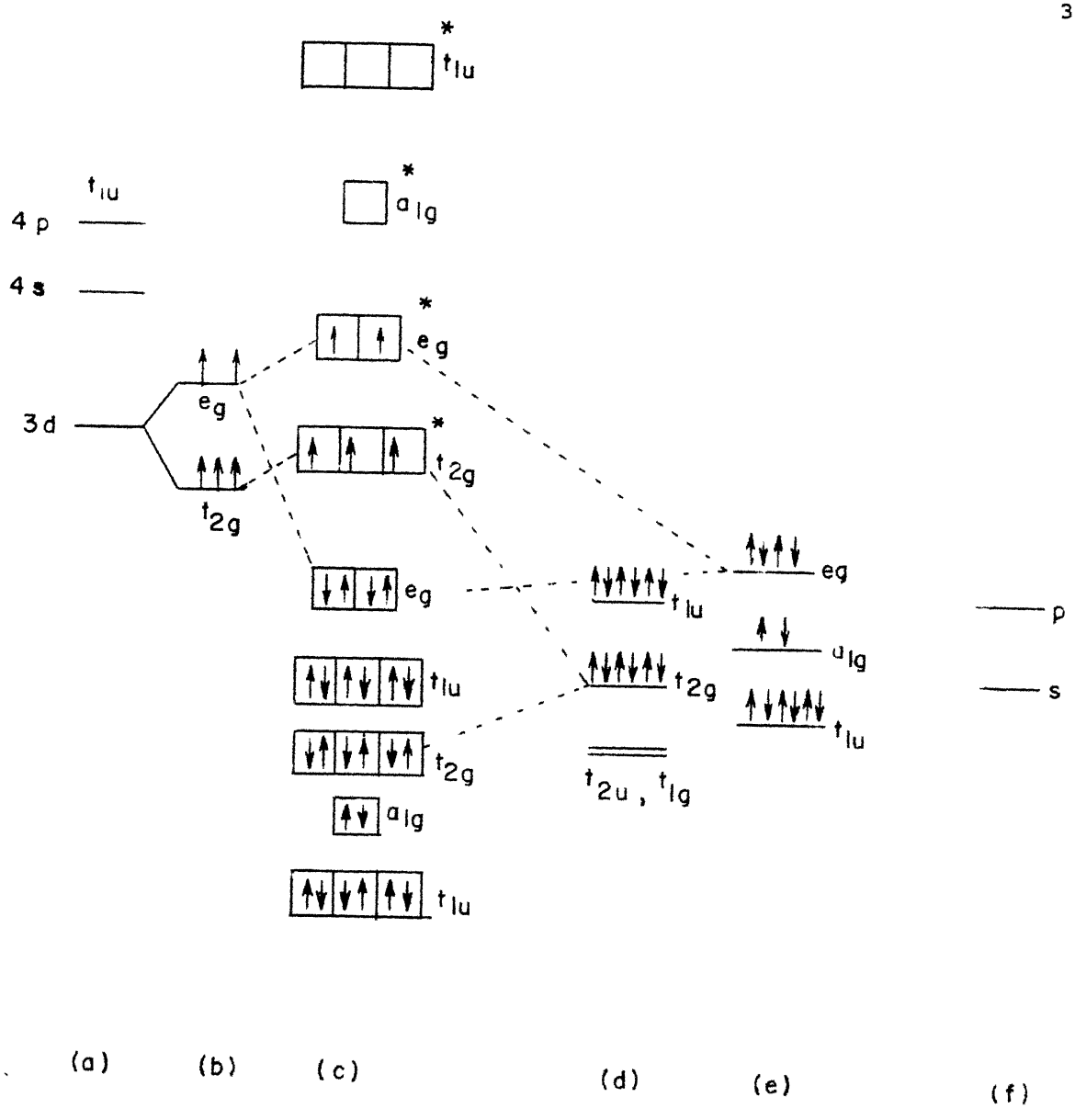

FIG. 2·6 BONDING ORBITALS IN AN OCTAHEDRAL COMPLEX. ARROWS INDICATE OCCUPATION OF THE LEVELS BY a d-ELECTRON. ASTERISKS INDICATE ANTIBONDING ORBITALS.

(a) ENERGY LEVELS OF FREE METALS ION
(b) SPLITTING BY AN ELECTRIC FIELD OF O_h SYMMETRY
(C) BONDING CENTRAL ION AND THE P-ORBITALS OF THE SURROUNDING LIGANDS
(d) TT-BONDING ORBITALS
(e) σ - BONDING ORBITALS
(f) ENERGY LEVELS OF FREE LIGAND IONS

2.10 Spin Hamiltonian Parameters

For a crystal with an ion embedded in it, in the absence of a theory to calculate parameters from first principles, paramagnetic resonance fields can be made to fit the spin Hamiltonian. Omitting nuclear terms which do not involve electron operators, the Zeeman interaction is taken into account by

$$\beta (g_x S_x H_x + g_y H_y S_y + g_z S_z H_z);$$

the fine structure is taken care of by the parameters D and E in

$$D\left[S_z^2 - \frac{1}{3}S(S+1)\right] + E(S_x^2 - S_y^2);$$

the hyperfine structure is accounted for by

$$A_z I_z S_z + A_x I_x S_x + A_y I_y S_y ;$$

and the ligand hyperfine structure, if present, is taken care of by equation (2.8).

2.11 EPR of Liquids

In the present study, the EPR spectra of VO^{2+} in alkali chlorides show certain features characteristic of liquids rather than solids. So it is felt necessary to briefly outline the theory of EPR spectra of liquids[14].

The paramagnetic complexes in liquid solutions can be considered as microcrystals tumbling in a random way as they are jostled by the molecular motions of the solvent liquid. The immediate environment of the paramagnetic ion in these microcrystals can be as high as cubic with strong possibility of an axial component. In a coordinate system (p,q,r) fixed in the molecule the axial spin Hamiltonian can be written as [14,15]

$$\mathcal{H} = \beta\left[g_{\parallel} H_r S_r + g_{\perp}(H_p S_p + H_q S_q)\right] + DS_r^2 + A_{\parallel} I_r S_r + A_{\perp}(I_p S_p + I_q S_q)$$

This can be transformed into laboratory coordinate system by using the following transformation equations:

$$H_r = H_o \cos\theta$$

$$S_r = S_z \cos\theta + S_x \sin\theta\cos\phi + S_y \sin\theta \sin\phi$$

$$= S_z \cos\theta + \tfrac{1}{2}(S_+ e^{-i\phi} + S_- e^{+i\phi})\sin\theta$$

After transforming into the laboratory coordinate system x,y,z the Hamiltonian takes the form[14,15]

$$\mathcal{H} = g\beta H_o S_z + a\underline{I}.\underline{S} + (D/2).(3\cos^2\theta - 1)S_z^2$$

$$+(D/2)\sin\theta\cos\theta\left[(S_zS_+ + S_+S_z)e^{-i\phi}\right.$$

$$\left.+(S_zS_- + S_-S_z)e^{i\phi}\right] + (1/3).(\Delta g\beta H_o + bI_z).$$

$$(3\cos^2\theta - 1)S_z$$

$$+(b/2)\sin\theta\cos\theta(I_+e^{-i\phi} + I_-e^{+i\phi})S_z$$

$$+\tfrac{1}{2}(\Delta g\beta H_o + bI_z)\sin\theta\cos\theta(S_+e^{-i\phi} + S_-e^{+i\phi})$$

$$+(b/4)\sin^2\theta(I_+S_+e^{-2i\phi} + I_-S_-e^{2i\phi})$$

$$-(b/12).(3\cos^2\theta - 1).(I_+S_- + I_-S_+) \qquad .. \qquad (2.9)$$

where $g = (1/3)(g_{\parallel} + 2g_{\perp})$, $\Delta g = g_{\parallel} - g_{\perp}$

$a = (1/3)(A + 2B)$, $b = A - B$

with $A = A_{\parallel}$ and $B = A_{\perp}$ while $I_{\pm}$ and $S_{\pm}$ are the usual raising and lowering operators, operating on nuclear and electronic spin states respectively. As the molecule tumbles, θ becomes time dependent, and the above Hamiltonian (2.9) can be written as $\mathcal{H} = \mathcal{H}_o + \mathcal{H}(t)$, where $\mathcal{H}_o$ is time independent and isotropic and is given by the first two terms in the above Hamiltonian (2.9), viz., $g\beta H_o S_z + a\underline{I}.\underline{S}$. $\mathcal{H}(t)$ contains rest of the terms and is time dependent due to random time dependence of θ. If the random motions are extremely rapid, which means, if the motional frequency times h exceeds the interaction energy in question, the time dependent terms

average out to zero and have little effect. This is the limiting case of situation which can be seen in the experiment. In general, however, the time dependent terms lead to important effects. McConnell[14] has shown that the anisotropies in g and A terms, which are averaged out to zero due to rapid tumbling of the molecule, ($\langle \overline{\mathcal{H}'(t)} \rangle = 0$), contribute to the line widths of the isotropic spectrum given by the Hamiltonian $\mathcal{H}_0$; and the line widths are predicted to obey a formula of the type

$$\Delta\nu \sim 1/T_2 \simeq \tau_c (\Delta g \beta H_0 + b m_I)^2 / \hbar^2$$

where τ_c is the correlation time, describing the random motion of the molecule. Rogers and Pake[16] first observed these line width effects in their study of EPR of VO^{2+} complexes in solutions. Similar effects are observed in the present study and are discussed in chapter 6 of this thesis.

2.12 REFERENCES (GENERAL)

The manuscript is written with the help of the following books and monographs. In the text the letter G is added when reference is specifically made to any one of the references listed in this category.

1. B.Bleaney and K.W.H.Stevens:Repts.Prog.in Physics., 16,108(1953).
2. A.Carrington and A.D.McLachlan, INTRODUCTION TO MAGNETIC RESONANCE WITH APPLICATIONS TO CHEMISTRY AND CHEMICAL PHYSICS, Harper and Row, New York (1967).
3. K.D.Bowers and J.Owen, Repts.Prog.in Phys.,18, 304(1955).
4. W.Low,PARAMAGNETIC RESONANCE IN SOLIDS, Academic Press, New York & London(1960).
5. G.E.Pake,PARAMAGNETIC RESONANCE, W.A.Benjamin Inc., New York, (1962).
6. S.A.Al'Tshuler and B.M.Kozyrev, ELECTRON PARAMAGNETIC RESONANCE, Academic Press, New York, London, (1964).
7. M.T.Hutchins, POINT CHARGE CALCULATIONS OF ENERGY LEVELS OF MAGNETIC IONS IN CRYSTALLINE ELECTRIC FIELDS, Solid State Physics 16, Academic Press,(1964).
8. H.M.Assenheim, INTRODUCTION TO ELECTRON SPIN RESONANCE,Hilger and Watts Ltd., London,(1966).
9. J.Owen and J.H.M.Thornley,Repts.Prog.in Phys., 29,675(1966).
10. P.B.Ayscough, ELECTRON SPIN RESONANCE IN CHEMISTRY, Methuen & Co., Ltd.,(1967).

2.13 REFERENCES (1 to 16)

The manuscript is written with the help of these original publications in various journals. These references are referred to as superscripts in the main body of the text.

1. R.Schlapp and W.G.Penney, Phys.Rev.,42,666(1932).
2. A.Abragam and M.H.L.Pryce, Proc.Roy.Soc.,A205,135 (1951).
3. W.Low, Phys.Rev.,105,793(1957).
4. H.Bethe, Ann.Phys.Lpz.,3,133(1929); English Translation, Consultants' Bureau, New York,(1958).
5. F.J.Milford, Am.J.Phys.,28,521(1960).
6. M.Tinkham, Proc.Roy.Soc.,A236,535,549(1956).
7. K.W.H.Stevens, Proc.Roy.Soc.,A219,542(1953).
8. J.H.E.Griffiths and J.Owen, Proc.Roy.Soc.,A226,96 (1954).
9. J.Owen, Disc.Faraday Soc.,19,127(1955).
10. R.G.Shulman and V.Jaccarino, Phys.Rev.,103,1126(1956).
11. P.W.Anderson,Phys.Rev.,79,350(1950).
12. A.M.Clogston, J.P.Gordon, V.Jaccarino, M.Peter, and L.R.Walker,Phys.Rev.,117,1222(1960).
13. T.P.P.Hall,W.Hayes,R.W.H.Stevenson, and J.Wilkens, J.Chem.Phys.,38,1977(1963).
14. H.M.McConnell, J.Chem.Phys.25,709(1956).
15. G.E.Pake, PARAMAGNETIC RESONANCE, W.A.Benjamin,Inc., New York,(1962).
16. R.N.Rogers and G.E.Pake,J.Chem.Phys.,33,1107 (1960).

CHAPTER III

ELECTRON PARAMAGNETIC RESONANCE OF Mn^{2+} IN SINGLE CRYSTALS OF CAESIUM SULPHATE, Cs_2SO_4

ABSTRACT

The electron paramagnetic resonance (EPR) spectrum of divalent manganese ion has been studied at 9.5 Gc/sec. These studies reveal that Mn^{2+} substitutes Cs^{+} ion and the charge compensation is restored by formation of cation vacancies—the Mn^{2+} ion substitutes at a β-Cs^{+} site and gets associated itself with a vacancy at a nearest neighbour β-Cs^{+} site. This gives rise to a complex in the ab-crystallographic plane. All the spectra observed in the temperature range from room temperature (300 ^{o}K) to liquid nitrogen temperature (77 ^{o}K) have been described by the spin-Hamiltonian for Mn^{2+} in rhombic crystalline field. The temperature variation of the parameters D and E has been studied in the above temperature range. The spectra for the observed complex along its three principal axes have been analysed using second order perturbation equations. The relevant energy matrix is diagonalised to determine the influence of the off-diagonal elements which may be significant in the present case. The parameters which satisfy a least-square fit are:

g_z = 1.999(5), g_x = 2.014(9), g_y = 2.008(9);

A_z = -93 Oe, A_x = -91 Oe, A_y = -92 Oe;

D = -941 Oe, E = -14 Oe;

b_4^0 = 0.0 Oe, b_4^2 = 13 Oe, b_4^4 = -77 Oe;

ϕ = 25^{o}; where ϕ is the angle the direction of the complex making with the longest crystallographic axis b in the ab-plane.

3.1 INTRODUCTION

During the past few years the technique of electron paramagnetic resonance (EPR) has been used for studying impurity ions in alkali sulphates[1-4]. The value of EPR methods to study the phase transition[3-7] is well-known. Moreover, EPR has been an important structural tool in perovskites, spinels and garnets[8]. Chowdari and Venkateswarlu[3] found indications of a probable phase transition around -130 °C in Mn^{2+} doped K_2SO_4 single crystal. It was felt that it would be interesting to see whether such a transition occurs in the case of the isomorphous sulphates[†] which are not ferro-electric. Information about the lattice defects such as positive ion vacancies is valuable for the solid state studies in general. In the present studies Mn^{2+} which is an S-state ion belonging to the iron group transition elements is doped in single crystals of caesium sulphate which is not ferroelectric. Exhaustive analysis of the observed paramagnetic resonance spectra is made in the temperature range of 77 °K to 300 °K and the spin-Hamiltonian parameters of the system $Mn^{2+}:Cs_2SO_4$ for the observed complex in the ab-crystallographic plane have been obtained. To our knowledge such studies have not been reported in the literature.

---

† $(NH_4)_2SO_4$ is known to become ferroelectric[4] below -50 °C.

3.2 CRYSTAL STRUCTURE

The crystal structures of isomorphous sulphates of potassium, ammonium, rubidium and caesium have been determined by Ogg[9]. They belong to the symmetry group V_h^{16} and contain two reflection planes, four glide planes, twelve dyad screw axes, and sets of four centres of symmetry. The orthorhombic unit cell dimensions are

$$a = 6.218 \text{ Å}$$
$$b = 10.884 \text{ Å}$$
$$c = 8.198 \text{ Å}$$

The structure of Cs_2SO_4 consists of layers of atoms parallel to (100) planes the spacing between which is a/2. The reflection planes are $(100)_{1/4}$ and $(100)_{-1/4}$ if we assume the origin of coordinates is at the centre of the unit cell. The unit cell contains four formula weights. Depending on the oxygen environment the caesium atoms are classified as α- or β-type[9]. As a result there are four caesium ions of α-type and four caesium ions of β-type in the unit cell (Fig. 3.1). A knowledge of the positions of caesium atoms is necessary to interpret the various paramagnetic resonance spectra described in this work.

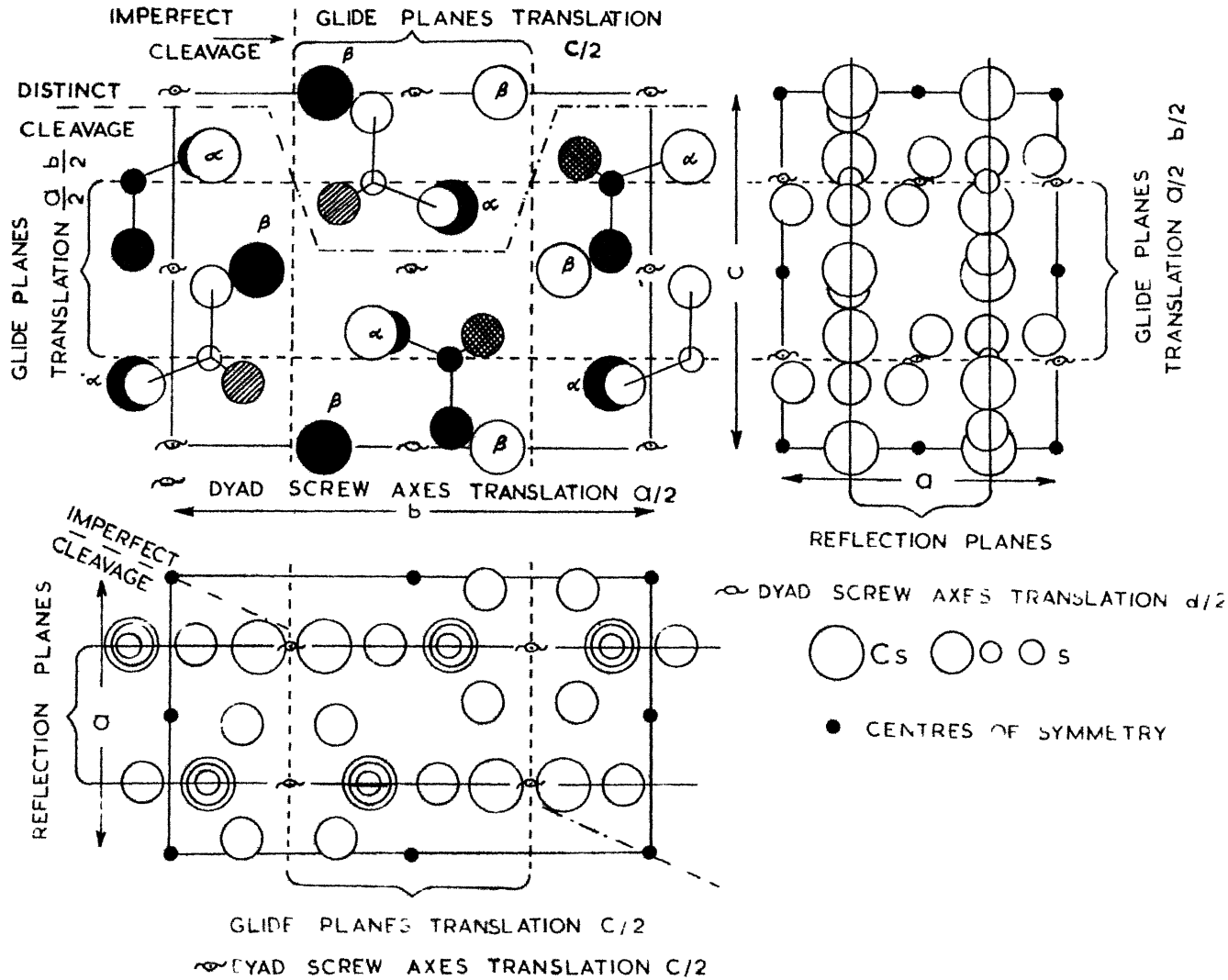

G.3·1. APPROXIMATE POSITONS OF ATOMS AND SYMMETRIES OF Cs_2 SO_4 IN THE THREE PRINCIPAL (AFTER A OGG[10])

3.3 EXPERIMENTAL

Caesium sulphate supplied by E.Merck and of analytical grade has been used. 0.3 mole percent of $MnSO_4$ has been added to a saturated aqueous solution of Cs_2SO_4. Slow evaporation yielded thin plates of transparent crystals, 1cm x 1cm x 0.2cm size, with well-developed {001} faces. Spectrophotometric analysis of the experimental crystal showed that the manganese content is less than 1250 parts per million. The crystal has no detectable traces of water either to give infra-red absorption bands on Cary-14 spectrophotometer or proton resonance signal on wide line NMR. Desired orientation of the experimental crystal with respect to the magnetic field has been easy because of the known axes <001> and <100> the former being perpendicular to the well-developed face of the crystal while the latter being the needle axis. X-ray rotation photographs taken along these directions confirmed the assignment of the axes. Measurements have been made at x-band with a Varian V-4502 EPR spectrometer having a 9-inch rotating magnet and 100 kc/sec field modulation. A Varian rotating cavity V-4533 has been used to determine the angular variation and the direction of the principal axes of the g-tensor. A speck of polycrystalline diphenylpicrylhydrazyl (DPPH) whose g-value is taken as 2.0036[10] placed alongside the crystal has been used as a field marker. The

magnetic field has been standardised using proton resonance in conjunction with a nuclear flux meter F-9 and Beckman 10-110 Mc convertor 7571. Temperature variation experiments have been done using a Varian V-4530 temperature controller. The spectrometer has been operated at low power the microwave power being one milliwatt.

3.4 THEORY

The ground state of Mn^{2+} with its $3d^5$ configuration is $^6S_{5/2}$. In a crystal field of low symmetry such as Cs_2SO_4 excited quartet levels get admixed into the ground state[11] and the ground state is split into three Kramers' doublets. In a magnetic field the degeneracy is completely removed and five fine structure transitions are possible. Due to the interaction with the nucleus of spin 5/2 each electronic transition gives rise to six hyperfine transitions. Thus the electron paramagnetic resonance absorption of Mn^{2+} in caesium sulphate is expected to contain thirty lines. In general, the spectrum has more lines due to the presence of angular parts due to Mn^{2+} ions in equivalent positions or at different sites. Additional lines due to forbidden transitions are also possible.

The thirty line EPR spectra of Mn^{2+} obtained in the present case have been analysed using a more general spin-Hamiltonian appropriate to the low symmetry:

$$\mathcal{H} = g_z\beta H_z S_z + g_x\beta H_x S_x + g_y\beta H_y S_y + \frac{1}{3}b_2^0 O_2^0 + \frac{1}{3}b_2^2 O_2^2$$
$$+ \frac{1}{60}b_4^0 O_4^0 + \frac{1}{60}b_4^2 O_4^2 + \frac{1}{60}b_4^4 O_4^4$$
$$+ AS_zI_z + BS_xI_x + CS_yI_y \qquad .. \quad (3.1)$$

The operators O_n^m are given in an explicit form by Orbach[12] and $\underline{g}$, b_i^k are parameters to be fixed by experiment. The matrix of this spin-Hamiltonian (3.1)[13] in the manifold of S=5/2 was diagonalised to a second order and the following expressions [3,13] have been used to calculate the fine structure positions at resonance when H$\|$z. The usual parameters D, E and a replace the constants b_2^0, $\frac{1}{3}b_2^2$ and $2b_4^0$ respectively.[14]

$$H_1(M=5/2 \leftrightarrow 3/2) = H_o - 4D + 9E^2/(H_1+D) - 5E^2/(H_1+3D) - 2a - 3Eb_4^2/H_o$$

$$H_2(M=3/2 \leftrightarrow \tfrac{1}{2}) = H_o - 2D - 9E^2/(H_2+D) + 9E^2/(H_2-D) - 5E^2/(H_2+3D) + 5/2(a) - 1.5Eb_4^2/H_o - \frac{(b_4^4)^2}{20H_o}$$

$$H_3(M=\tfrac{1}{2} \leftrightarrow -\tfrac{1}{2}) = H_o - 9E^2/(H_3-D) + 5E^2/(H_3+3D) + 5E^2/(H_3-3D) - 9E^2/(H_3+D) + 6Eb_4^2/H_o$$

$$H_4(M=-\tfrac{1}{2} \leftrightarrow -3/2) = H_o + 2D + 9E^2/(H_4+D) - 9E^2/(H_4-D) - 5E^2/(H_4-3D) - 5/2(a) - 1.5Eb_4^2/H_o - \frac{(b_4^4)^2}{20H_o}$$

$$H_5(M=-3/2 \leftrightarrow -5/2) = H_o + 4D + 9E^2/(H_5-D) - 5E^2/(H_5-3D) + 2a - 3Eb_4^2/H_o \quad .. \quad (3.2)$$

To take account of the hyperfine structure a term HFS has been added to each of the above equations (3.2):

$$HFS = -Am - \frac{B^2 + C^2}{4H_o}\{I(I+1) - m^2\} - \{(2M-1)m\}BC/H_o \quad .. \quad (3.2a)$$

$$= H(m \leftrightarrow m)$$

The same expressions have been used cyclically when the static field H is parallel to x or y. The corresponding D^*, E^*, a^*, b_4^{2*} and b_4^{4*} are related by standard transformation relations listed in Table (3.1). A,B and C are hyperfine constants when $H \| z$, $H \| x$ and $H \| y$ respectively.

To keep up the generality a term containing Q is usually added to the Hamiltonian (3.1) to take account of the quadrupole interaction. The contribution due to this to HFS in $\theta = 90^o$ part of the spectrum is the addition of the extra term[15]

$$\frac{-Q^2 m.2\{I(I+1)\} - 2m^2 - 1}{8BM(M-1)} \quad .. \quad (3.2b)$$

TABLE 3.1

Relationship† among the constants of the spin-Hamiltonian for three mutually perpendicular orientations of the magnetic field $\underline{H}$

Effective value of the constants	$H\|\|z$	$H\|\|x$	$H\|\|y$
D^* (b_2^{o*})	D $(\equiv b_2^o)$	$\frac{1}{2}(-D+3E)$ $(\equiv -\frac{1}{2}(b_2^o - b_2^2))$	$-\frac{1}{2}(D+3E)$ $(\equiv -\frac{1}{2}(b_2^o + b_2^2))$
E^* $(\equiv b_2^{2*})$	E $(\equiv b_2^2/3)$	$-\frac{1}{2}(D+E)$ $(-(3b_2^o + b_2^2)/6))$	$\frac{1}{2}(D-E)$ $(\equiv (3b_2^o - b_2^2)/6))$
b_4^{o*} $(\equiv a^*/2)$	b_4^o $(a/2)$	$\frac{1}{12}(3b_4^o + b_4^2 + b_4^4)$	$\frac{1}{3}(3b_4^o - b_4^2 + b_4^4)$
b_4^{2*}	b_4^2	$-\frac{1}{2}(5b_4^o + b_4^2 - b_4^4)$	$-\frac{1}{2}(5b_4^o - b_4^2 - b_4^4)$
b_4^{4*}	b_4^4	$\frac{1}{24}(35b_4^o - 7b_4^2 + b_4^4)$	$\frac{1}{24}(35b_4^o + 7b_4^2 + b_4^4)$
A^*	A	B	C
B^*	B	C	A
C^*	C	A	B
g^*	g_z	g_x	g_y

† We are thankful to Dr. Daniel Schechter of Solid State Physics Laboratory, TRW Systems, for kindly sending a memo which discussed in detail the effects of interchanging site axes.

For manganese I=5/2 so that m takes the values -5/2 to +5/2. However, this term (3.2b) has been neglected in the present analysis as the quadrupole effects are found to be negligible.

The spin-Hamiltonian parameters obtained by using relations obtained with the help of second order perturbation theory are not necessarily correct as the validity of the use of the perturbation theory when the parameters form a sizable percentage of the fields at which resonance occurs is open to question. So they have been improved upon by diagonalising the relevent energy matrix for the case when E/D is a minimum. Taking the z-axis as the axis of quantisation one can see that the off-diagonal elements for $H_x g_x S_x$ and $H_y g_y S_y$ in equation (3.1) do not exist. The diagonal elements involve terms containing $g_z H_z S_z$, D, a and A_z. The off-diagonal elements due to $E(S_x^2 - S_y^2)$ and $A_x S_x I_x + A_y S_y I_y$ have been evaluated. To keep up the generality, the components A_x, A_y and A_z are all assumed to be different in this work. The off-diagonal elements in A_x and A_y have been obtained using the following relations:

$$\langle M,m|A_xS_xI_x|N,n\rangle = A_x/4\{\delta_{M,N+1}\sqrt{S(S+1) - N(N+1)} + \delta_{M,N-1}\sqrt{S(S+1) - N(N-1)}\}x \{\delta_{m,n+1}\sqrt{I(I+1) - n(n+1)} + \delta_{m,n-1}\sqrt{I(I+1) - n(n-1)}\}$$

$$\langle M,m|A_yS_yI_y|N,n\rangle = -A_y/4\{\delta_{M,N+1}\sqrt{S(S+1) - N(N+1)} - \delta_{M,N-1}\sqrt{S(S+1) - N(N-1)}\}x \{\delta_{m,n+1}\sqrt{I(I+1) - n(n+1)} - \delta_{m,n-1}\sqrt{I(I+1) - n(n-1)}\}$$

The elements of (2S+1).(2I+1) matrix with S=I=5/2 are shown in Table (3.2).

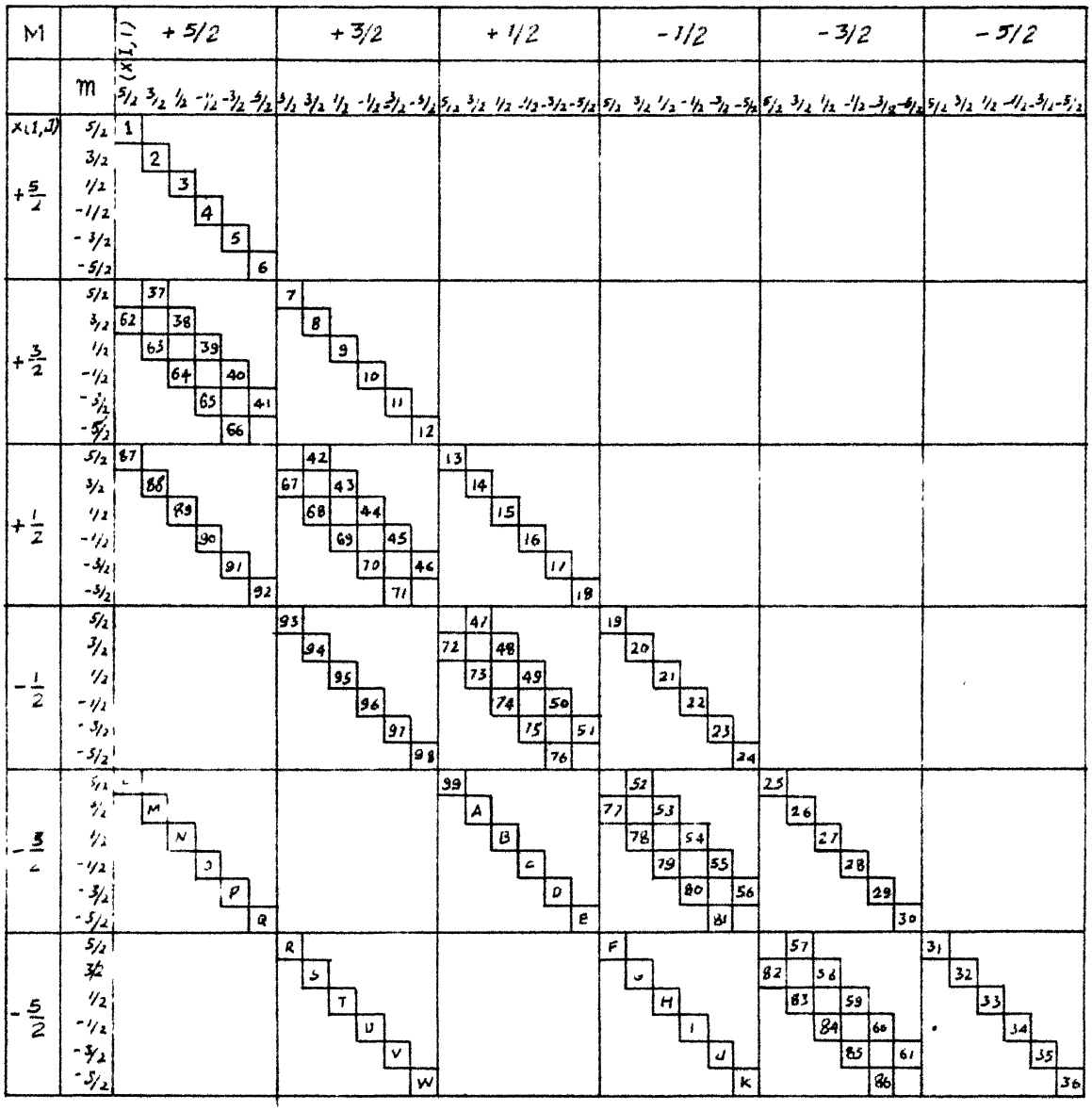

TABLE. 3.2

MATRIX FOR EVALUATING THE ENERGY LEVELS IN THE EPR SPECTRUM OF Mn^{2+} in Cs_2SO_4

TABLE 3.2

The 36x36 Matrix connected with the Energy Levels of EPR Spectrum

Numbered square	Matrix Element	Value
	Diagonal elements 1-36	
1	x(1,1)	$2.5H_o + 10/3.D + 6.25A + b_4^o$
2	x(2,2)	$2.5H_o + 10/3.D + 3.75A + b_4^o$
3	x(3,3)	$2.5H_o + 10/3.D + 1.25A + b_4^o$
4	x(4,4)	$2.5H_o + 10/3.D - 1.25A + b_4^o$
5	x(5,5)	$2.5H_o + 10/3.D - 3.75A + b_4^o$
6	x(6,6)	$2.5H_o + 10/3.D - 6.25A + b_4^o$
7	x(7,7)	$1.5H_o - 2/3.D + 3.75A - 3b_4^o$
8	x(8,8)	$1.5H_o - 2/3.D + 2.25A - 3b_4^o$
9	x(9,9)	$1.5H_o - 2/3.D + 0.75A - 3b_4^o$
10	x(10,10)	$1.5H_o - 2/3.D - 0.75A - 3b_4^o$
11	x(11,11)	$1.5H_o - 2/3.D - 2.25A - 3b_4^o$
12	x(12,12)	$1.5H_o - 2/3.D - 3.75A - 3b_4^o$
13	x(13,13)	$0.5H_o - 8/3.D + 1.25A + 2b_4^o$
14	x(14,14)	$0.5H_o - 8/3.D + 0.75A + 2b_4^o$
15	x(15,15)	$0.5H_o - 8/3.D + 0.25A + 2b_4^o$
16	x(16,16)	$0.5H_o - 8/3.D - 0.25A + 2b_4^o$
17	x(17,17)	$0.5H_o - 8/3.D - 0.75A + 2b_4^o$
18	x(18,18)	$0.5H_o - 8/3.D - 1.25A + 2b_4^o$
19	x(19,19)	$-0.5H_o - 8/3.D - 1.25A + 2b_4^o$
20	x(20,20)	$-0.5H_o - 8/3.D - 0.75A + 2b_4^o$

TABLE 3.2 (CONTINUED)

Numbered square	Matrix Element	Value
21	x(21,21)	$-0.5H_o - 8/3.D - 0.25A + 2b_4^o$
22	x(22,22)	$-0.5H_o - 8/3.D + 0.25A + 2b_4^o$
23	x(23,23)	$-0.5H_o - 8/3.D + 0.75A + 2b_4^o$
24	x(24,24)	$-0.5H_o - 8/3.D + 1.25A + 2b_4^o$
25	x(25,25)	$-1.5H_o - 2/3.D - 3.75A - 3b_4^o$
26	x(26,26)	$-1.5H_o - 2/3.D - 2.25A - 3b_4^o$
27	x(27,27)	$-1.5H_o - 2/3.D - 0.75A - 3b_4^o$
28	x(28,28)	$-1.5H_o - 2/3.D + 0.75A - 3b_4^o$
29	x(29,29)	$-1.5H_o - 2/3.D + 2.25A - 3b_4^o$
30	x(30,30)	$-1.5H_o - 2/3.D + 3.75A - 3b_4^o$
31	x(31,31)	$-2.5H_o + 10/3.D - 6.25A + b_4^o$
32	x(32,32)	$-2.5H_o + 10/3.D - 3.75A + b_4^o$
33	x(33,33)	$-2.5H_o + 10/3.D - 1.25A + b_4^o$
34	x(34,34)	$-2.5H_o + 10/3.D + 1.25A + b_4^o$
35	x(35,35)	$-2.5H_o + 10/3.D + 3.75A + b_4^o$
36	x(36,36)	$-2.5H_o + 10/3.D + 6.25A + b_4^o$
Off-diagonal elements in (B + C) 37-61		
37	x(7,2)	$1.25(B + C)$
38	x(8,3)	$1.25(B + C)\sqrt{40}$
39	x(9,4)	$1.25(B + C)\sqrt{45}$
40	x(10,5)	$1.25(B + C)\sqrt{40}$
41	x(11,6)	$1.25(B + C)$
42	x(13,8)	$1.25(B + C)\sqrt{40}$
43	x(14,9)	$2(B + C)$

TABLE 3.2 (CONTINUED)

Numbered square	Matrix Element	Value
44	x(15,10)	$1.25(B + C)\sqrt{72}$
45	x(16,11)	$2(B + C)$
46	x(17,12)	$1.25(B + C)\sqrt{40}$
47	x(19,14)	$1.25(B + C)\sqrt{45}$
48	x(20,15)	$1.25(B + C)\sqrt{72}$
49	x(21,16)	$2.25(B + C)$
50	x(22,17)	$1.25(B + C)\sqrt{72}$
51	x(23,18)	$1.25(B + C)\sqrt{45}$
52	x(25,20)	$1.25(B + C)\sqrt{40}$
53	x(26,21)	$2(B + C)$
54	x(27,22)	$1.25(B + C)\sqrt{72}$
55	x(28,23)	$2(B + C)$
56	x(29,24)	$1.25(B + C)\sqrt{40}$
57	x(31,26)	$1.25(B + C)$
58	x(32,27)	$1.25(B + C)\sqrt{40}$
59	x(33,28)	$1.25(B + C)\sqrt{45}$
60	x(34,29)	$1.25(B + C)\sqrt{40}$
61	x(35,30)	$1.25(B + C)$
	Off-diagonal elements in (B - C) 62-86	
62	x(8,1)	$1.25(B - C)$
63	x(9,2)	$1.25(B - C)\sqrt{40}$
64	x(10,3)	$1.25(B - C)\sqrt{45}$
65	x(11,4)	$1.25(B - C)\sqrt{40}$
66	x(12,5)	$1.25(B - C)$
67	x(14,7)	$1.25(B - C)\sqrt{40}$
68	x(15,8)	$1.25(B - C)$
69	x(16,9)	$1.25(B - C)\sqrt{72}$
70	x(17,10)	$1.25(B - C)$
71	x(18,11)	$1.25(B - C)\sqrt{40}$

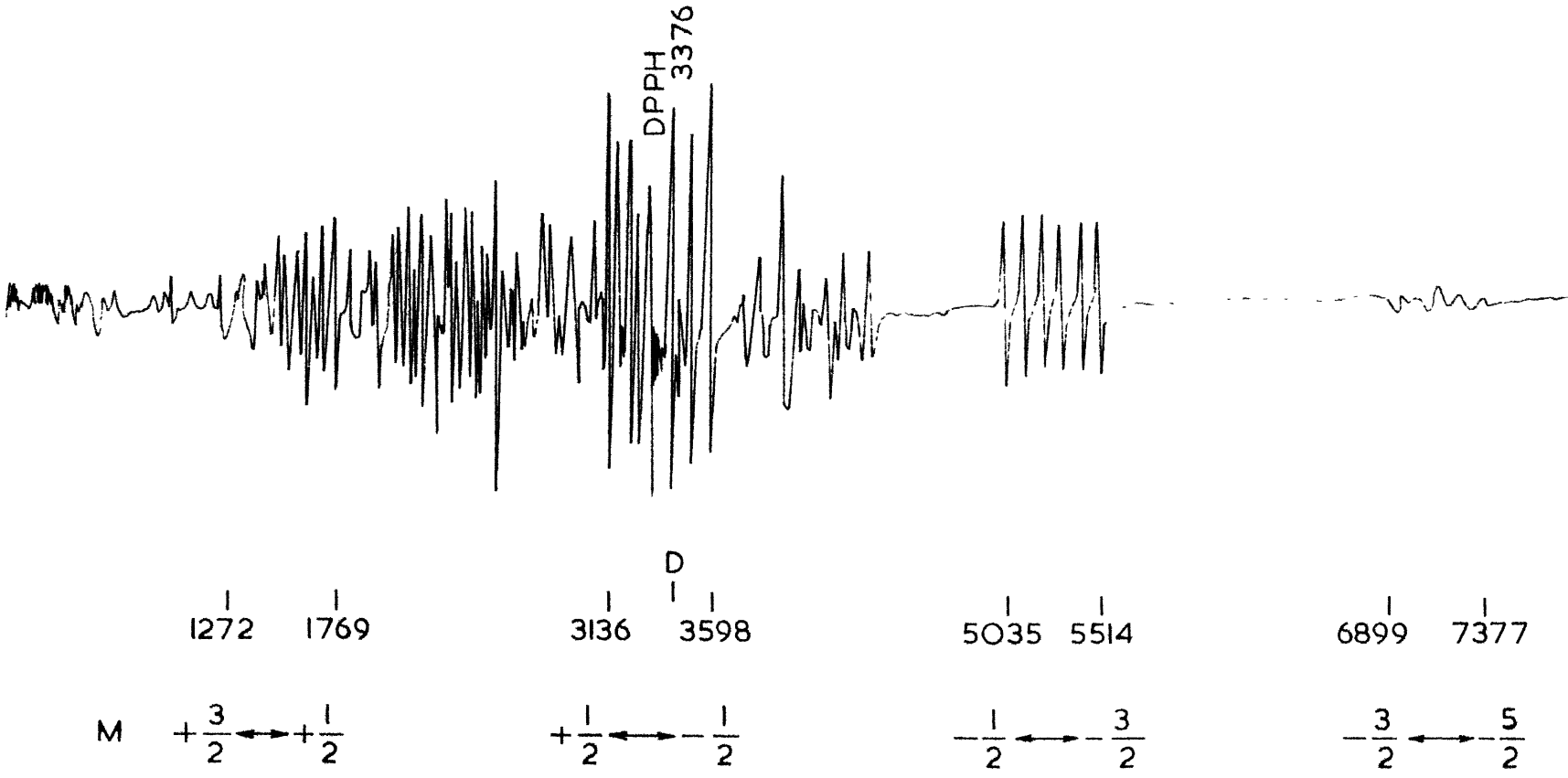

FIG.3.2 EPR SPECTRUM OF Mn^{2+} IN Cs_2SO_4 SINGLE CRYSTAL AT ROOM TEMPERATURE (20°C). THE DIRECTION OF THE MAGNETIC FIELD IS MAKING 25° WITH THE b AXIS OF THE CRYSTAL IN ab PLANE H// TO Z AXIS. DPPH IS THE FIELD MARKER. NUMBERS INDICATE FIELD VALUES IN OERSTED

TABLE 3.2 (CONTINUED)

Numbered square	Matrix Element	Value
98	x(24,12)	$3\sqrt{2}E - \sqrt{2}/4.b_4^2$
99	x(25,13)	$3\sqrt{2}E - \sqrt{2}/4.b_4^2$
A	x(26,14)	$3\sqrt{2}E - \sqrt{2}/4.b_4^2$
B	x(27,15)	$3\sqrt{2}E - \sqrt{2}/4.b_4^2$
C	x(28,16)	$3\sqrt{2}E - \sqrt{2}/4.b_4^2$
D	x(29,17)	$3\sqrt{2}E - \sqrt{2}/4.b_4^2$
E	x(30,18)	$3\sqrt{2}E - \sqrt{2}/4.b_4^2$
F	x(31,19)	$\sqrt{10}E + \sqrt{10}/20.b_4^2$
G	x(32,20)	$\sqrt{10}E + \sqrt{10}/20.b_4^2$
H	x(33,21)	$\sqrt{10}E + \sqrt{10}/20.b_4^2$
I	x(34,22)	$\sqrt{10}E + \sqrt{10}/20.b_4^2$
J	x(35,23)	$\sqrt{10}E + \sqrt{10}/20.b_4^2$
K	x(36,24)	$\sqrt{10}E + \sqrt{10}/20.b_4^2$
	Off-diagonal elements in b_4^4	
L	x(25,1)	$b_4^4/\sqrt{5}$
M	x(26,2)	"
N	x(27,3)	"
O	x(28,4)	"
P	x(29,5)	"
Q	x(30,6)	"
R	x(31,7)	"
S	x(32,8)	"
T	x(33,9)	"
U	x(34,10)	"
V	x(35,11)	"
W	x(36,12)	"

3.5 RESULTS AND DISCUSSION

Angular variation studies when the magnetic field is swept in the ab plane with the c-axis of the crystal as rotation axis indicate the existence of four distinct spectra over a 180°-scan. These spectra can be grouped into two categories:

(i) two identical spectra which have been obtained when the magnetic field is making an angle of 25° with the b axis of the crystal on either side of it. Each one of them has been identified as the z-axis of the complex;

(ii) two identical spectra which have been obtained when the magnetic field is making an angle of 65° with the b-axis of the crystal on either side of it, each one of them having been identified as the y-axis of the complex.

Angular variation studies by rotating the magnetic field in the bc plane with the shortest axis a of the crystal as the rotation axis gave a clear, well-spread spectrum when the magnetic field is parallel to the c axis of the crystal. This has been identified as the x-axis of the complex which has its z and y axes in the ab plane.

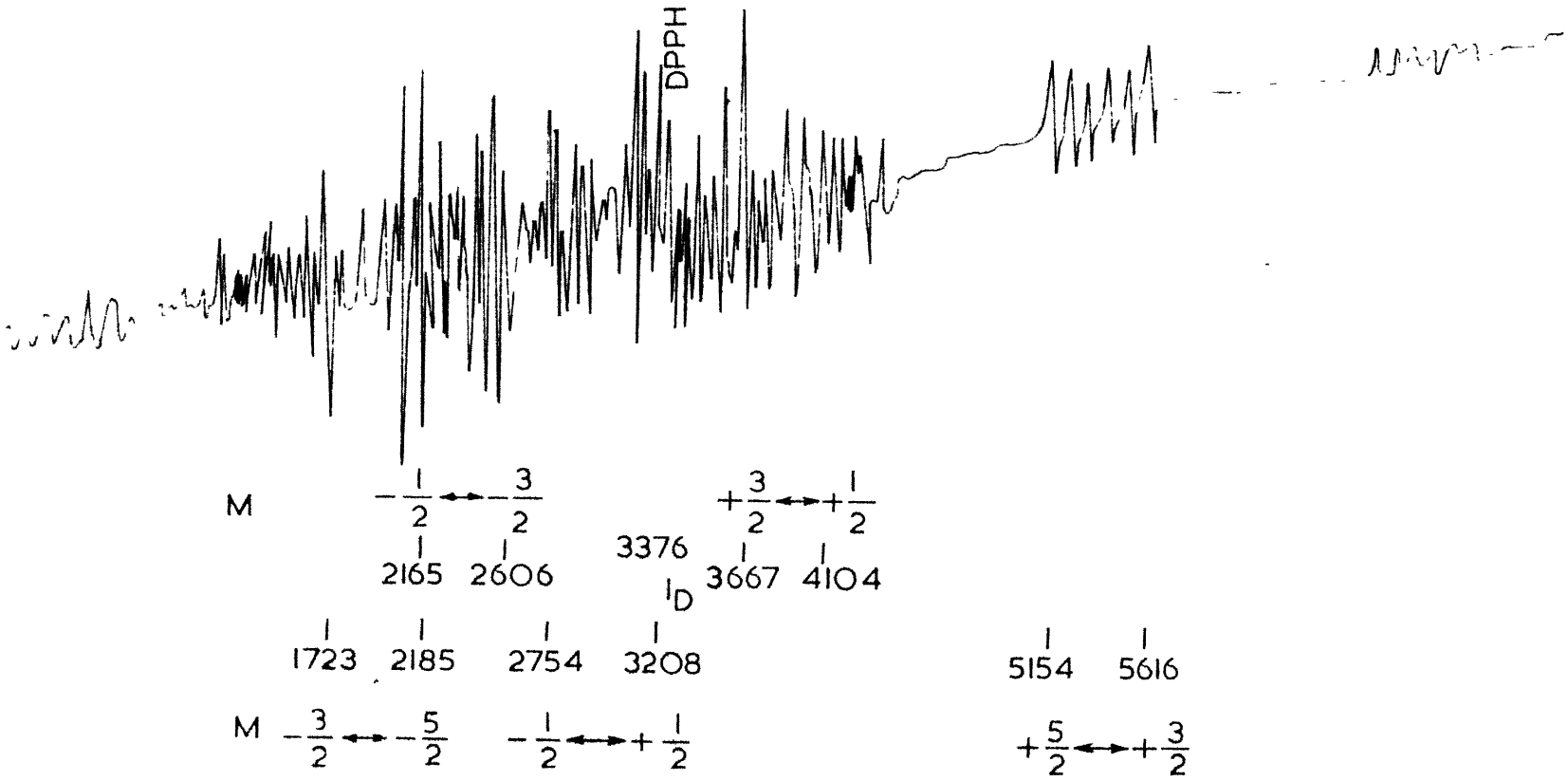

FIG·3·3 EPR SPECTRUM OF $Mn^{2+}:Cs_2SO_4$ SINGLE CRYSTAL AT ROOM TEMPERATURE.(20°C) THE DIRECTION OF MAGNETIC FIELD IS 65° TO THE b-AXIS OF THE CRYSTAL IN THE ab PLANE H// TO Y-AXIS. DPPH IS THE FIELD MARKER. NUMBERS INDICATE FIELD VALUES IN OERSTED.

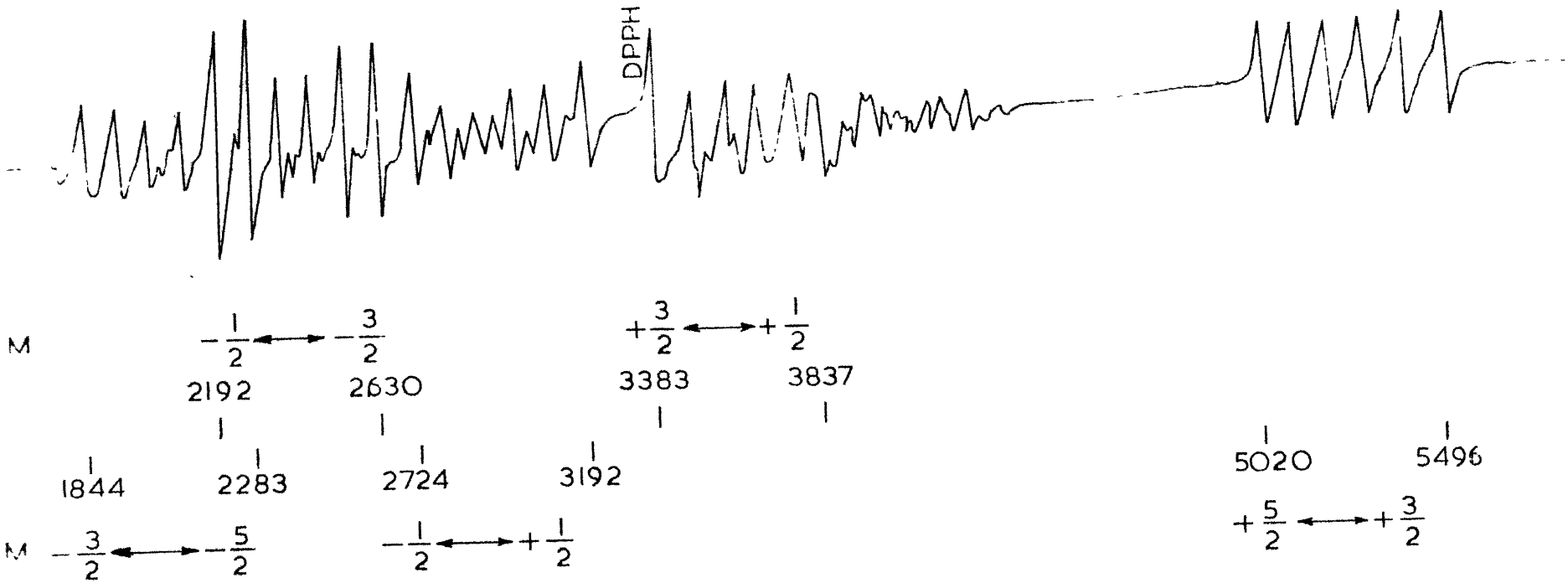

FIG·3·4 EPR SPECTRUM OF Mn^{2+} IN Cs_2SO_4 SINGLE CRYSTAL AT ROOM TEMPERATURE (20°C). THE DIRECTION OF MAGNETIC FIELD IS PARALLEL TO THE C - AXIS OF THE CRYSTAL IN THE ac PLANE. H// TO X-AXIS. NUMBERS INDICATE FIELD VALUES IN OERSTED

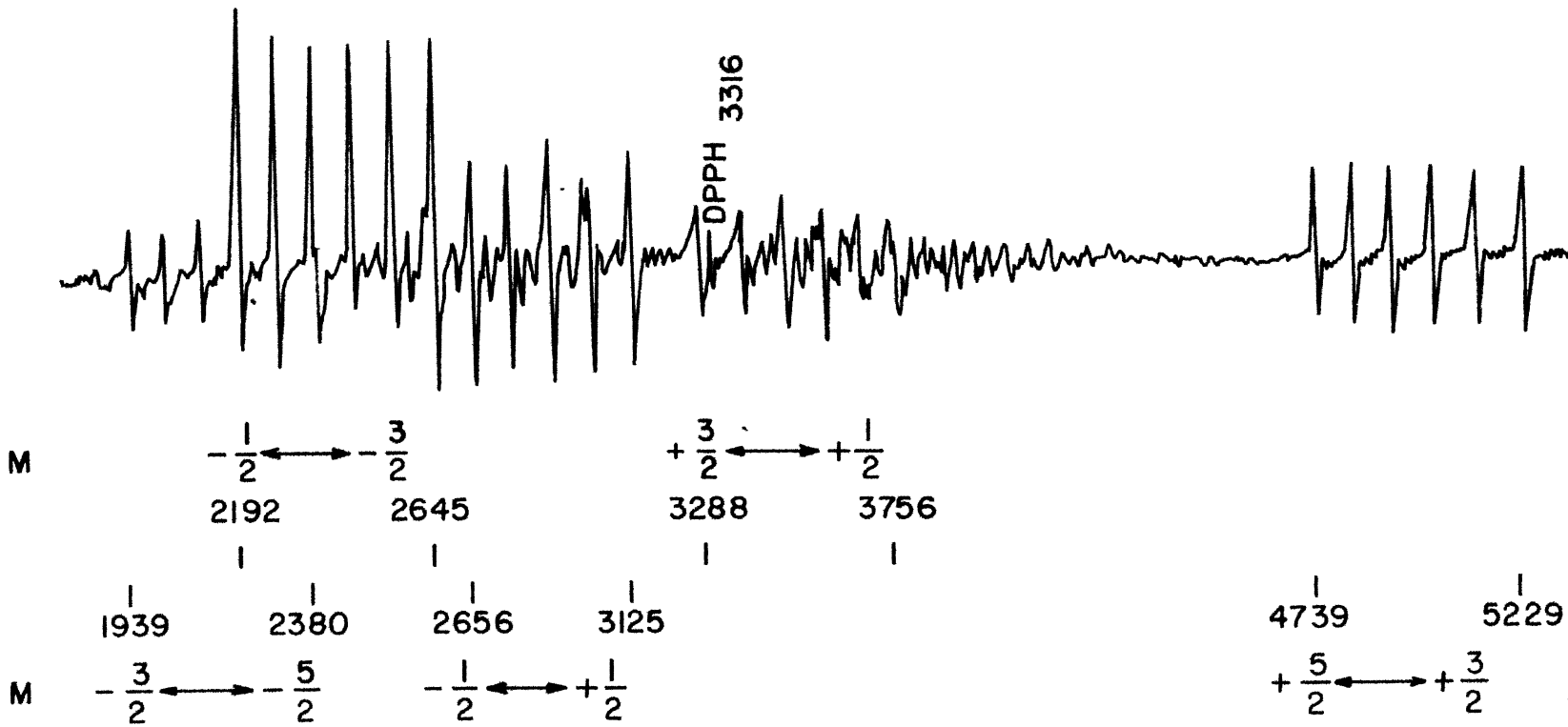

FIG. 3·6. EPR SPECTRUM OF Mn^{2+} IN Cs_2SO_4 SINGLE CRYSTA AT 77 °K. THE DIRECTION OF MAGNE FIELD IS PARALLEL TO THE C-AXIS OF THE CRYSTAL IN bc PLANE.

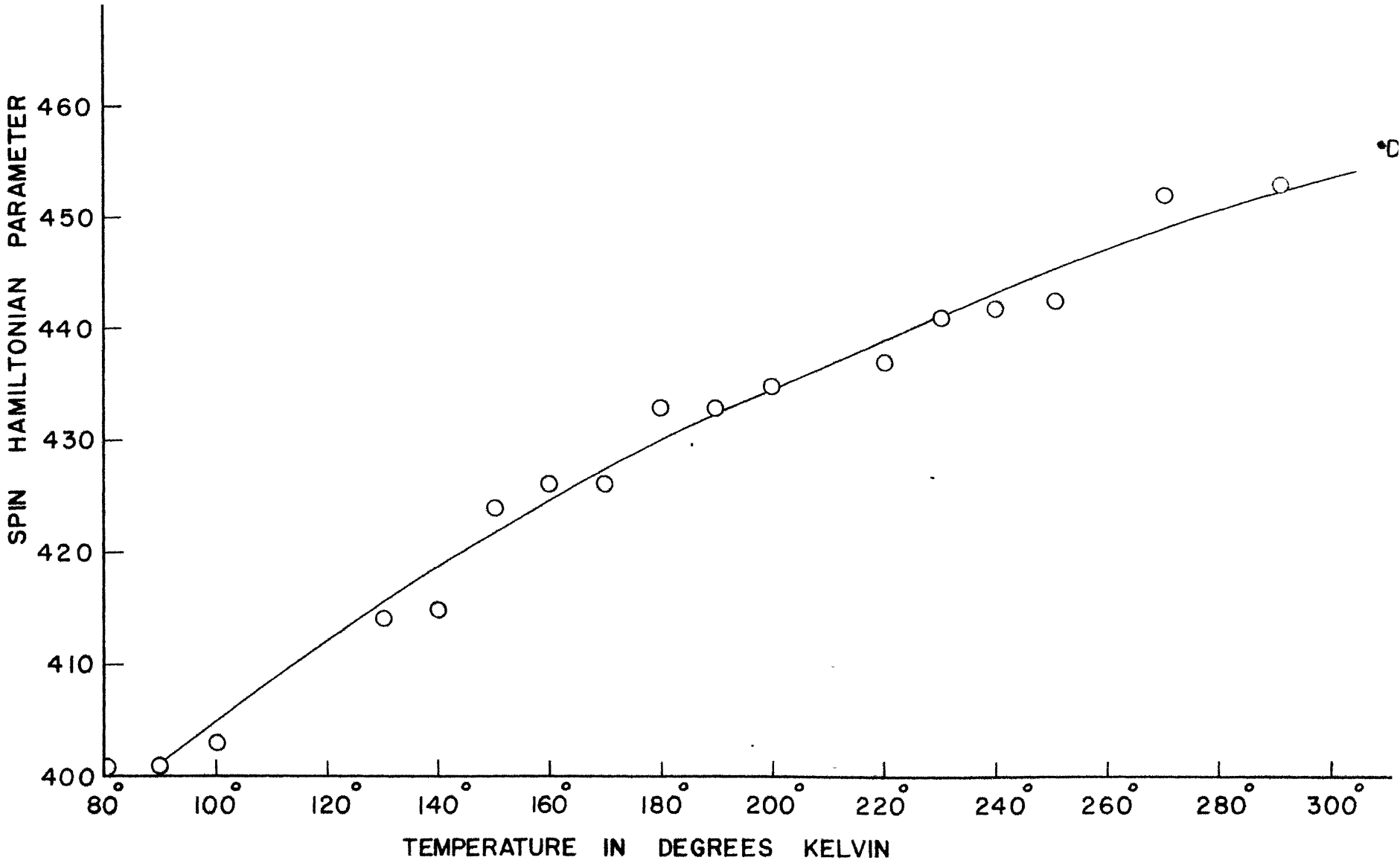

FIG.3·7 .TEMPERATURE VARIATION OF SPIN HAMILTONIAN PARAMETERS D AND E IN THE RANG

300°K TO 77°K FOR THE Cs_2SO_4: Mn^{2+} SINGLE CRYSTAL FOR THE OBSERVED β

strains which may tilt the paramagnetic axis as found by Bronstein and Maniv[17] in melt-grown crystals.

3.6 ANALYSIS OF THE SPECTRA

All the three spectra of the complex with H$\|$z, H$\|$y and H$\|$x axes have been analysed at room temperature by the spin-Hamiltonian method. One of these with H$\|$x axis has been further analysed at 10^{o} intervals between 77 ^{o}K and 300 ^{o}K and the spin-Hamiltonian parameters have been determined at various temperatures within this range.

The procedure which has been adopted for analysis is as follows: the three spectra relevent to the complex are examined. By inspection the M-values are assigned to each of the well-defined sextets. Assuming A's to be negative[18], the relative sign of D and the sequence of M and m are determined by comparing the separation between the extreme hyperfine components of fine structure groups in high and low fields[19]. In the present case D is found to be negative, that is, has the same sign as A. Approximate values for the components of hyperfine tensor A,B, and C are obtained from the high field sextet specially taken with a low sweep rate of the magnetic field of about 0.4 kilooersted per minute. The first and the sixth lines of each transition fixed the position of the fine structure line. Using these fields the parameters have been found by a least square analysis with the help

of equations (3.2). Then the field values corresponding to the thirty lines have been utilised and the terms (3.2a) and (3.2b) are added to equations (3.2) and the process is repeated to get the parameters. For the spectrum which has a large effective value of D,(that is, for the spectrum with H$\|$z axis), the very low field transitions cannot be obtained with an x-band spectrometer. For this case a computer program is written for an IBM computer to diagonalise the relevant 36x36 energy matrix. The approximate parameters obtained have been used in the usual transformation relations[20] to get the values of D* and E* which served as input parameters. They are varied until the calculated values compared favourably with the experimental values for a least-square fit. Thus to avoid inaccuracies inherent in second order perturbation formulae and to get the probable low-field values at x-band frequencies the D parameter obtained by diagonalising the energy matrix corresponding to the largest spread spectrum has been taken to be correct. For the value of E the effective values of D* as obtained by the x and y axes spectra are taken as guide lines. The effective E* values of the x and y axes together with D* values serve to fix the parameters D and E ultimately. This is particularly necessary as small variations in E have great influence on the parameters obtained in x and y directions. In principle it is

possible to minimise the parameters to get the agreement between the observed and the calculated values by utilising the relations (3.2) to within 10 oersted which is the order of line width in the present case. The minimised value of H_o is utilised for calculating the corresponding g-value of the spectrum. However, to obtain the correlation among the spectra taken along the three axes z,x, and y as determined by the transformation relations[20] given in Table (3.1), values of the parameters which are slightly different from the minimised values are taken (at the risk of increasing the standard deviation between the experimental and calculated values). This procedure served as an additional check on the preliminary assignments made and enabled to sort out the lines in question from the angular parts. This method is a sophisticated version of that followed by Bronstein and Maniv[17] who tried different assignments of the transitions to obtain the expected relation between the parameters D* and E* in the spin-Hamiltonian. Table (3.3) gives the observed and calculated fields at resonance for the fine structure positions only while tables (3.4), (3.5), and (3.6) give the observed and calculated fields at resonance for the entire spectrum of thirty lines for the three spectra with the input parameters as indicated in each case. The main analysis of the observed complex is contained in these tables. Table (3.7) gives

TABLE 3.3

Influence of the Parameters b_4^0 and b_4^2 on Resonant Field Values (Fine Structure)*

Designation	With b_4^0 and b_4^2					Without b_4^0 and b_4^2		
	Experimental Oe	Calculated Oe	b_4^0 Oe	b_4^2 Oe	Standard deviation	Experimental Oe	Calculated	Standard deviation
Spectrum z D=-941 E=-14 H_o = 3383 Oe g_z= 1.9995	7138	7147	0	13	13	7138	7147	13
	5275	5264				5275	5264	
	3367	3384				3367	3384	
	1521	1503				1521	1503	
	-383	-383				-383	-383	
Spectrum y D*=496 E*=-461 H_o^*= 3366 Oe g_y= 2.0096	1954	1923	-18	7	22	1954	1854	78
	2386	2357				2386	2448	
	2982	3001				2982	2996	
	3886	3876				3886	3787	
	5385	5394				5385	5469	
Spectrum x D*=452 E*=475 H_o^*= 3357 Oe g_x= 2.0149	2064	2039	-8	-45	23	2064	2026	44
	2411	2431				2411	2481	
	2958	2955				2958	2917	
	3610	3648				3610	3617	
	5258	5247				5258	5298	

* Least square fit using Equations 3.2(a).

TABLE 3.4

The Lines of $Mn^{2+}:Cs_2SO_4$ at Room Temperature 20 °C

H ∥ z-axis of the complex
(All values in Oersted)

DPPH[a] 3376

Line	+5/2 ↔ +3/2		+3/2 ↔ +½		+½ ↔ -½		-½ ↔ -3/2		-3/2 ↔ -5/2	
	Observed	calculated	Observed	calculated	Observed	calculated	Observed	calculated	Observed	calculated
	X	-612	1272	1271	3136	3150	5035	5032	6899	6914
	X	-520	1384	1384	3230	3243	5137	5125	7019	7007
	X	-427	1478	1456	3325	3336	5231	5218	7104	7100
	X	-334	1563	1549	3410	3429	5317	5311	7189	7193
	X	-241	1666	1642	3496	3523	5419	5404	7292	7286
	X	-148	1769	1735	3598	3616	5514	5497	7377	7379

X Not observed at x-band; [a]Diphenylpicrylhydrazyl Standard deviation 16

Input parameters (for 36x36 Energy Matrix):

$A_z(\equiv A)=-93$ $A_x(\equiv B)=-91$ $A_y(\equiv C)=-91$

$H_{oz}=3383$ ($g_z=1.9995$); D=-941; E=-14; $b_4^0=0$; $b_4^2=13$; $b_4^4=-77$

TABLE 3.5

The Lines of $Mn^{2+}:Cs_2SO_4$ at Room Temperature 20 °C

H ∥ y-axis of the complex
(All values in Oersted)

DPPH[a] 3376

Line	-3/2 ↔ -5/2		-½ ↔ -3/2		-½ ↔ +½		+½ ↔ +3/2		+3/2 ↔ +5/2	
	Observed	calculated	Observed	calculated	Observed	calculated	Observed	calculated	Observed	calculated
	1723	1703	2165	2129	2754	2771	3667	3639	5154	5152
	1819	1784	2258	2213	2846	2857	3752	3728	5246	5243
	1920	1867	2350	2299	2932	2946	3834	3819	5338	5337
	2025	1953	2446	2387	3024	3037	3922	3912	5430	5433
	2093	2042	2555	2478	3116	3130	4010	4008	5512	5531
	2185	2133	2606	2572	3208	3226	4104	4107	5616	5633

Standard deviation 34 [a]Diphenylpicrylhydrazyl

Input parameters (for second order perturbation equations 3.2(a)):

$A_y(\equiv C)=-91$; $A_z(\equiv A)=-93$; $A_x(\equiv B)=-91$

$H_{oy}=3366$ ($g_y=2.00955$); $D_y=496.5$; $E_y=-461$; $(b_4^0)_y=-18$; $(b_4^2)_y=7$

the values of the parameters obtained at 77 ^{o}K.

3.7 SUMMARY

The paramagnetic resonance of divalent manganese doped in caesium sulphate single crystals has been studied. A complex has been identified and a vacancy complex model has been proposed. The spectra have been obtained and analysed in all the three principal directions of g-tensor at room temperature, (~20 ^{o}C). One of the spectra is also analysed at liquid nitrogen temperature. In this temperature range of approximately 220^{o} the rhombic field parameter $(E^*)_x$ has decreased from 487 oersted to 470 oersted and the axial field parameter $(D^*)_x$ has decreased from 453 oersted to 401 oersted as the temperature is lowered. The variations are smooth and no detectable changes in the spectral features occured to suggest a phase transformation of either kind as has been indicated in the case of isomorphous K_2SO_4 crystals[3].

The spin-Hamiltonian parameters with deviations as suggested by correlating those obtained from transformed site axes are summarised in Table (3.8). The spectrum is broadly insensitive to the parameter b_4^4 and as such its value is chosen to have consistency in the transformed parameters b_4^{2*} and b_4^{0*}.

TABLE 3.8

Spin Hamiltonian Parameters
for Mn^{2+} in Cs_2SO_4 at Room Temperature

Parameter	Value
g_z	2.000 ± 0.003
g_x	2.015 ± 0.003
g_y	2.000 ± 0.003
$A_z(\equiv A)$ [a]	93 ± 1 Oe
$A_x(\equiv B)$	91 ± 1 Oe
$A_y(\equiv C)$	91 ± 1 Oe
D [b]	941 ± 7 Oe
E	14 ± 3 Oe
b_4^0 (or a/2)	0 ± 1 Oe
b_4^2	13 ± 1 Oe
b_4^4	-77 Oe
ϕ [c]	25° ± 1°

(a) A's are assumed to be negative

(b) The sign of D is relative to A

(c) The angle between the direction of the complex taken as z axis and the longest crystallographic axis.

3.8 General comments on the consistency of the spin-Hamiltonian parameters obtained from the $H \| z$, $H \| y$ and $H \| x$ spectra

The parameters D, E, b_4^0, b_4^2 and b_4^4 given in Table (3.8) are those obtained from the analysis of the spectrum taken with $H \| z$ axis of the complex. The effective values of these parameters in the x and y directions have been obtained from the analysis of the spectra with $H \| y$ and $H \| x$ axes and are listed in Tables (3.5) and (3.6). Expressions showing the relationships between the effective values of the parameters D, E, b_4^0, b_4^2 and b_4^4 along the z, x, and y directions are given in Table (3.1). The first column in Table (3.9) shows the effective values of the parameters along the z direction which are the same as those given in Table (3.4) and also in Table (3.8) and designated D, E, b_4^0, b_4^2 and b_4^4. Column 2 in Table (3.9) shows these parameters calculated using the effective values obtained from the analysis of the spectrum with $H \| x$ along with the necessary relations given in Table (3.1). Similarly column 3 of Table (3.9) shows the parameters derived using the constants obtained from the analysis of the spectrum with $H \| y$ along with the necessary relations given in Table (3.1). The values of the parameters D are consistent within ± 2.5 oersted while those of E are consistent within ± 4 oersted. The magnitude of these deviations can probably be taken as the error

in the determination of the values of the parameters D and E. It is satisfactory to see that these deviations are not large. However, the inconsistencies or deviations can probably be reduced by using expressions involving higher orders of perturbation than used here as the term D in general and the effective values of the term E in the y and z directions have large magnitudes.

As pointed out earlier the parameter obtained from the analysis of the spectrum with H $\|$z are probably taken to be more accurate than those obtained from the other two spectra as the higher order terms in E are the least effective when H is parallel to the z axis of the complex.

It is interesting to note, though alarming in a way, that the deviations in the values of the parameters b_4^0 and b_4^2 in the columns 2,3 and 4 of table (3.9) are as large as the magnitude of their values. This raises a question about the usefulness of keeping these parameters in the present analysis. Table (3.3) shows the magnetic resonance field values (fine structure)calculated with and without the parameters b_4^0 and b_4^2. The observed values are also included in the table for comparison and it can be seen that the standard deviation decreases to some extent when the parameters b_4^0 and b_4^2 are included in the analysis.

3.9 REFERENCES

1. K.N.Shrivastava, Electron Paramagnetic Resonance of Mn^{2+} in Single Crystals, Doctoral Thesis, Indian Institute of Technology, Kanpur, India (1966).
2. G.Chaddha, J.Phys.Soc.Japan,24,976(1968).
3. B.V.R.Chowdari and Putcha Venkateswarlu, J.Chem.Phys 48,318(1968).
4. B.V.R.Chowdari and Putcha Venkateswarlu, Proc.Ind. Acad. of Sciences, 67A, 130(1968).
5. J.G.Chambers, W.R.Datars and C.Calvo, J.Chem.Phys. 41, 806(1964).
6. C.Calvo, J.S.Leung, and W.R.Datars, J.Chem.Phys. 46, 796(1967).
7. A.I.Kaslinskij and V.T.Cecernikov, Acta.Cryst. (Internat.)21,Pt.7,Suppl.A197(1966) Seventh International Congress and Symposium, International Union of Crystallography, Moscow,1966.
8. W.Low and E.L.Offenbacher, Solid State Physics, 17,135,Academic Press (1965).
9. A.Ogg, Phil.Mag.,5,354(1928).
10. A.N.Holden, C.Kittel, F.R.Merritt and W.A.Yager, Phys.Rev.77,147(1950).
11. R.R.Sharma, T.P.Das, and R.Orbach, Phys.Rev.155, 338(1967).
12. R.Orbach, Proc.Roy.Soc.(London) A264,458(1961).
13. V.M.Vinokurov, M.M.Zapirov and V.G.Stepanov, Soviet Phys. Solid State (English Transl.)6, 870(1964).

14. M.T.Hutchings, Solid State Phys.16,227(1964).

15. W.Low, Paramagnetic Resonance in Solids (Academic Press, Inc., New York,(1960) p62.

16. G.D.Watkins, Phys.Rev.113,79(1959).

17. J.Bronstein and S.Maniv, Phys.Rev.153,303(1967).

18. G.E.Pake, PARAMAGNETIC RESONANCE (W.A.Benjamin, Inc., New York, 1962).

19. W.Low, Solid State Physics. Suppl.2,71(1960).

20. Daniel Schechter, Bell Telephone and Electronic Laboratories Inc., Technical Memorandum 125.3, September 14,(1961).

CHAPTER IV

ELECTRON PARAMAGNETIC RESONANCE STUDIES OF VO^{2+} IN SINGLE CRYSTALS OF CAESIUM SULPHATE †

† A preliminary account of the work was reported at the Nuclear Physics and Solid State Physics Symposium held at I.I.T., Powai, Bombay during December 1968.

ABSTRACT

The electron paramagnetic resonance of VO^{2+} doped in caesium sulphate single crystals has been studied in three crystallographic planes. The spectrum obtained is somewhat complicated. A tentative analysis of the spectrum suggests that the VO^{2+} ions substitute the α-Cs^{+} ions. The V-O bond has been found to have three preferential directions: one along the c-axis of the crystal, one in a direction making an angle of 30° with the c-axis in the bc plane and yet another making an angle of 9° with the a-axis in the ab-plane. These directions are the directions of nearest approach from the position of α-Cs^{+} to the neighbouring oxygens. Optical absorption studies confirm the formation and existence of VO^{2+} ion in the crystal.

magnetic field H. The units of H, H_o, K, A, B and C are in gauss or oersted. The A,B and C of equation 4.1 are obtained by dividing those of the Hamiltonian by $g\beta$.

The EPR spectrum taken at any general orientation furnishes the effective g-value, g_{eff}. The square of the g-value can be expressed as[12]

$$g^2 = \sum_{i,j=1}^{3} \tilde{A}_{ij} l_i l_j \qquad (A_{ij} = A_{ji}) \quad .. \quad (4.2)$$

So, for the general case of canted axes, the principal values of $\tilde{\underline{g}}$ and $\tilde{A}$ tensors can be determined by measuring g_{eff} at several angles θ in the three principal crystallographic planes[13,14]. If ϕ_x is the angle made by H with the crystallographic y-axis when the plane of rotation is the yz plane, and if ϕ_y, ϕ_z represent the analogous angles for the rotations respectively in zx and xy planes, we have,

yz plane:

$$g_{eff}^2 = (\underline{g}^2)_{yy}\cos^2\phi_x + (\underline{g}^2)_{zz}\sin^2\phi_x + 2(\underline{g}^2)_{yz}\cos\phi_x\sin\phi_x$$

zx plane:

$$g_{eff}^2 = (\underline{g}^2)_{zz}\cos^2\phi_y + (\underline{g}^2)_{xx}\sin^2\phi_y + 2(\underline{g}^2)_{zx}\cos\phi_y\sin\phi_y$$

xy plane:

$$g^2_{eff} = (\underline{g}^2)_{xx} \cos^2\phi_z + (\underline{g}^2)_{yy} \sin\phi_z + 2(\underline{g}^2)_{xy} \cos\phi_z \sin\phi_z \quad .. \quad (4.3)$$

Here $(g^2)_{ij}$, i and j taking values from 1 to 3, are the elements of the g^2-tensor. The principal g-values are found by diagonalising the matrix $\underline{\tilde{A}}$,(not given explicitly, equation 4.2), which is formed using the relations (4.3) or the equivalent form

$$g^2 = \alpha + \beta \cos 2\theta + \gamma \sin 2\theta \quad .. \quad (4.4)$$

where α , β and γ are found by a least-square fit of the experimental data. The sign of the off-diagonal elements is to be determined from a g^2-θ plot and noting the position of maxima and minima with respect to the reference axes.

4.3 EXPERIMENTAL PROCEDURE

Single crystals of caesium sulphate containing small concentration of vanadyl ion are grown by slow evaporation of aqueous solution of caesium sulphate of E.Merck, analar quality, with an initial concentration of 0.5 mol percent of vanadyl sulphate. Well developed, rectangular, boat-shaped crystals have been obtained the sizes varying from one centimeter to a few millimeters in length. Spectrophotometric analysis of the experimental

crystal yielded 300 ppm of vanadium. Optical absorption measurements were done on a Cary-14 spectrophotometer. The remaining experimental details are the same as those discussed in chapter III.

4.4 RESULTS AND DISCUSSION

The structure of caesium sulphate with the metal oxygen directions marked in the bc and ac planes is shown in Figs. 4.1(a) and 4.2(b) respectively. The positional coordinates of the atoms are listed by Ogg.[15] The Cs^+ ions and two of the oxygens of the sulphate group lie in the bc plane. Depending upon the oxygen environment the Cs^+ ions are divided[15] into two types α and β. Considering an α-Cs^+ ion, there is an oxygen atom along the c-axis at a distance of 3.1 Å. Another oxygen atom is at an angle of $27^{\circ}36'$ to the c-axis in the bc plane and is at a distance of 3.28 Å. A third oxygen atom is at an angle of $7^{\circ}36'$ to the a-axis in the ab-plane and is at a distance of 3.2 Å. These three oxygen atoms are designated in this work as I, II and III respectively, Fig.(4.1).

Angular variation of the EPR spectra of VO^{2+} in Cs_2SO_4 is carried out in the three crystallographic planes, viz., ab, bc and ca of the crystal. The spectra obtained in different important directions are shown in Figures 4.2 — 4.6. Three complexes which are magnetically inequivalent are found to exist. The spectrum of complex I

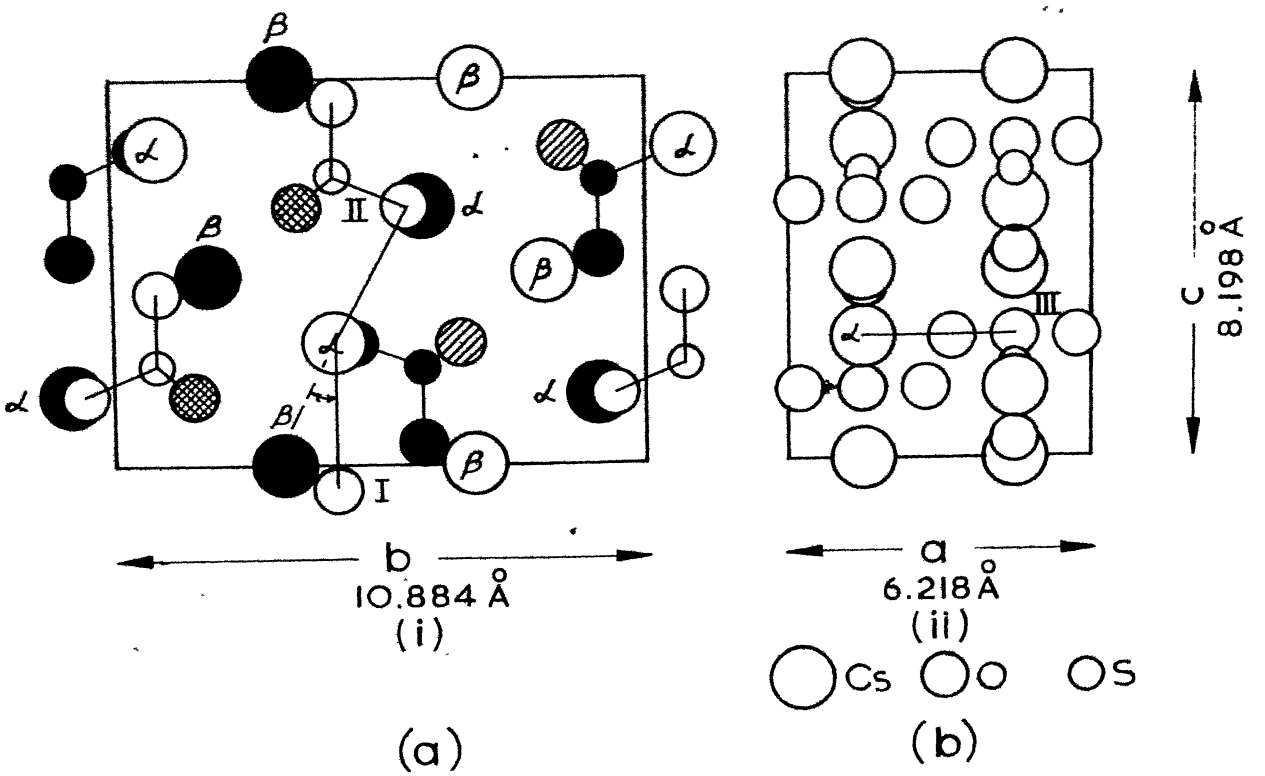

FIG. 4.1 - PROJECTION OF ATOMS OF CAESIUM SULPHATE CRYSTAL IN bc AND ac PLANES

$Cs_{\alpha} - O_{I}$ COMPLEX I ALONG THE c-AXIS

$Cs_{\alpha} - O_{II}$ COMPLEX II AT ANGLE OF 30° TO c-AXIS

$Cs_{\alpha} - O_{III}$ COMPLEX III ALONG a-AXIS

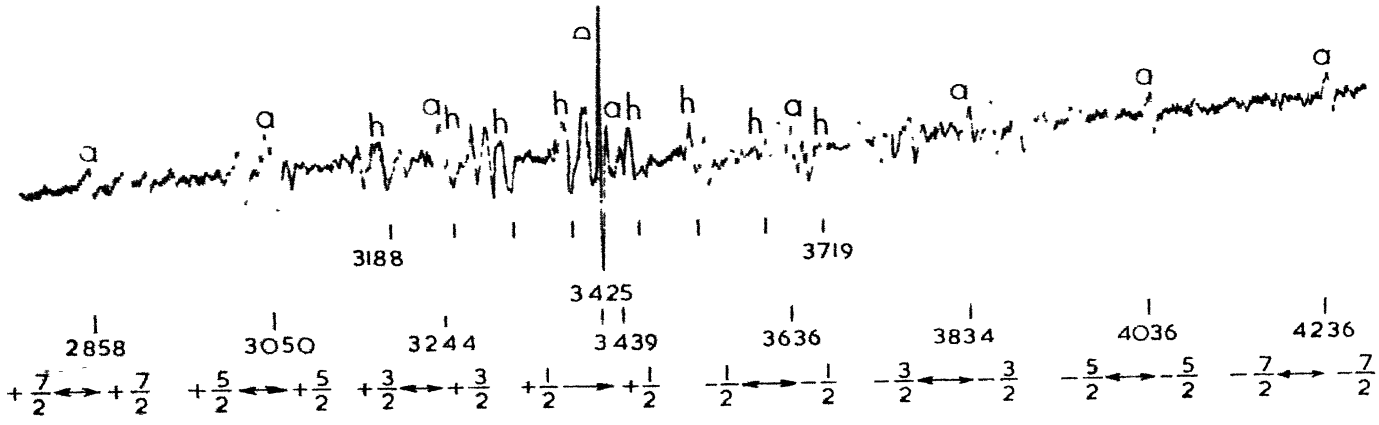

FIG. 4.2 EPR SPECTRUM OF VO^{++} IN CS_2SO_4 SINGLE CRYSTAL AT ROOM TEMPERATURE. H//C (b-AXIS VERTICAL) a'S REFER TO I_Z, h'S REFER TO III_X; D IS THE FIELD MARKER FIELD VALUES IN OERSTED.

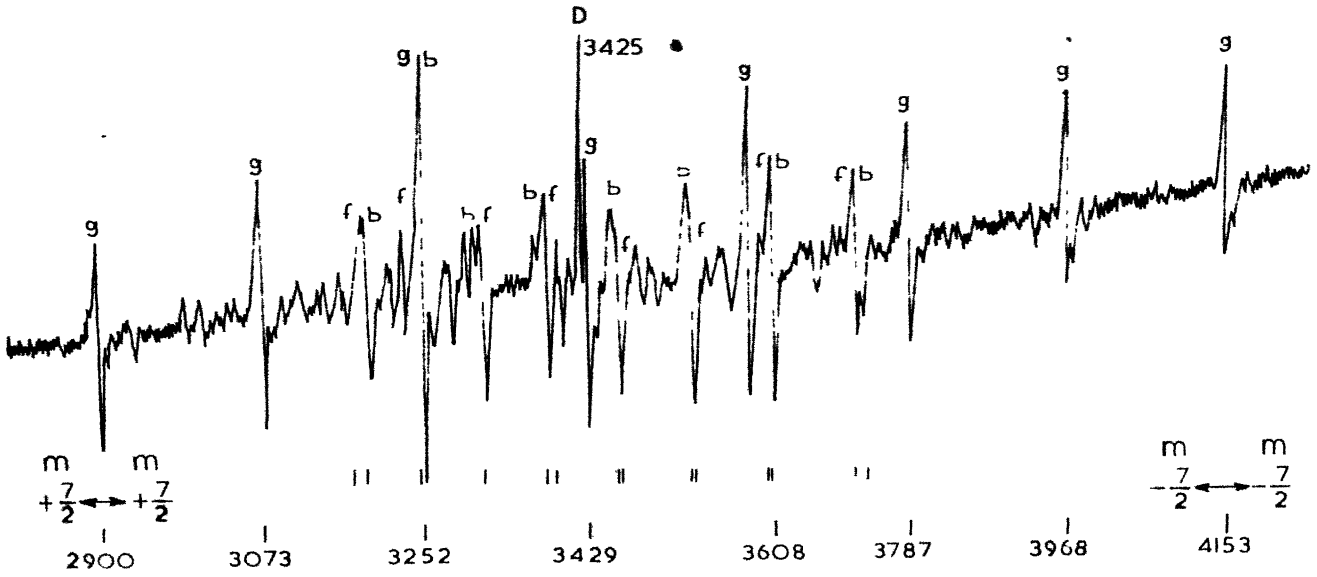

FIG.43 EPR SPECTRUM OF VO^{++} IN CS_2SO_4 SINGLE CRYSTAL AT ROOM TEMPERATURE H||a AXIS (b-AXIS VERTICAL) g'S DENOTE VO III Z-AXIS, b'S DENOTE VO I X-AXIS, f'S DENOTE VO II Y-AXIS, D IS THE FIELD MARKER ALL VALUES ARE IN OERSTED.

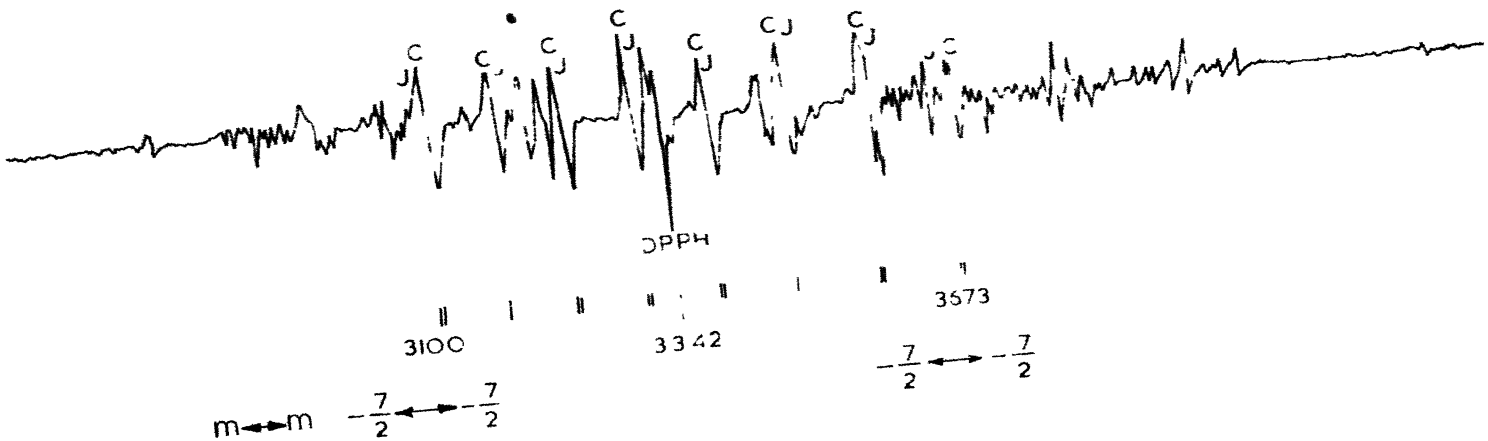

FIG.4.4 EPR SPECTRUM OF VO^{2+} IN CS_2SO_4 SINGLE CRYSTAL AT ROOM TEMPERATURE. H // b-AXIS (c-AXIS VERTICAL) C'S DENOTE I_Y, J'S DENOTE III_Y, DPPH IS THE FIELD MARKER, FIELD VALUES ARE IN OERSTED.

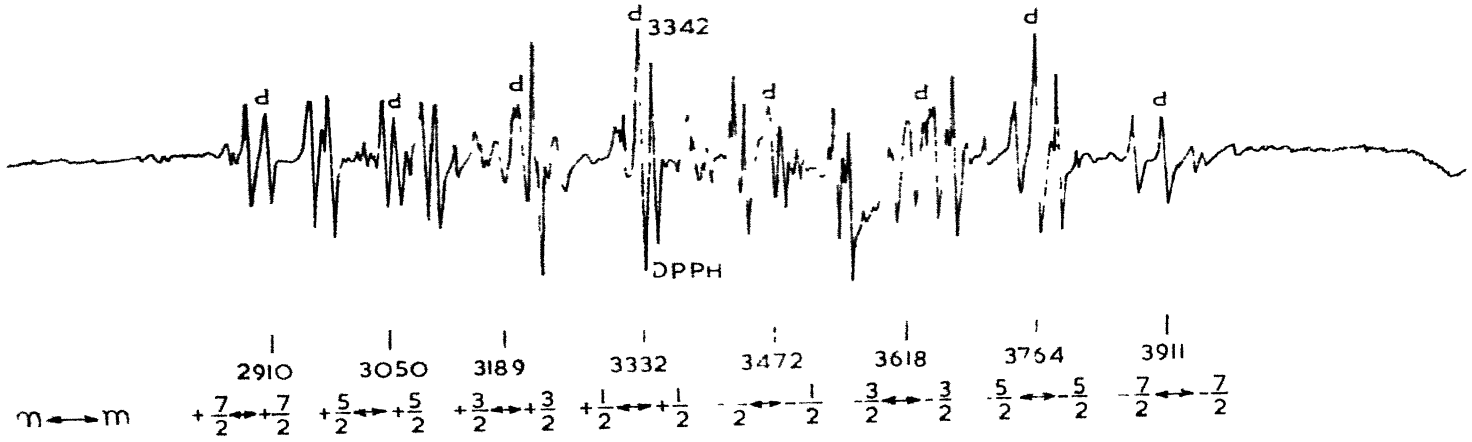

FIG.4.5 EPR SPECTRUM OF VO^{2+} IN CS_2SO_4 SINGLE CRYSTAL AT ROOM TEMPERATURE. H AT AN ANGLE OF 30° TO C-AXIS (a-AXIS VERTICAL) d'S DENOTE II_Z, DPPH IS THE FIELD MARKER FIELD VALUES ARE IN OERSTED

and their direction cosines have been determined by adopting the procedure outlined briefly in section 4.2. The angle which the principal z axis of the g tensor makes with the crystallographic a axis in the ab plane comes out to be $9^{o}6'$ as compared to $7^{o}36'$ calculated from the structural parameters[15]. The acute angles which the other principal components (x and y) of the g-tensor make respectively with the crystallographic b and c axes are found to be $9^{o}6'$ and $8^{o}42'$.

The angular variations of the spectral lines in complexes I, II and III indicate that the principal axes of the g and A tensors coincide in all the complexes.

The z directions of the complexes I, II and III nearly coincide with the directions of nearest approach from the position of α-Cs^{+} to three neighbouring oxygens marked I, II and III in Fig.4.1 and referred to in the earlier part of the chapter. This suggests that the VO^{2+} substitutes the α-Cs^{+} ions and the VO-bonds of the complexes are along the z directions of the respective complexes.

The observed and the calculated magnetic field resonance values are given in Tables 4.1 to 4.3. Calculations for the least square fit are done with the help of an IBM 1620 computer. The spin-Hamiltonian parameters obtained for the different complexes are included in the Tables 4.1 to 4.3 at the appropriate places.

TABLE 4.1

Observed and Calculated Field Values of the Spectrum I

(Result of the least-square fit)
Field values in Oersted

Transition m↔m	Spectrum I_z H||c Fig.4.3 a's		Spectrum I_x H| a Fig.4.4 b's		Spectrum I_y H||b Fig.4.5 c's	
	Observed	Calculated	Observed	Calculated	Observed	Calculated
+7/2 ↔ +7/2	2858	2859	3195	3194	3100	3100
+5/2 ↔ +5/2	3050	3050	3252	3252	3161	3162
+3/2 ↔ +3/2	3244	3244	3318	3316	3228	3230
+½ ↔ +½	3439	3439	3385	3387	3303	3305
-½ ↔ -½	3636	3636	3465	3465	3387	3386
-3/2 ↔ -3/2	3834	3835	3547	3549	3476	3474
-5/2 ↔ -5/2	4036	4035	3640	3640	3568	3569
-7/2 ↔ -7/2	4236	4238	3737	3737	3673	3671
	Standard Deviation Δ =1.2		Standard Deviation Δ =1.2		Standard Deviation Δ =1.4	
	A_z(≡A)=197 Oe		A_x(≡B)=77.5Oe		A_y(≡C)=81.5 Oe	
	H_{oz}=3540.5 Oe		H_{ox}=3437.5 Oe		H_{oy}=3357.0 Oe	
	g_z = 1.9382		g_x = 1.9963		g_y = 1.9947	

TABLE 4.2

Observed and Calculated Field Values
of the Spectrum II
(Result of the least-square fit)
Field values in Oersted

Transition m↔ m	Spectrum II_z H in bc plane 30° to c		Spectrum II_x H in bc plane 120° to c		Spectrum II_y H‖a	
	Fig.4.6 d's		Fig.4.7 e's		Fig.4.4 f's	
	Observed	Calculated	Observed	Calculated	Observed	Calculated
+7/2 ↔ +7/2	2910	2910	3138	3137	3183	3182
+5/2 ↔ +5/2	3050	3049	3192	3191	3248	3248
+3/2 ↔ +3/2	3189	3189	3249	3248	3318	3319
+½ ↔ +½	3332	3330	3309	3310	3393	3392
-½ ↔ -½	3472	3473	3377	3375	3470	3470
-3/2 ↔ -3/2	3618	3618	3444	3445	3551	3551
-5/2 ↔ -5/2	3764	3764	3517	3518	3636	3636
-7/2 ↔ -7/2	3911	3911	3596	3595	3724	3724
	Standard Deviation$^{\Delta}$ =0.9 $A_z(\equiv A)$=143 Oe H_{oz}=3404.5 Oe g_z=1.9669		Standard Deviation$^{\Delta}$=1.0 $A_x(\equiv B)$=65.5 Oe H_{ox}=3349.5 Oe g_x=1.9992		Standard Deviation$^{\Delta}$ =0.6 $A_y(\equiv C)$=77.5 Oe H_{oy}=3437.5 Oe g_y=1.9963	

TABLE 4.3

Observed and Calculated Field Values
of the Spectrum III
(Result of the least-square fit)
Field values in Oersted

Transition m↔m	Spectrum III$_z$ H ∥ a		Spectrum III$_x$ H ∥ c		Spectrum III$_y$ H ∥ b	
	Fig.4.4 g's		Fig.4.3 h's		Fig.4.5 j's	
	Observed	Calculated	Observed	Calculated	Observed	Calculated
+7/2 ↔ +7/2	2900	2901	3188	3188	3096	3095
+5/2 ↔ +5/2	3073	3074	3246	3247	3161	3161
+3/2 ↔ +3/2	3252	3250	3312	3312	3232	3231
+½ ↔ +½	3429	3427	3383	3382	3307	3308
-½ ↔ -½	3608	3606	3459	3458	3391	3390
-3/2 ↔ -3/2	3787	3787	3540	3540	3476	3477
-5/2 ↔ -5/2	3968	3969	3627	3627	3572	3571
-7/2 ↔ -7/2	4153	4154	3719	3720	3669	3669
	Standard Deviation =1.5		Standard Deviation 0.7		Standard Deviation 1.5	
	$A_z(\equiv A)$=179 Oe		$A_x(\equiv B)$=76 Oe		$A_y(\equiv C)$=82 Oe	
	H_{oz}=3519.5 Oe		H_{ox}=3430 Oe		H_{oy}=3358.5 Oe	
	g_z = 1.9498		g_x = 2.0006		g_y = 1.9939	

It may be noted here that for all the complexes A_z is much larger than A_x and A_y. It is also found that the values of g_z are comparatively much smaller than the values of g_x and g_y for all the three complexes. Again, the values of g_x and g_y are nearer to one another in all the complexes, the value of g_x being slightly larger than that of g_y.

From the crystal structure structure data[15] the distances Cs_{α}— O(I), Cs_{α}— O(II) and Cs_{α}— O(III) are respectively 3.1 Å, 3.28 Å and 3.2 Å. The magnitudes of the hyperfine constants (A_z) for the complexes I, II and III are respectively 197, 143 and 179 Oersted. The values of $g_z - g_x$ for complexes I, II and III are respectively 0.0581, 0.0323 and 0.0508. Again, the values of g_z are 1.9382, 1.9669 and 1.9498 respectively for the complexes I, II and III. It is interesting to note that the changes in A_z, $(g_z - g_x)$ or $(g_z - g_y)$ and g_z as we go from complex I to complex III are related to the respective Cs_{α}— O(I, II, III) distances.

In order to fonfirm the formation and existence of VO^{2+} ion in the vanadyl doped Cs_2SO_4 crystal, optical absorption spectrum of the crystal has been recorded. The spectrum obtained is shown in Fig.(4.7). It reveals a broad absorption band with a maximum at about 8000 Å ($12,500\ cm^{-1}$) along with a shoulder at about 6250 Å ($16,000\ cm^{-1}$). This is consistent with the spectrum that one expects for VO^{2+} ion. The VO^{2+} in vanadyl solutions

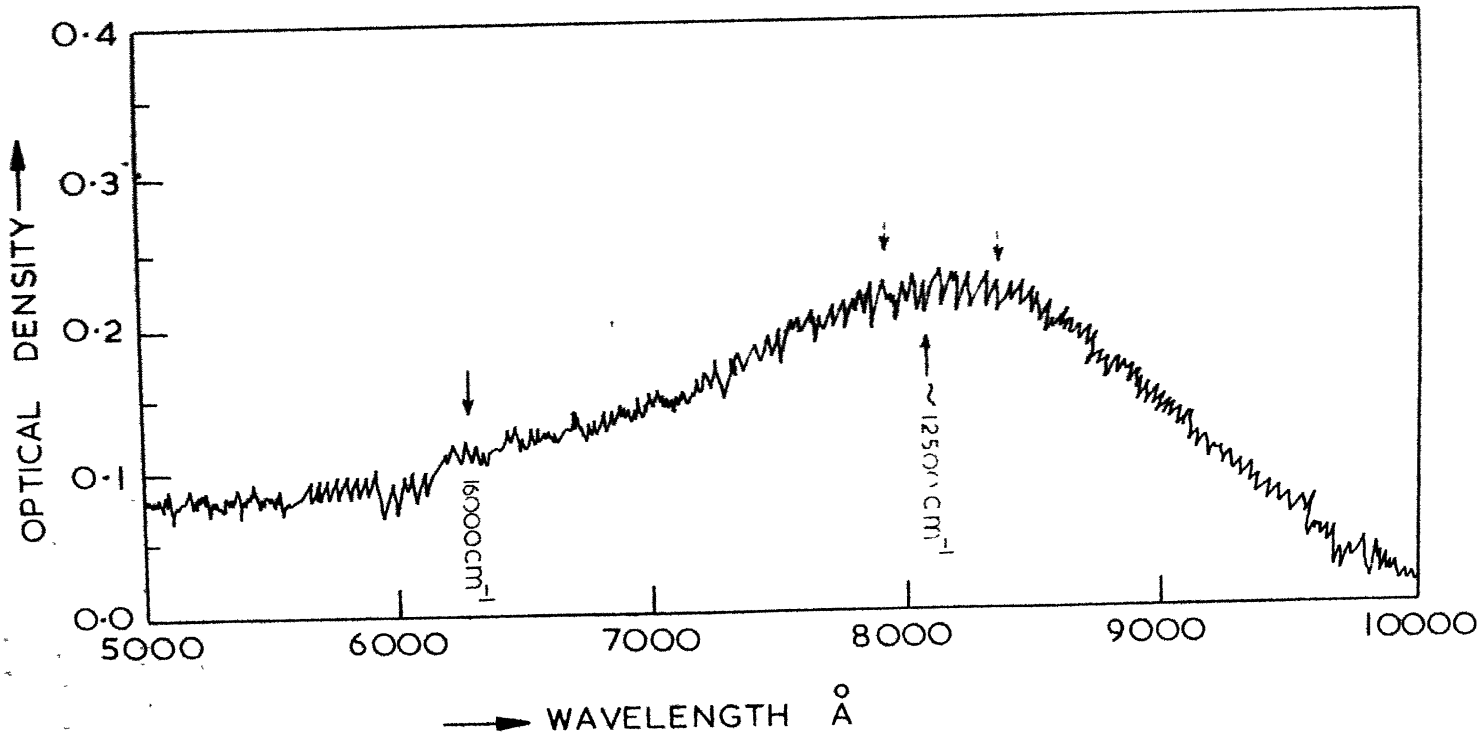

FIG.4.7 OPTICAL ABSORPTION SPECTRUM OF VO^{2+} IN CS_2SO_4 SINGLE CRYSTAL.

is known[16] to give an absorption with a maximum at 13,000 cm^{-1} and a shoulder at 16,000 cm^{-1}. In potassium aluminium (KAl) alum and ammonium aluminium (NH_4Al) alum[6] doped with VO^{2+} absorption bands have been obtained at 13,000 cm^{-1} and 15,700 cm^{-1} while in methyl ammonium gallium (MAG) alum[7] they are at 12,700 cm^{-1} and 15,200 cm^{-1} respectively. The VO^{2+} is known to replace the trivalent metal ion in the alums and form $\left[\underline{VO(H_2O)_5}\right]^{2+}$ with the neighbouring water molecules. Thus VO^{2+} in these crystals appears to have a distorted octahedral coordination. The two absorption bands of VO^{2+} in the visible region in the vanadyl solutions have been interpreted by Jorgensen[17] treating the molecule as a strongly tetragonally distorted octahedron $\left[\underline{VO(H_2O)_5}\right]^{2+}$ and by Furlani[18] by considering only $C_{\infty v}$ point symmetry. Jorgensen interprets the spectrum of VO^{2+} in terms of an energy level diagram[19] shown in Fig.(4.8). The left of the figure shows the effect of an axial tetragonal component appropriate to the d^1 ions while the right of the diagram shows the effect of a square tetragonal component. The observed transitions are thought to be $^2B_2 \rightarrow E$ and $^2B_2 \rightarrow {}^2B_1$. According to Ballhausen[16] the band at 13,000 cm^{-1} is due to the first transition and the one at 16,000 cm^{-1} is due to the second transition.

It is difficult to visualize a tetragonally distorted octahedral coordination for the vanadyl ion at the $\alpha - Cs^+$ site. If it is an octahedral coordination, it must

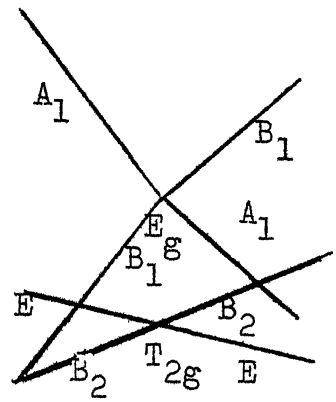

LINEAR CUBIC SQUARE

Fig.4.8. Energy levels of a single d-electron in fields of octahedral and tetragonal symmetry. The right side of the diagram applies to the case in which the polar ligands are farther away (or have a lower charge) than the equatorial ligands of the octahedron The left side is for the opposite case. (From reference 19).

CHAPTER V

ELECTRON PARAMAGNETIC RESONANCE OF Mn^{2+} IN NaF SINGLE CRYSTALS*

* This work has been recently published: A.V.Jagannadham and Putcha Venkateswarlu, Proc.Ind.Acad.Sci.69,67(1969).

ABSTRACT

The electron paramagnetic resonance of Mn^{2+} in NaF single crystals is investigated at different temperatures from 573 °K to 93 °K. Four different spectra designated as I, II, III_2 and III_4 are observed. Spectrum I consists of a single broad resonance corresponding to precipitated Mn^{2+} ions. Spectrum II is isotropic and centred near g=2.00. This spectrum corresponds to substitutional Mn^{2+} ions with remote charge compensati· sites and therefore with local cubic symmetry. Spectrum III_2 with g=2.014 and spectrum III_4 with g=1.995 are also due to substitutional Mn^{2+} ions but subjected to tetragonal crystalline fields and are the same as those reported by earlier workers. Superhyperfine structure has been observed in spectra II, III_2 and III_4. The analysis of that structure in spectra II and III_2 has been carried out for the first time and the constants A_s and A_σ are given. The spectra are analysed by the usual spin-Hamiltonian method.

5.1 INTRODUCTION

It is known that when alkali halide crystals are doped with divalent impurities like Mn^{2+}, alkali vacancies are created to maintain charge neutrality. The divalent ions could individually go in substitutionally or interstitially in the crystal or could also go in clusters or precipitates. The vacancy could be a nearby neighbour to the divalent ion or it could be far away from it. The electron paramagnetic resonance (EPR) spectra[1,7] clearly indicate the different ways in which the impurity ions go into the crystals. Earlier work[5,6] on Mn^{2+}:NaCl has shown that the following different types of EPR spectra could be obtained depending upon the way in which the crystal is grown: (I) a broad absorption due to clusters or precipitates of Mn^{2+}, (II) a spectrum showing only one hyperfine sextet which is due to Mn^{2+} in cubic symmetry the vacancies being far away, (III_1) an orthorhombic spectrum due to Mn^{2+} associated with a first neighbour alkali vacancy along the $\langle 110 \rangle$ direction, (III_2) a tetragonal spectrum due to Mn^{2+} associated with a second neighbour alkali vacancy along $\langle 100 \rangle$, (IV) an orthorhombic spectrum due to Mn^{2+} associated with a molecular oxygen ion in the first neighbour halogen site, and (V) a terragonal spectrum due to Mn^{2+} associated probably with a hydroxyl ion again in the first neighbour halogen site. Hayes and Jones[3] investigated the EPR of Mn^{2+}:NaF And reported a strong tetragonal spectrum which is called here for convenience as III_4

and also a weak spectrum of the same kind which is designated here as III_2. Both these spectra have also been analysed. They are reported to reveal super-hyperfine structure (SHFS) though the involved constants for only the strong spectrum III_4 had been obtained. In order to see whether the other types of the spectra reported for Mn^{2+}: NaCl could also be found the EPR of Mn^{2+}:NaF has been reinvestigated with larger samples at different temperatures in the range 573°-93°K. The present paper deals with the results obtained in such an investigation.

5.2 EXPERIMENTAL

Electron paramagnetic resonance (EPR) studies at room temperature are made with a large single crystal of NaF of an approximate volume of one cubic centimeter containing 0.1% of manganese. This crystal is cleaved from a melt-grown crystal supplied by OPTOVAC and is quite transparent. The crystal was grown in vacuum in a graphite crucible. Smaller crystals cut from the above large crystal are used for studying the spectra between 573 °K and 93 °K. A Varian X-band spectrometer V-4502-12 with 100 kc./sec. field modulation is used. Angular variation is studied with the sample in a V-4533 rotating cavity while the temperature studies are made with V-4547 variable temperature accessories. The magnetic field is measured with a model F-8 flux meter. The frequency of the proton resonance is measured with a Hewlett Packard

frequency counter HP-524C. The field has been standardised using a polycrystalline sample of the free radical α-α-diphenyl β-picryl hydrazyl (DPPH) as a field marker the g-value of which is taken as 2.0036 ± 0.0002.[8]

5.3 THEORY

The Mn^{2+} spectrum has been discussed well by various authors.[9-11] Divalent manganese has a $3d^5$ electron configurarion for which the ground term is $^6S_{5/2}$. This state splits into three Kramers' doublets in the presence of an electric field having an axial or lower symmetry. This splitting gives rise to five fine structure lines in the EPR spectrum of Mn^{2+} which further split into sextets due to hyperfine interaction with the nucleus. An axial spectrum is described by a spin-Hamiltonian

$$H = g\beta \underline{H}.\underline{S} + A^{55}\underline{S}.\underline{I} + \frac{a}{6}\left[S_x^4 + S_y^4 + S_z^4 - \left(\frac{1}{5}\right)S(S+1)(3S^2 + 3S - 1)\right] + D\left[S_z^2 - \left(\frac{1}{3}\right)S(S+1)\right] \quad .. \quad (5.1)$$

The first term in Equation (5.1) describes the Zeeman interaction of the electron spin (S=5/2) with the applied static magnetic field H, g is the spectroscopic splitting factor and β is the Bohr magneton. The second term is due to the nuclear hyporfine interaction, A^{55} being the hyperfine interaction constant due to manganese nucleus. 'I' is the nuclear spin of manganese (I=5/2). The third and

the fourth terms are related to the splittings of the electronic levels in the zero magnetic field due to the crystalline electric field. The crystal field parameters a and D correspond, respectively, to the cubic and tetragonal fields. In the present case a term of the type $\sum S.A^i.I^i_o$ is added to the spin-Hamiltonian since there exists a magnetic interaction between Mn^{2+} ion and the surrounding F^- ligand nuclei whose spin is $I_o(=½)$. This interaction produces a shift δH in the field at which resonance occurs[12,3]

$$\delta H = \Sigma_i I^i_{oz} \left\{ A^i_s + A^i_\sigma (3 \cos^2 \theta_{z,\sigma} - 1) \right\} \quad .. \quad (5.2)$$

where the summation is over the six fluorine nuclei. It is assumed that the magnetic electrons are partly in $p\sigma$ orbitals on fluorines and that the magnetic field is applied along the z-axis at an angle $\theta_{z,\sigma}$ with the axis of each σ bond. A_s is the isotropic part and is determined by the s electron contact interaction. A_σ is the anisotropic part and it includes the dipole-dipole interaction ans the coupling [illegible]h the $p\sigma$ orbitals. As the six fluorines form an octahedron around Mn^{2+}, the interaction parameters A_s and A_σ can be expected to be the same for all the fluorine nuclei. When the magnetic field is parallel to the crystallographic axis <100>, two fluorines along the field direction will be equivalent while the four fluorines in the plane perpendicular to the field direction will be equivalent among themselves. In such

a case Equation (5.1) takes the form

$$\delta H = A_s \sum_1^6 I_{oz}^i + 2A_\sigma \sum_1^4 I_{oz}^i - A_\sigma \sum_1^4 I_{oz}^i \quad .. \quad (5.2a)$$

where I_{oz} can take the values ½ or -½. The resulting number of lines in this case will be fifteen and the expressions for δH for the individual lines along with their relative intensities are given in columns 3 and 2 of Table 5.1. In practice the number of lines observed will be smaller than fifteen. This is because of the considerable line width and the overlaps will be dependent upon the relative magnitudes of A_s and A_σ. If A_σ is exactly equal to zero there will be seven lines all of which will be equally separated from one another.

The field values corresponding to the different transitions when the static magnetic field is parallel to the <100> direction are given by[5,6]

$$H(M=+\tfrac{1}{2} \leftrightarrows -\tfrac{1}{2}) = H_o \quad .. \quad (5.3)$$

$$H(M=\pm 3/2 \leftrightarrow \pm\tfrac{1}{2}) = H_o \mp 2D \pm 5a/2 \quad .. \quad (5.4)$$

$$H(M=\pm 5/2 \leftrightarrow \pm 3/2) = H_o \mp 4D \quad 2a \quad .. \quad (5.5)$$

to which the following expression for hyperfine structure is to be added:

$$H(m \leftrightarrow m\,) = -A^{55}m - A^2/2H_o \cdot \left[\underline{I}(I+1) - m^2 + (2M-1)\underline{m}\right] \quad (5.6)$$

Here $H_o = h\nu/g\beta$, ν being the microwave frequency.

and $A_\sigma = 3.3G$

($M = +5/2 \rightarrow 3/2$ and $m = -5/2 \rightarrow -5/2$)

Line Nos.	Relative statistical weight	δH	δH in gauss	δH expected peaks in gauss	Calculated relative intensity	H=iii+ 2128.0 in gauss	H observed in gauss	Observed relative intensity
1	1	$-3A_s$	-42.9	-42.9	1	2085.1	2083.9	1
2	4	$-(2A_s+A_\sigma)$	-31.9	-31.9	4	2096.1	2097.2	5
3	2	$-2(A_s-A_\sigma)$	-22.0	-21.2	8	2106.8	2106.9	10
4	6	$-(A_s+2A_\sigma)$	-20.9					
5	8	$-(A_s-A_\sigma)$	-11.0	-10.6	12	2117.4	2117.4	13
6	4	$-3A_\sigma$	-9.9					
7	1	$-(A_s-4A_\sigma)$	-1.1	0.0	14	2128.0	2128.3	14
8	12	0	0					
9	1	(A_s-4A_σ)	1.1					
10	4	$3A_\sigma$	9.9	10.6	12	2138.6	2138.9	14
11	8	(A_s-A_σ)	11.0					
12	6	$+(A_s+2A_\sigma)$	20.9	21.2	8	2149.2	2149.0	11
13	2	$2(A_s-A_\sigma)$	22.0					
14	4	$(2A_s+A_\sigma)$	31.9	31.9	4	2159.9	2159.4	6
15	1	$3A_s$	42.9	42.9	1	2170.9	2170.1	2

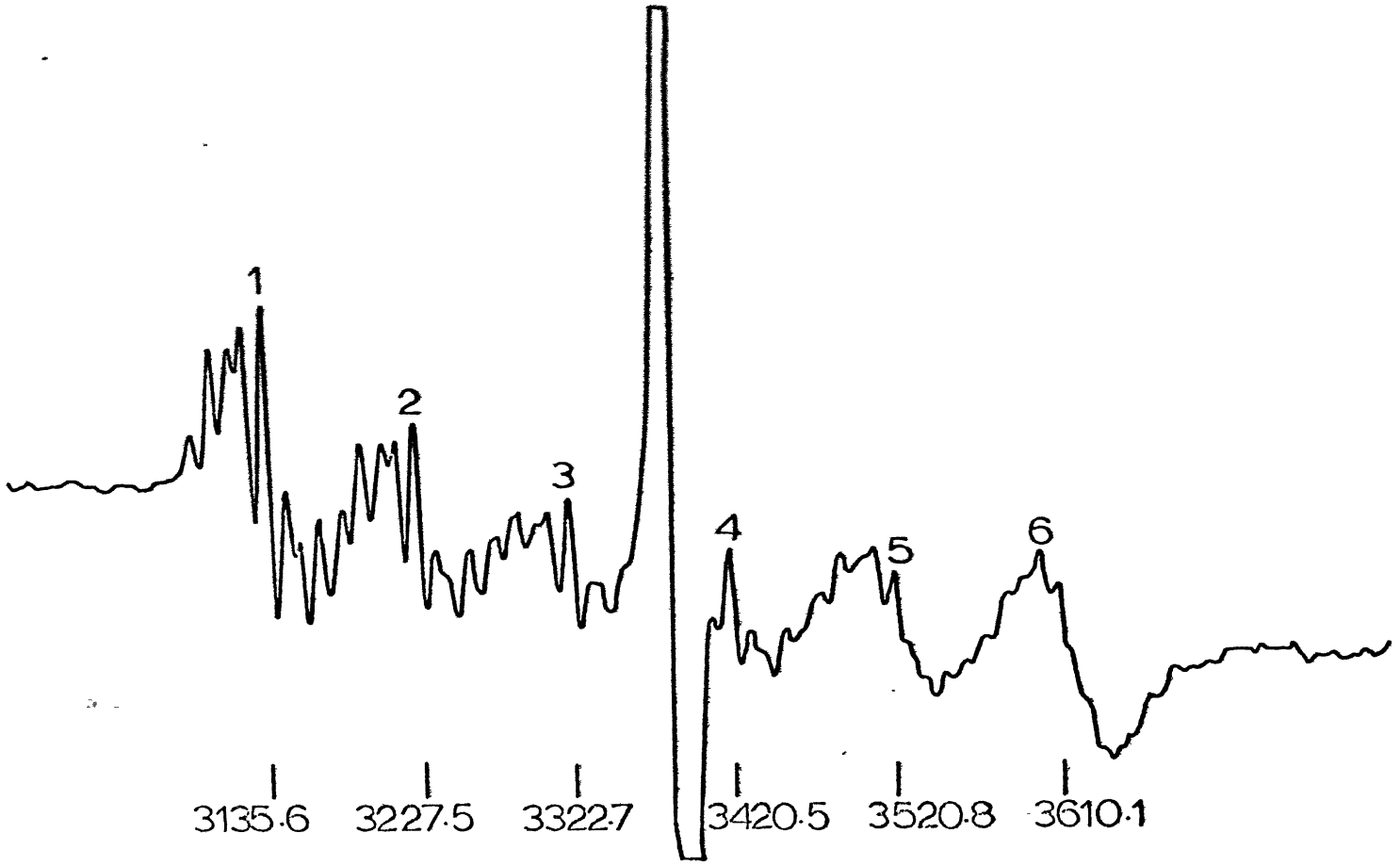

Fig. 5.1. The EPR spectrum II of Mn^{2+}: NaF powdered (Polycrystalline) sample at room temperature. Numbers indicate the field values in gauss. The central line is due to the field marker, DPPH.

It may be noted that one would be tempted to analyse the spectrum III_4 as a 90^o part of the spectrum III_2. Then one should see two components for III_2 when H is deviated from the <100>direction and such components have not been observed. Further, the spectrum III_4 is about tem times more intense than spectrum III_2 which will be difficult to understand unless these two are different spectra. A detailed analysis for these spectra confirmed that they are two different spectra. It appears that the $\theta = 90^o$ spectrum of III_2 is overlapped by the stronger spectrum III_4 and is not identifiable separately. Similarly the $\theta = 90^o$ part of the spectrum III_4 is overlapped by the spectrum II and is not observable.

5.5 EFFECT OF TEMPERATURE

High temperature studies are made up to 573 ^oK. One expects that the vacancies become mobile and get dissociated from Mn^{2+} ions at higher temperatures[14,15]. In the present study the intensity of the axial and cubic spectra increased in the first instance with the increase of temperature indicating that the number of the corresponding magnetic centres has increased in the initial stages. This happens probably at the expense of the intensity of the spectrum I which is found to be more prominent at the 93^oK. On further increase of temperature, at about 533^oK the 'SHFS' gets smeared up and the intensity of the

axial spectra start diminishing with a corresponding increase in the intensity of the cubic spectrum. One can infer from these observations that the charge compensation is occuring by the production of alkali vacancies and the vacancies become mobile above 533 ^{o}K and get dissociated at higher temperature thus making the local symmetry of Mn^{2+} cubic. This is reflected in the exchange of intensities between axial and cubic spectra, the intensity of the latter being enhanced at the cost of the intensity of the former.

The superhyperfine structure has been analysed following the procedure of Tinkham[12]. Here it may be mentioned that Clogston, Gordon, Jaccarino, Peter and Walker[16] have reported an extensive work on F^{19} superhyperfine structure in the EPR spectrum of Mn^{2+} in ZnF_2 and improved the work done earlier by Tinkham[12]. Clogston et al[16] worked at 23.3 and 54 GHz and obtained $\Delta m_F = \pm 1$ transitions apart from $\Delta m_F = 0$ in the observed SHFS. However, the present experimental conditions and the observed SHFS are more similar to that of Tinkham's and may be classified as "simple" in the notation of Clogston et al[16]. A comparison of the observed and calculated SHFS pattern for the transition M = +5/2 → +3/2, m = -5/2 → -5/2 in the spectra III_2 and III_4 is shown in Tables (5.1) and (5.2) respectively while that for the transition M = +½ → -½, m = -5/2 → -5/2 in the spectrum II is shown in Table (5.3).

TABLE II

The observed and calculated superhyperfine structure in spectrum III_4 with A_s = 14.3G and A_σ = 3.8G

(M = +5/2 → +3/2 and m = -5/2 → -5/2)

Relative statistical weight	δH	δH in gauss	δH expected peaks in gauss	Calculated relative intensity	H(calculated) =δH+ 2704.0 in gauss	H observed in gauss	Observed relative intensity
1	$-3A_s$	-42.9	-42.9	1	2661.1	2662.1	1
4	$-(2A_s+A_\sigma)$	-32.4	-32.4	4	2671.6	2672.0	3
6	$-(A_s+2A_\sigma)$	-21.9	-21.7	8	2682.3	2682.0	8
2	$-2(A_s-A_\sigma)$	-21.0					
4	$-3A_\sigma$	-11.4	-10.8	12	2693.2	2693.8	12
8	$-(A_s-A_\sigma)$	-10.5					
1	(A_s-4A_σ)	-0.9	0.0	14	2704.0	2703.1	14
12	0	0.0					
1	$-(A_s-4A_\sigma)$	0.9					
8	(A_s-A_σ)	10.5	10.8	12	2714.8	2714.8	12
4	$3A_\sigma$	11.4					
2	$2(A_s-A_\sigma)$	21.0	21.7	8	2725.7	2726.0	8
6	(A_s+2A_σ)	21.9					
4	$(2A_s+A_\sigma)$	32.4	32.4	4	2736.4	2736.7	4
1	$3A_s$	42.9	42.9	1	2746.9	2747.2	1

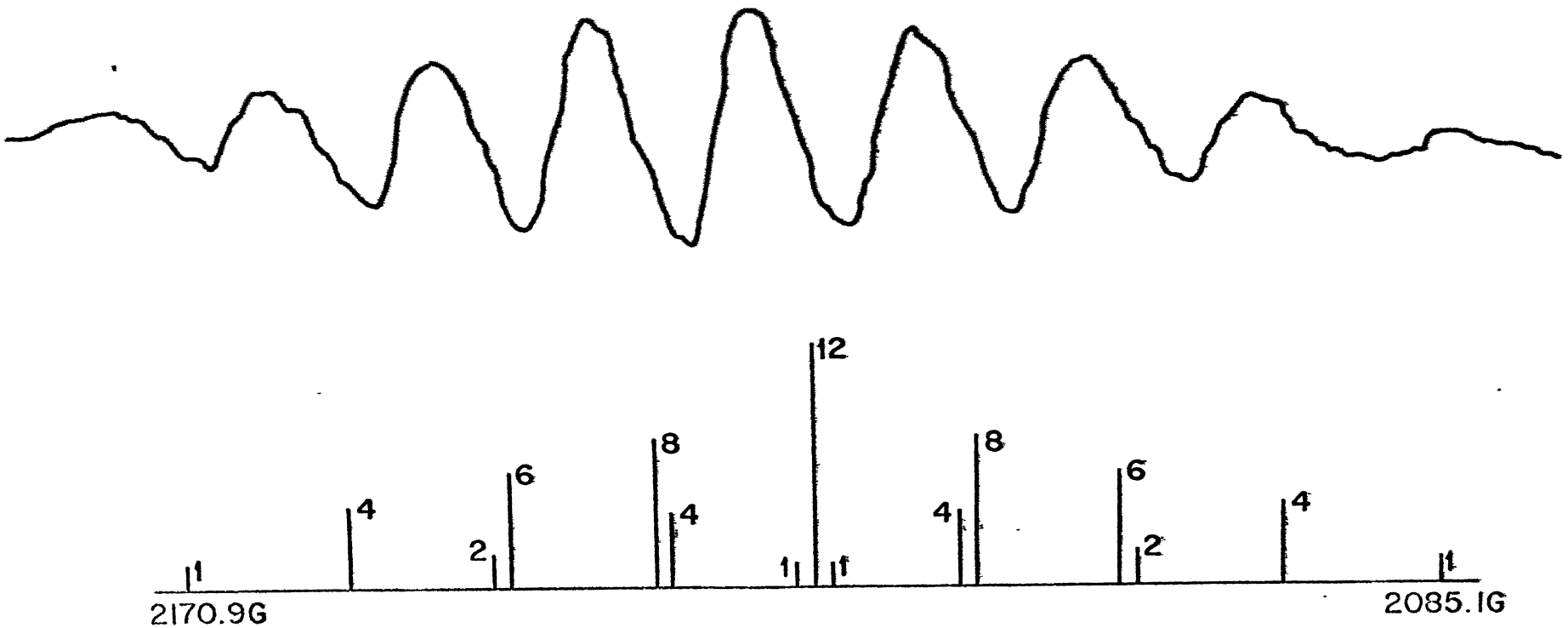

Fig. 5.2. The observed and calculated superhyperfine structure in the EPR spectrum III_2 of Mn^{2+}: NaF single crystal at room temperature with H parallel to the (100) axis of the crystal for the transition M = + 5/2 → + 3/2 and m = - 5/2 → - 5/2.

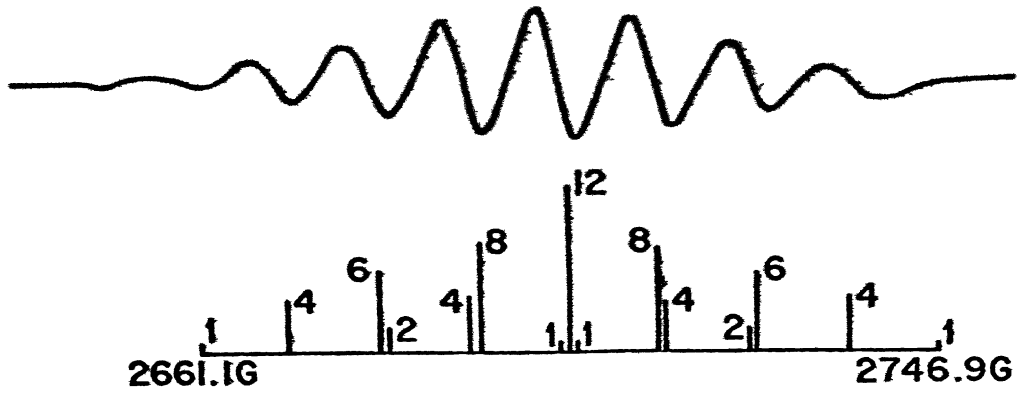

Fig. 5.3. The observed and calculated superhyperfine structure in the EPR spectrum III_4 of Mn^{2+}: NaF single crystal at room temperature with H parallel to the (100) axis of the crystal for the transition M = + 5/2 → + 3/2 and m = - 5/2 → - 5/2.

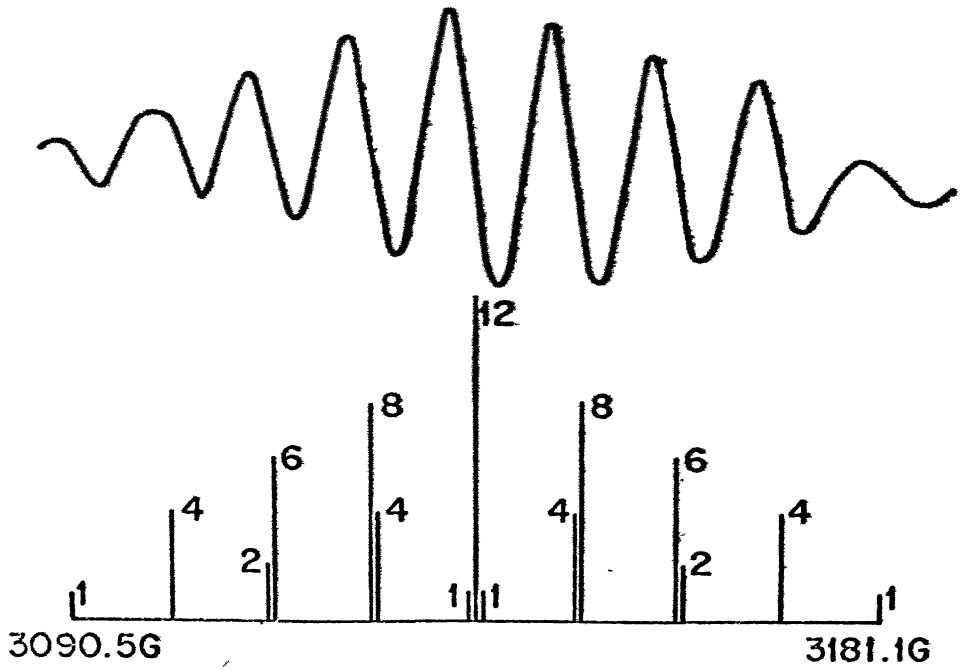

Fig. 5.4. The observed and calculated superhyperfine structure in the EPR spectrum II of Mn^{2+}: NaF single crystal at room temperature with H parallel to the (100) axis of crystal for the transition $M = +\frac{1}{2} \rightarrow -\frac{1}{2}$ and $m = -5/2 \rightarrow -5/2$.

The observed and calculated superhyperfine structure in spectrum II with A_s = 15.1G and A_σ = 3.7G

(M = +1/2 ↔-1/2 and m =-5/2 ↔-5/2)

Line Nos.	Relative statistical weight	δH	δH in gauss	δH expected peaks in gauss	Calculated relative intensity	H=III+ 3135.8 in gauss	H observed in gauss	Observed relative intensity
1	1	$-3A_s$	-45.3	-45.3	1	3090.5	3091.4	1
2	4	$-(2A_s+A_\sigma)$	-33.9	-33.9	4	3101.9	3102.4	4
3	2	$-2(A_s-A_\sigma)$	-22.8	-22.6	8	3113.2	3112.6	8
4	6	$-(A_s+2A_\sigma)$	-22.5					
5	8	$-(A_s-A_\sigma)$	-11.4	-11.3	12	3124.5	3123.7	13
6	4	$-3A_\sigma$	-11.1					
7	1	$-(A_s-4A_\sigma)$	-0.3	0	14	3135.8	3135.6	14
8	12	0	0					
9	1	(A_s-4A_σ)	0.3					
10	4	$3A_\sigma$	11.1	11.3	12	3147.1	3146.7	13.5
11	8	(A_s-A_σ)	11.4					
12	6	(A_s+2A_σ)	22.5	22.6	8	3158.4	3157.7	10
13	2	$2(A_s-A_\sigma)$	22.8					
14	4	$(2A_s+A_\sigma)$	33.9	33.9	4	3169.7	3169.6	6
15	1	$3A_s$	45.3	45.3	1	3181.1	3182.4	2

5.6 REFERENCES

1. P.A.Forrester and E.E.Schneider, Proc.Phys.Soc.(London), 69B, 883(1956).
2. B.Bleaney and W.Hayes, Proc.Phys.Soc.(London), 70B, 626, (1957).
3. W.Hayes and D.A.Jones, Proc.Phys.Soc.(London), 71, 503, (1958).
4. T.P.P.Hall, W.Hayes and F.I.B.Williams, Proc.Phys.Soc. (London), 78, 883(1961).
5. G.D.Watkins, Phys.Rev., 113, 79, (1959).
6. K.N.Shrivastava and P.Venkateswarlu, Proc.Ind.Acad.Sci., 53A, 284(1966).
7. K.Morigaki, M.Fujimoto and J.Itoh, J.Phys.Soc.Japan, 13, 1174(1958).
8. A.N.Holden, C.Kittel, F.Merritt and W.A.Yager, Phys.Rev., 77, 147(1950).
9. B.Bleaney and K.W.H.Stevens, Reports on Progress in Physics, 16, 108(1953).
10. K.D.Bowers and J.Owen, Reports on Progress in Physics, 18, 304(1955).
11. W.Low, PARAMAGNETIC RESONANCE IN SOLIDS, Academic Press, New York and London, 1960.
12. M.Tinkham, Proc.Roy.Soc.(London), 236A, 536, 549(1956).
13. T.P.P.Hall and W.Hayes, and R.W.H.Stevenson and J.Wilkens, J.Chem.Phys., 38, 1977(1963).
14. W.J.Veigele and W.H.Tantilla, J.Chem.Phys., 41, 274(1964).
15. G.A.Persyn and A.W.Nolle, Phys.Rev., 140A, 1610(1965).
16. A.M.Clogston, J.P.Gordon, V.Jaccarino, M.Peter and L.R. Walker, Phys Rev., 117, 1222(1960).
17. R.Bötcher, W.Windsch and W.Lüdke, Physica.Stat.Solidi, 20, 121(1967).

CHAPTER VI

ELECTRON PARAMAGNETIC RESONANCE of VO^{2+} IN THE ALKALI CHLORIDES

ABSTRACT

Electron paramagnetic resonance (EPR) of VO^{2+} radicals incorporated in face-centred single crystals of NaCl, KCl and RbCl has been studied in the temperature range of 77 °K to 330 °K. At liquid nitrogen temperature, anisotropic spectra have been recorded in each case while spectra recorded at room and higher temperatures are isotropic suggesting the existence of a fast readjustment of VO^{2+} molecular ions in the crystals at higher temperature while this motion gets hindered at liquid nitrogen temperatures. Spin-Hamiltonian constants are calculated from the recorded isotropic and anisotropic spectra. The line widths in each case are found to obey a parabolic law originally proposed by Kivelson. The constants which give a close fit have been evaluated. The random orientation and readjustment of V-O bond in these alkali chloride crystals is explained on the assumption that the medium exhibits a "liquid-like" nature for VO^{2+} molecular ion as far as the electron paramagnetic resonance absorption is concerned.

6.1 INTRODUCTION

Electron paramagnetic resonance (EPR) of VO^{2+} doped in NH_4Cl single crystal has been recently studied by Sastry and Venkateswarlu[1] and that in KNO_3 and $CsNO_3$ by Rao, Sastry and Venkateswarlu[2]. It has been found from these studies that the molecular ion VO^{2+} does not have a fixed orientation in these crystals and undergoes a fast readjustment at room temperature while it shows the effects of hindered rotation at low temperatures. On the other hand, VO^{2+} is known to have preferred orientation in Tutton salts[3] and in rubidium and caesium alims.[4] Very recently Rao, Sastry and Venkateswarlu[5] have also found from their EPR studies that the VO^{2+} ion has preferred orientation in the potassium and ammonium aluminium alums and MAG alum. The present work has been undertaken to get information about the VO^{2+} complex in the alkali halide crystals, NaCl, KCl and RbCl. Further it was felt that if these systems exhibit a "liquid-like" behaviour they might represent better examples than $NH_4Cl:VO^{2+}$, $KNO_3:VO^{2+}$ and $CsNO_3:VO^{2+}$ to examine the applicability of Kivelson's theory[6] of paramagnetic relaxation in liquids as these crystals (alkali halides) exhibit a liquid-like nature as far as VO^{2+} is concerned.

6.2 EXPERIMENTAL PROCEDURE

0.5 mol percent of vanadyl chloride is added to E.Merck, A.R.Quality chlorides of sodium, potassium and rubidium. Slow evaporation of aqueous solution yielded well-developed cubes. EPR measurements are carried at

X-band, 9.5 kMc/sec. nominal frequency, with a Varian V-4502 EPR spectrometer and a V-3400 nine-inch rotating electromagnet using a 100 kc/sec field modulation. The magnetic field is calibrated using DPPH* as a field marker. The proton resonance is monitored with a Varian Flux-meter model F-8A connected to a Beckmann 10-110 Mc/sec. convertor 7571. Spectra are recorded at various temperatures ranging from +60 °C to -180 °C with the help of a Varian V-4540 variable temperature accessory. General microwave 459A thermoelectric power meter has been used for measuring the power output. IBM electronic computers 1620 and 7044 have been used for calculations and least square fit.

6.3 THEORY

The electronic state of the VO^{2+} ion is mainly dependent on the $3d^1$ electron of vanadium. In a crystalline field of symmetry less than cubic the lowest level will be an orbital singlet. In such a case only one fine structure transition can be expected in EPR, and the hyperfine structure would show eight lines because of the V^{51} nucleus whose spin is 7/2. As the EPR is due to the molecular ion which has itself an axial field, the spectrum cannot be expected to reveal cubic site symmetry even if VO^{2+} goes in substitutionally and the expected positive vacancy is too far off from it. If the VO^{2+} ion goes in substitutionally in the present alkali halides as Mn^{2+}

*Diphenylpicrylhydrazyl whose g-value is taken as 2.0036

in NaCl, it might get associated with a first neighbour positive vacancy in which case the site symmetry will be orthorhombic or it might get associated with a second neighbour positive vacancy in which case the site symmetry will be tetragonal. However, the EPR spectra of VO^{2+} obtained in the present experiments are found to be independent of the crystal orientation with respect to the magnetic field indicating clearly that the VO^{2+} ion has no preferred orientation in the present crystals.

For a paramagnetic ion placed in a matrix which does not exhibit directional properties the spectra can be interpreted using a simple model of random array[7] of magnetic ions. The EPR spectrum of VO^{2+} in tetragonal symmetry or of randomly oriented VO^{2+} molecular ions in solutions can be described by the spin-Hamiltonian,[8-10] of the type

$$\mathcal{H} = g_{\parallel}\beta H_z + g_{\perp}\beta(H_x S_x + H_y S_y) + A I_z S_z + B(I_x S_x + I_y S_y). \quad .. \quad (6.1)$$

The Hamiltonian (6.1) leads to the following magnetic field resonance[10] values for the hyperfine structure components in the EPR spectrum of VO^{2+}:

$$H = H_o - \frac{K m_I}{g\beta} - \frac{B^2(A^2+K^2)}{4H_o g^2\beta^2K^2}\left[I(I+1) - m_I^2\right] - \frac{(A^2-B^2)g_{\parallel}^2 g_{\perp}^2}{2H_o g^2\beta^2K^2g^4}\sin^2\theta\cos^2\theta m_I^2 \quad .. \quad (6.2)$$

TABLE 5.4

SPIN-HAMILTONIAN PARAMETERS* OF Mn^{2+} IN NaF AT 300 °K

Parameter	Spectrum I	Spectrum II	Spectrum III_2	Spectrum III_4
g	2.0	2.003±0.002	2.014±0.004	1.995±0.003
			(2.00±0.01)†	(1.996±0.006)†
A^{55} x10^{-4}cm^{-1}	..	-90.4±1.6	-92.8±0.5	-93.8±1.0
		(88.6±0.1)§	(92±4)†	(91±4)†
D x10^{-4}cm^{-1}	..	...	221.0±0.2	89.0±0.5
			(225±8)†	(89±5)†
a x10^{-4}cm^{-1}	..	...	0.2	-1.3
A_s^{19} x10^{-4}cm^{-1}	..	14.2±0.4	13.4±0.2	13.3±0.3
		(12.9±0.2)§		(14.4±0.3)†
A_σ^{19} x10^{-4}cm^{-1}	..	3.5±0.6	3.1±0.3	3.5±0.5
		(3.2±0.2)§		(2.8±0.7)†

*It is to be noted that the constants A_s and A_σ are given in units of 10^{-4}cm.$^{-1}$ here while they are given in gauss in Tables (5.1),(5.2) and (5.3).

†These values are those obtained by Hayes and Jones[3] at 90 °K.

§ Hall, Hayes, Stevenson and Wilkens[13].

is also angular independent. Figs. 6.1 and 6.2 show the typical spectra obtained in the case of $NaCl:VO^{2+}$ system. The parallel and perpendicular components are labelled "a" and "b" respectively. The gradual change of spectrum to spectrum II with lowering of temperature is reversible. The isotropic spectrum I is similar to those reported by Rao et al[2] in the case of $CsNO_3:VO^{2+}$ and $KNO_3:VO^{2+}$ at room temperature, and O'Reilly[8] for Vanadyl etioporphirin I (VEPI) in benzene solution. On the other hand, the anisotropic spectrum II obtained at liquid nitrogen temperature as in the case of KNO_3, $CsNO_3$ and NH_4Cl[1,2] is similar to the spectrum obtained by Hochstrasier[11] for VO^{2+} in amorphous glass and to those obtained by O'Reilly[8] for VEPI dissolved in high viscous petroleum oil and for solid asphaltenes containing vanadium. This similarity suggests that the VO^{2+} in alkali chlorides behaves as if it were in a liquid medium as far as the results of EPR are concerned. The isotropic spectrum at room temperature is probably due to a fast reorientation of the V-O bond which results in the averaging out of anisotropies in g and A tensors. As the temperature is lowered, the fast reorientation gets hindered and at liquid nitrogen temperature the reorientation rate is slow enough that the anisotropies in g and A tensors are not averaged out and can be seen in the spectrum. However, even at liquid nitrogen temperature the orientation of the V-O bond is random enough to make the EPR spectrum angular independent. The appearance of

spectrum II only at liquid nitrogen temperature is probably due to the hindrance (or freezing) of the motion of VO^{2+} ion due to the lowering of temperature and as such appears to be a purely temperature effect as unlike in NH_4Cl there are no phase transformations in the crystals studied here.

O'Reilly[8] and McConnel[13] obtained the following expressions for the isotropic values of g and A in terms of $g_{\parallel}$ and $g_{\perp}$ for the cases where the molecule is rotating with a correlation time much shorter than the reciprocal of the frequency spread of this spectrum:

$$g_o = \frac{g_{\parallel} + 2g_{\perp}}{3} \qquad .. \quad (6.3a)$$

$$A_o = \frac{A + 2B}{3} \qquad .. \quad (6.3b)$$

The values obtained for g_o and A_o from the analysis of the spectrum I are listed in Table 6.1 for the different alkali halides studied.

The Hamiltonian (6.1) remains anisotropic for cases where the correlation time is long. The existence of anisotropic spectra at liquid nitrogen temperature in all cases is confirmed by varying the microwave power level from 1.0 mW to 110 μW. There were no saturation effects and the intensities followed the power levels, their relative values remaining the same.

TABLE 6.1

Spin-Hamiltonian Constants for VO^{2+} in NaCl and RbCl Single Crystals

(Values of A_o, $A_{\parallel}$ and $A_{\perp}$ are in units of $10^{-4}cm^{-1}$)

Crystal System	Spectrum I	Spectrum II
$NaCl:VO^{2+}$	$g_o = 1.971 \pm 0.001$	$g_{\parallel} = 1.925 \pm 0.002$
	$A_o = 104.0 \pm 1.0$	$g_{\perp} = 1.996 \pm 0.002$
		$A_{\parallel} = 176.8 \pm 2.0$
		$A_{\perp} = 64.2 \pm 2.0$
$KCl:VO^{2+}$	$g_o = 1.969 \pm 0.002$	$g_{\parallel} = 1.932 \pm 0.002$
	$A_o = 106.8 \pm 2.0$	$g_{\perp} = 1.988 \pm 0.002$
		$A_{\parallel} = 186.8 \pm 3.0$
		$A_{\perp} = 70.4 \pm 5.0$
$RbCl:VO^{2+}$	$g_o = 1.967 \pm 0.002$	$g_{\parallel} = 1.939 \pm 0.002$
	$A_o = 106.0 \pm 2.0$	$g_{\perp} = 1.968 \pm 0.002$
		$A_{\parallel} = 188.7 \pm 3.0$
		$A_{\perp} = 63.9 \pm 3.0$

All the spectra obtained, type I and type II, have been analyzed using equation (6.2) and the results are tabulated in Table (6.1).

6.5 LINE WIDTH STUDIES

The spin resonance studies have clearly shown that VO^{2+} in alkali chlorides exhibit a "liquid-like" nature as far as the paramagnetic resonance and relaxation are concerned similar to what has been reported earlier in the case of NH_4Cl[1], KNO_3 and $CsNO_3$[2]. An attempt is therefore made to see the applicability of Kivelson's theory[6] of paramagnetic relaxation in liquids, to the single crystal systems of the present study.

It has been shown[6,13] that the anisotropies in g and A tensors contribute to the line broadening in the EPR spectra. When there are considerable anisotropies in g and A, the line widths can be given by the following expression[14]

$$1/t_2 = a_1 + a_2 m_I + a_3 m_I^2 \qquad .. \quad (6.4)$$

where a's+ depend upon the factors $(g_{\parallel} - g_{\perp})$ and $(A - B)$. The experimental line widths are measured by the method used by Rogers and Pake[14] and Rao et al[2] where it is

---

+The a's given here are related to those in reference 14 by a multiplicative constant $\pi\sqrt{3}$.

All the spectra obtained, type I and type II, have been analyzed using equation (6.2) and the results are tabulated in Table (6.1).

6.5 LINE WIDTH STUDIES

The spin resonance studies have clearly shown that VO^{2+} in alkali chlorides exhibit a "liquid-like" nature as far as the paramagnetic resonance and relaxation are concerned similar to what has been reported earlier in the case of NH_4Cl[1], KNO_3 and $CsNO_3$[2]. An attempt is therefore made to see the applicability of Kivelson's theory[6] of paramagnetic relaxation in liquids, to the single crystal systems of the present study.

It has been shown[6,13] that the anisotropies in g and A tensors contribute to the line broadening in the EPR spectra. When there are considerable anisotropies in g and A, the line widths can be given by the following expression[14]

$$1/t_2 = a_1 + a_2 m_I + a_3 m_I^2 \qquad .. \quad (6.4)$$

where a's+ depend upon the factors $(g_{\parallel} - g_{\perp})$ and $(A - B)$. The experimental line widths are measured by the method used by Rogers and Pake[14] and Rao et al[2] where it is

---

+The a's given here are related to those in reference 14 by a multiplicative constant $\pi\sqrt{3}$.

assumed that the population difference between the different m_I levels is small. The m_I dependence of the line widths is shown in Figs. 6.3, 6.4 and 6.5. These curves fit in very well with equation (6.4), and a least square calculation yields the constants a_1, a_2 and a_3 given in Table 6.2. Wilson and Kivelson[15] have added cubic and fourth order terms to the polynomial in equation 6.4; but such terms are not found to be necessary in the present case.

TABLE 6.2

Line Width Parameters of the EPR of VO^{2+} in Alkali Halides

Crystal	a_1 in gauss	a_2 in gauss	a_3 in gauss
NaCl	23.40	2.30	1.23
KCl	19.40	1.30	0.54
RbCl	20.13	1.62	0.72

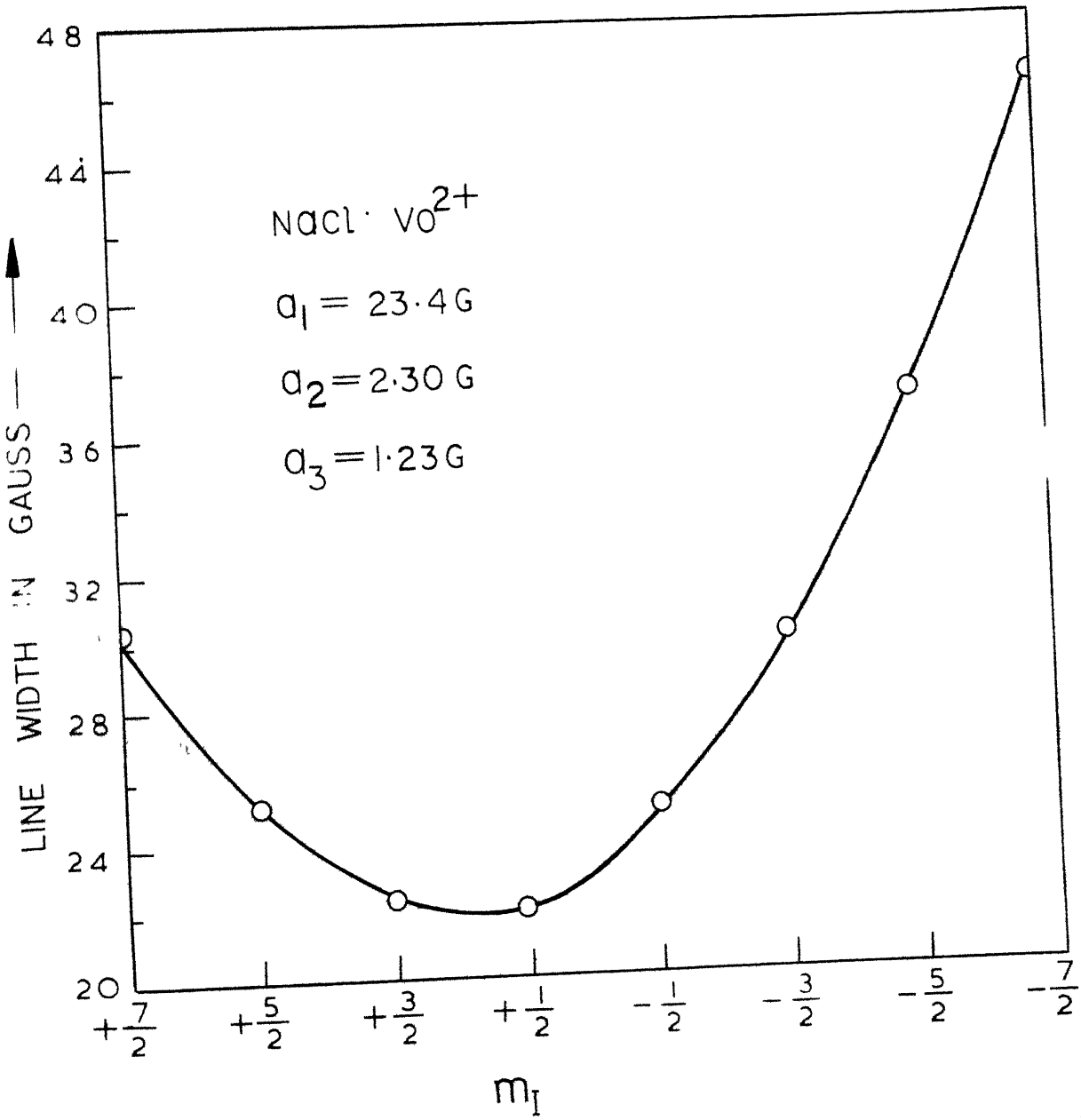

FIG. 6.3 PLOT OF LINE WIDTH VERSUS m_I IN THE EPR OF NaCl:VO^{2+} SYSTEM. THE SOLID CURVE REPRESENTS PREDICTED VARIATION OF THE LINE WIDTH WHILE CIRCLES INDICATE ACTUAL EXPERIMENTAL VALUES AT ROOM TEMPERATURE

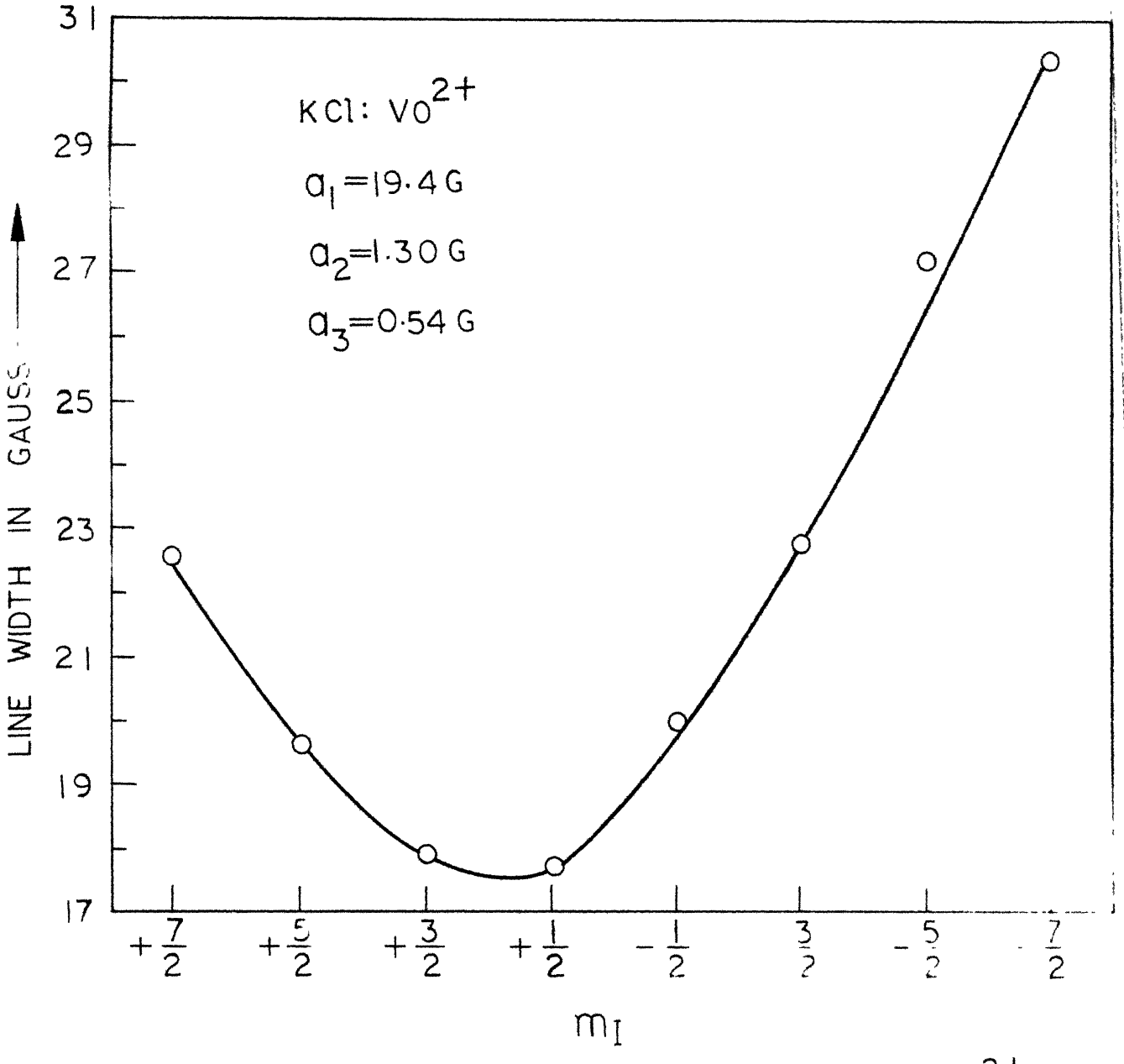

FIG. 6·4 PLOT OF LINE WIDTH VERSUS m_I IN THE EPR OF KCl·VO^{2+} SYSTEM THE SOLID CURVE REPRESENTS PREDICTED VARIATION OF THE LINE WIDTH WHILE CIRCLES INDICATE ACTUAL EXPERIMENTAL VALUES AT ROOM TEMPERATURE.

APPENDICES A and B

Appendix A comprises of two Tables, 7.1 and 7.2 which list respectively the spin Hamiltonian constants of the divalent ions Mn^{2+} and VO^{2+} studied in this thesis when they are doped in different host lattices. Appendix B contains some of the computer programs used in calculations.

TABLE 7.1

Mn^{2+}

Crystal	g	D	E	A	Reference	Note
Diopside $CaMgSi_2O_6$	2.0017	452.95 G	-102.8 G	84.4 G	7.1	a
	2.0016			84.4		
	2.0016			81.9		
	2.0015	379.84 G	17.09 G	91.3	7.1	a
	2.0013			91.7		
	2.0008			90.8		
Tremolite $2(H_2Ca_2Mg_5(SiO_3)_8)$	1.998	-448.3 G	-78.2 G	77.9 G	7.2	b
	1.997			76.7		
	1.995	-442.9 G	-79.4 G	79.9 G	7.2	b
	1.993			79.0		
Spodumene (Kunzite) $LiAl(SiO_3)_2$	2.0013	579 G	81.3 G	89.5 G	7.3	c
	2.0011			87.5		
	2.0012	947 G	122 G	88.3	7.3	c
	2.0024			83.9		
$Cd_2V_2O_7$	2.0004	-418 G	+41.7 G	-86.7 G	7.4	d
	1.9995			-87.0		
	2.0001			-87.4		
NH_4Cl	2.0012	1603.6 G		88.6 G	7.5	e
	2.0012			90.7		
NaCl	1.95	-1450 G	107 G	-85	7.6	f
$MnBCl_2 6H_2O$	2.01	1300 G			7.7	g

TABLE 7.1(CONTINUED)

Mn^{2+}

Crystal	g	D	E	A	Reference	Note
Cs_2SO_4	2.000	941 Oe	14 Oe	93 Oe	Present work	p
	2.015			91 "		
	2.000			91 "		

TABLE 7.2

VO^{2+} or V^{4+}

Crystal	g	A	Reference	Note
TiO_2	$g_x=1.915$ $g_y=1.913$ $g_z=1.956$	$A_x=0.0031$ cm^{-1} $A_y=0.0043$ cm^{-1} $A_z=0.0142$ cm^{-1}	7.8	h
Sapphire	$g_{\parallel}=1.97$	$A_{\parallel}=0.0132$ cm^{-1}	7.9	i
GeO_2	$g_{\parallel}=1.929$ $g_{\perp}=1.976$	$A_{\parallel}=175.5\times10^{-4}$cm^{-1} $A_{\perp}=68.2\times10^{-4}$cm^{-1}	7.10	j
GeO_2	$g_z=1.963$ $g_x=1.921$ $g_y=1.921$	$A_z=134.36\times10^{-4}$cm^{-1} $A_x=36.69$ " $A_y=37.54$ "	7.10	k
$Zn(NH_4)_2(SO_4)_2\cdot 6H_2O$ Tutton salt	$g_x=1.9813$ $g_y=1.9801$ $g_z=1.9331$	$A_x=0.007120$ cm^{-1} $A_y=0.007244$ " $A_z=0.018281$ "	7.11	l
$K_2V_2O_2(C_2O_4)_3\cdot 4H_2O$	$g_1=1.95_4$ $g_2=1.98_5$ $g_3=1.96_7$		7.12	m
Rb Alum	$g_{\parallel}=1.932$ $g_{\perp}=1.975$	$A=182.2\times10^{-4}$cm^{-1} $B=66.6$ "	7.13	
Cs Alum	$g_{\parallel}=1.932$ $g_{\perp}=1.979$	$A=183.4$ " $B=65.7$ "		
Potassium Alum	$g_{\parallel}=1.936$ $g_{\perp}=1.977$	$A=177$ " $B=68$ "	7.14	n
Ammonium Alum	$g_{\parallel}=1.940$ $g_{\perp}=1.978$	$A=176.0$ " $B=67$	7.14	n
Triglycine Sulphate	$g_{\parallel}=1.922$ $g_{\perp}=1.974$	$A=179.3$ " $B=70.4$ "	7.15	o

TABLE 7.2(CONTINUED)

Crystal	g	A	Reference	Note
Caesium sulphate	g_z=1.9382	A_z=197.0 oe	Present work	q
	g_x=1.9963	A_x= 77.5 "		
	g_y=1.9947	A_y= 81.5 "		
	g_z=1.9669	A_z=143.0 "	"	"
	g_x=1.9992	A_x= 65.5 "		
	g_y=1.9963	A_y= 77.5 "	"	"
	g_z=1.9498	A_z=179.0 "		
	g_x=2.0006	A_x= 76.0 "		
	g_y=1.9939	A_y= 82.0 "		

References to Tables 7.1 and 7.2:

7.1 V.M.Vinokurov, M.M.Zapirov, and V.G.Stepanov, Soviet Phys.Solid State (English Translation) 6,870(1964).

7.2 A.Manoogian, Can.J.Phys.46,129(1968).

7.3 F.Holuj, Can.J.Phys.46,287(1968).

7.4 C.V.Stager, Can.J.Phys.46,807(1968).

7.5 M.M.Zapirov and G.K.Chirkin, Zh.Strukt.Khim. 5,36(1964); A.Forman and J.A.Van Wyk, J.Chem.Phys.44,73(1966).

7.6 M.Ikoya, N.Itoh and T.Suita, Jour.Phys.Soc.Japan, 26,291(1969).

7.7 A.Van Heuvelen, M.D.Lundeen, H.G.Hamilton,J.R., and M.Dale Alexander, J.Chem.Phys.,50,489(1969).

7.8 H.J.Gerritsen and H.R.Lewis, Phys.Rev.119,1010(1960).

7.9 J.Lambe and C.Kikuchi (1959) unpublished.

7.10 I.Siegel, Phys.Rev.134A,193(1964).

7.11 R.H.Borcherts and C.Kikuchi, J.Chem.Phys.40,2270(1964)

7.12 Griffiths, Owen and Ward(1955)unpublished.

7.13 A.Manoogian and J.A.MacKinnon,Can.J.Phys.45,2769(1967)

7.14 K.V.S.Rao and M.Dattatreya Sastry and Putcha Venkateswarlu, J.Chem.Phys.49,4984(1968).

7.15 W.Windsch and E.Hartmann,Phys.Stat.Solid.29,K11,(1968)

Notes to Tables 7.1 and 7.2

(a) Work was done at two approximate frequencies of 10 Gc/s and 36 Gc/s.
Two complexes have been observed.
The error in g_z is 0.0005 while the error in g_x and g_y is 0.0008.
The error in hyperfine constant is 0.5G
For complex I b_4^0=0.34, b_4^2= -4.74, b_4^4=15.88 G.
For complex II b_4^0= -6.58, b_4^2= -2.93, b_4^4=32.47 G.
Error in D and E is not stated.

(b) Work was done at 9.2 GHz.
Values are given for two varieties, pink tremolite and white tremolite.
The error in g_z and g_y is 0.001
The error in hyperfine constant is 0.5G

For pink tremolite $b_4^0 = -0.96$, $b_4^2 = 33.0$, $b_4^4 = -34.6$ G
For white tremolite $b_4^0 = -0.43$, $b_4^2 = -19.0$, $b_4^4 = 18.2$ G

(c) Work was done at k-bank frequencies
As many as 6 complexes are reported
The error in g's is 0.0003 for complex I
The error in g's is 0.0005 for complex VI
The error in D is 2G for complex I and 15G for complex VI.
The error in E is 1G for complex I and 5G for complex VI.
The error in A_z, A_y is 0.5G for complex I
The error in A_z is 4G and that in A_y is 2G for complex VI.
For complex I $b_4^0 = -1 \pm 2$G, $b_4^2 = -4 \pm 2$ and $b_4^4 < 0.5 \pm 2$G.
The direction cosines of the ESR spectral axes with relative signs are:

Spectrum	Complex I	Complex VI	Axis
x	0	0.26989	bxc
	-1	-0.55335	b
	0	0.78801	c
y	0.91355	0.80115	bxc
	0	-0.58207	b
	-0.40674	-0.13917	c
z	+0.40674	0.57449	bxc
	0	0.55478	b
	0.91355	0.60182	c

(d) Work was done at 35 Gc/s
Error in g-values is 0.0008
Error in D is 1G while that in E is 2G
Error in A_x is 3G, A_y is 10G and A_z is 5G
$b_4^0 = -1 \pm 1$, $b_4^2 = 1 \pm 6$, $b_4^4 = -15 \pm 7$

(e) Work was done at 37Gc/sec and 51 Gc/sec
0.01% manganese as $MnCl_2$ added to NH_4Cl with pectin to get doped single crystals.
Error in A and B is 0.5G
Error in g's is 0.0005.
Cubic field constant referred to as D_4 is -2.3 ± 0.5G.

(f) Work was done at k-band spectrum
Doped crystals were x-irradiated
Error in g is 0.01; error in A is 1G and error in E is 10G.
Cubic field parameter a is 40G.

(g) A typical five line spectrum is obtained
Manganese is in spin 5/2 state
B is a macroscopic ligand
$b_4^0=0$, $b_4^4= -100G$
Absolute signs are not determined but the sign of b_0^2 is opposite to that of b_4^4.

(h) Rutile form of TiO_2; nearly tetragonal z-axis.
Direction cosines of the magnetic axes relative to the crystal axes are:

	a	a	c
x	$-\sqrt{2}/2$	$\pm\sqrt{2}/2$	0
y	0	0	1
z	$\pm\sqrt{2}/2$	$\sqrt{2}/2$	0

(i) Axial crystal; g is isotropic

(j) Amorphous; this is attributed to VO^{2+}
Error in g's is 0.001; error in A's is $0.1\times10^{-4}cm^{-1}$.

(k) Tetragonal; vanadium appears as V^{4+}
Error in g_z is 0.0003; error in g_x is 0.0006 and error in g_y is 0.0001
Error in A_z is $0.02\times10^{-4}cm^{-1}$
Error in A_x and A_y is $0.01\times10^{-4}cm^{-1}$.

( ) Work was done at x-band
g and A tensors displaced by 23° 20'
V-O axis is found to have three possible orientations.

(m) Work was done at two temperatures 290 °K and 90 °K
K.D.Bowers and J.Owen, Repts.Prog.in Phys.18,304(1955)

(n) Error in g's is 0.001; error in A and B is $1.0\times10^{-4}cm^{-1}$

(o) Ferroelectric crystal
Error in $g_{\parallel}$ is 0.002 and error in $g_{\perp}$ is 0.006
Error in A is 2.5 and error in B is $2.0\times10^{-4}cm^{-1}$.

```
      DO 12 I=1,5
12    SUM=SUM+DIF(I)
      AVE=SUM/5.
      VE=SQRTF(AVE)
      G=PH*PPH/FNOT
      PRINT 444,FNOT,G RD,RE,BFZ,BFT
      PRINT 444,VE,(HC(I),I=1,5)
444   FORMAT(6F10.4)
555   CONTINUE
      STOP
      END
```

APPENDIX B2

Computer programme used to diagonalize the 36x36 energy matrix.
Y(I) are the thirty field values of the entire spectrum
G is the DPPH field value and BFF is b_4.

The matrix elements (Table 7.3) are generated.
This program also can be used to either iterate or diagonalize any number of times NUM for different values of any parameter.

```
£JOB    PHR006,  TIME005  ,     PAGES025,     NAME A V J
£IBJOB
£IBFTC MAIN     NODECK
      DIMENSION X(36,36),E(36,36),H(36),HH(36),Y(30),DEF(30
      ),HF(36)
      DIMENSION HFC(12),DEFS(30),DIS(30)
      DOUBLE PRECISION X,E,H,Y,DEF,HF,HFC,DEFS
      HDPPH=2.0036
      READ 3333,NUM
3333  FORMAT(I3)
      READ 10,(Y(I),I=1,30)
      PRINT 10,(Y(I),I=1,30)
10    FORMAT(10F8.2)
      READ 1009,G,RD,RE,AZ,AX,AY,HNOT
1009  FORMAT(1X,7F8.2)
      PRINT 1000,G,RD,RE,AZ,AX,AY,HNOT
      READ 1109,BFZ,BFT,BFF
      PRINT 1109,BFZ,BFT,BFF
1109  FORMAT(1X,3F6.1)
      NDIM=36
1011  FORMAT(6E12.5)
600   AXYS=AX+AY
      RF=SQRT(40.)
      RFF=SQRT(45.)
      RS=SQRT(72.)
      DO 555 INDEX=1,NUM
C     COMPUTE X MATRIX
      DO 5I=1,NDIM
      DO 5 J=1,NDIM
5     X(I,J)=0.
C     DIAGONAL ELEMENTS
      P=2.5*G+10.*RD/3.
      X(1,1)=P+6.25*AZ
      X(2,2)=P+3.75*AZ
      X(3,3)=P+1.25*AZ
      X(4,4)=P-1.25*AZ
      X(5,5)=P-3.75*AZ
      X(6,6)=P-6.25*AZ
      PP=1.5*G-2.*RD/3.
      X(7,7)=PP+3.75*AZ
      X(8,8)=PP+2.25*AZ
      X(9,9)=PP+0.75*AZ
      X(10,10)=PP-0.75*AZ
```

```
      X(11,11) = PP-2.25*AZ
      X(12,12) = PP-3.75*AZ
      PPP=G/2.-8.*RD/3.
      X(13,13) = PPP+1.25*AZ
      X(14,14) = PPP+0.75*AZ
      X(15,15) = PPP+0.25*AZ
      X(16,16) = PPP-0.25*AZ
      X(17,17) = PPP-0.75*AZ
      X(18,18) = PPP-1.25*AZ
      Q=-G/2.-8.*RD/3.
      X(19,19)=Q-1.25*AZ
      X(20,20)=Q-0.75*AZ
      X(21,21)=Q-0.25*AZ
      X(22,22)=Q+0.25*AZ
      X(23,23)=Q+0.75*AZ
      X(24,24)=Q+1.25*AZ
      QQ=-1.5*G-2.*RD/3.
      X(25,25)=QQ-3.75*AZ
      X(26,26)=QQ-2.25*AZ
      X(27,27)=QQ-0.75*AZ
      X(28,28)=QQ+0.75*AZ
      X(29,29)=QQ+2.25*AZ
      X(30,30)=QQ+3.75*AZ
      QQQ=-2.5*G+10.*RD/3.
      X(31,31)=QQQ-6.25*AZ
      X(32,32)=QQQ-3 75*AZ
      X(33,33)=QQQ-1.25*AZ
      X(34,34)=QQQ+1.25*AZ
      X(35,35)=QQQ+3.75*AZ
      X(36,36)=QQQ+6.25*AZ
      DO 67 I=1,36
   67 HF(I)=X(I,I)
    C    OFF DIAGONAL ELEMENTS IN E
  463 STEN=SQRT(10.0)*RE
      STH=SQRT(2.0)*3.0*RE
      DO 61 I=1,6
      J=I+12
   61 X(I,J)=STEN
      DO 62 I=7,12
      J=I+12
      X(I,J)=STEN
      AXYD=AX-AY
      AXYS=AX+AY
    C    OFF DIAGONAL ELEMENTS IN AX,AY
      X(7,2)=1.25*AXYS
      X(8,3)=1.25*RF*AXYS
      X(9,4)=1.25*RFF*AXYS
      X(10,5)=X(8,3)
      X(11,6)=X(7,2)
      X(8,1)=1.25*AXYD
      X(9,2)=1.25*RF*AXYD
      X(10,3)=1.25*RFF*AXYD
```

```
      X(11,4)=X(9,2)
      X(12,5)=X(8,1)
      X(13,8)=1.25*RF*AXYS
      X(14,9)=2.*AXYS
      X(15,10)=1.25*RS*AXYS
      X(16,11)=X(14,9)
      X(17,12)=X(13,8)
      X(14,7)=1.25*RF*AXYD
      X(15,8)=2.*AXYD
      X(16,9)=1.25*RS*AXYD
      X(17,10)=X(15,8)
      X(18,11)=X(14,7)
      X(19,14)=1.25*RFF*AXYS
      X(20,15)=1.25*RS*AXYS
      X(21,16)=2.25*AXYS
      X(22,17)=X(20,15)
      X(23,18)=X(19,14)
      X(20,13)=1.25*RFF*AXYD
      X(22,15)=2.25*AXYD
      X(21,14)=1.25*RS*AXYD
      X(23,16)=X(21,14)
      X(24,17)=X(20,13)
      X(25,20)=1.25*RF*AXYS
      X(26,21)=2.*AXYS
      X(27,22)=1.25*RS*AXYS
      X(28,23)=X(26,21)
      X(29,24)=X(25,20)
      X(26,19)=1.25*RF*AXYD
      X(27,20)=2.*AXYD
      X(28,21)=1.25*RS*AXYD
      X(29,22)=X(27,20)
      X(30,23)=X(26,19)
      X(31,26)=1.25*AXYS
      X(32,27)=1.25*RF*AXYS
      X(33,28)=1.25*RFF*AXYS
      X(34,29)=X(32,27)
      X(35,30)=X(31,26)
      X(32,25)=1.25*AXYD
      X(33,26)=1.25*RE*AXYD
      X(34,27)=1.25*RFF*AXYD
      X(35,28)=X(33,26)
      X(36,29)=X(32,25)
C     ADDITIONAL TERMS CONTAINING B4ZERO(BFZ),B4TWO(BFT)
      AND B4FOUR(BFF)
C     DIAGONAL TERMS
      DO 401 I=1,6
401   X(I,I)=X(I,I)+BFZ
      DO 402 I=7,12
402   X(I,I)=X(I,I)-3.0*BFZ
      DO 403 I=13,24
403   X(I,I)=X(I,I)+2.0*BFZ
```

```
      DO 404 I=25,30
404   X(I,I)=X(I,I)-3.0*BFZ
      DO 405 I=31,36
405   X(I,I)=X(I,I)+BFZ
C     NONDIAGONAL TERMS IN E
      DO 406 I=1,6
      J=I+12
406   X(I,J)=X(I,J)+0.0&*SQRT(10.0)*BFT
      DO 407 I=7,18
      J=I+12
407   X(I,J)=X(I,J))0.25*SQRT(2.0)*BFT
      DO 4071 I=19,24
      J=I+12
4071  X(I,J)=X(I,J)+0.05*SQRT(10.0)*BFT
C     ADDITIONAL NONDIAGONAL TERMS
      DO 408 I=25,36
      J=I-24
408   X(I,J)=0.25*SQRT(5.0)*BFF
      DO 3 I=1,NDIM
      DO 3 J=1,NDIM
3     X(J,I)=X(I,J)
      PRINT 167
167   FORMAT(5X,*P,PP,PPP,Q,QQ,QQQ
      PRINT 1008,P,PP,PPP,Q,QQ,QQQ
      PRINT 168
168   FORMAT(5X,*DIAGONAL MATRIX ELEMENTS*)
      PRINT 1008,(X(I,I),I=1,36)
C     MATRIX DIAGONALIZATION ROUTINE-5116 SPACES
C     ARRAYS USED X(I,J),E(I,J)(EIGENVECTORS),DIMENSION-
      NDIM
250   DO 253 I=1,NDIM
      DO 253 J=1,NDIM
      IF(I-J)251,252,251
251   E(I,J)=0.
      GO TO 253
252   E(I,J)=1.0
253   CONTINUE
200   LA=1
      LB=2
      BX=DABS(X(2,1))
      DO 202 J=3,NDIM
      JA=J-1
      DO 202 I=1,JA
      D=BX-DABS(X(I,J))
      IF(D)201,202,202
201   BX=DABS(X(I,J))
      LA=I
      LB=J
202   CONTINUE
      IF(BX-0.00001)320,320,300
```

```
C       COMPUTE ROTATION
300     BX=X(LA,LB)*X(LA,LB)
        D=X(LA,LA)-X(LB,LB)
        R=SQRT(D*D+4.*BX)
        A=SQRT(ABS((R+D)/(2.0*R)))
        IF(0.707-A)302,302,301
301     B=0.0-A
        A=SQRT(1.0-B*B)
        GO TO 303
302     B=-SQRT(1.0-A*A)
303     IF(D/X(LA,LB))304,310,310
304     B=0.0-B
C       ORTHOGONAL ROTATION OF MATRIX
310     DO 313 J=1,NDIM
        IF(LA-J)311,313,311
311     IF(LB-J)312,313,312
312     X(LA,J)=A*X(J,LA)-B*X(J,LB)
313     CONTINUE
        DO 314 J=1,NDIM
        X(J,LA)=X(LA,J)
314     X(J,LB)=X(LB,J)
        D=X(LA,LA)+X(LB,LB)
        X(LA,LA)=A*A*X(LA,LA)+B*B*X(LB,LB)-2.*A*B*X(LA,LB)
        X(LB,LB)=D-X(LA,LA)
        X(LA,LB)=0.0
        X(LB,LA)=0.0
C       ENTER ROTATION MATRIX
        DO 315 J=1,NDIM
        BX=E(J,LA)
        E(J,LA)=A*BX-B*E(J,LB)
315     E(J,LB)=B*BX+A*E(J,LB)
        GO TO 200
C       TEST DIAGONALIZED MATRIX
320     BX=0.00004
        JA=NDIM-1
        DO 323 I=1,JA
        JB=I+1
        DO 323 J=JB,NDIM
        IF(X(I,J))321,323,321
321     R=ABS(X(I,J)/(X(I,I)-X(J,J)))
        IF(R-BX)323,323,322
322     BX=R
        LA=I
        LB=J
323     CONTINUE
        IF(BX-0.00005)450,450,300
C       CALC TRANSITION INTENSITIES AND FREQUENCIES
450     DO 451 I=1,NDIM
451     H(I)=X(I,I)
        PRINT 169
169     FORMAT(5X,*ENERGY LEVELS*)
```

```
      PRINT 1008,(H(I),I=1,36)
1000  FORMAT(/3H G=,F11.5,4H RD=,F14.1,4H RE=,F10.5,
      4H AZ=F10.5,4H AX=,F
     110.5,4H AY=,F10.5,7H HDPPH=,F8.2//)
1008  FORMAT(2X,6F10.2)
      DO 65 I=1,30
65    HH(I)=H(I)-H(I+6)
500   FORMAT(2X,10HCALCULATED,3X,12HEXPERIMENTAL)
50    FORMAT(2X,F8.2,5X,F8.2)
      GZ=HDPPH*HNOT/G
2000  FORMAT(7H GXAXIS)
      N1=1
      DO 5020 IJ=1,3
      N2=N1+9
      PRINT 5000,(I,I=N1,N2)
5000  FORMAT(//25X,10I10/)
      PRINT 5001,(Y(I),I=N1,N2)
      PRINT 5002,(HH(I) I=N1,N2)
5001  FORMAT(5X,*OBSERVED*,12X,10F10.2)
5002  FORMAT(5X,*CALCULATED*,10X,10F10.2)
5020  N1=N1+10
2001  FORMAT(5X,8E12.5)
      PRINT 2001,G,GZ,HNOT,RD,RE,AZ,AX,AY
      DO 324 I=1,30
      DEF(I)=Y(I)-HH(I)
324   DEFS(I)=DEF(I)**2
      DSUM=0.0
      DO 325 I=1,30
325   DSUM=DSUM+DEFS(I)
      DAVE=DSUM/30.0
      DELA=SQRTF(DAVE)
      PRINT 76
76    FORMAT(5X,*STANDARD DEVIATION FOR THE THIRTY LINE
      SPECTRUM*)
      PRINT 100,DELA
      HH(37)=HH(1)-HH(6)
      HH(38)=HH(7)-HH(12)
      HH(39)=HH(13)-HH(18)
      HH(40)=HH(19)-HH(24)
      HH(41)=HH(25)-HH(30)
      H(37)=Y(1)-Y(6)
      H(38)=Y(7)-Y(12)
      H(39)=Y(13)-Y(18)
      H(40)=Y(19)-Y(24)
      H(41)=Y(25)-Y(30)
      PRINT 70
 70   FORMAT(30HSEPARATION FOR EACH TRANSITION)
      PRINT 500
      PRINT 50,(HH(I),H(I),I=37,41)
      DO 69 I=1,36
 69   HF(I)=H(I)-HF(I)
```

```
      DO 68 I=1,5
      J=6*I
      K=J-5
      JEP=J+6
      KEP=J+1
68    HFC(I)=-(Y(J)-Y(K)+HF(K)+HF(JEP)-HF(J)-HF(KEP))/5.
      PRINT 99,(HFC(I),I=1,5)
99    FORMAT(1X,5F8.2)
      SUM=0.
      DO 700 I=1,5
700   SUM=SUM+HFC(I)
120   AVE=SUM/5.0
      PRINT 75
75    FORMAT(18HHYPERFINE CONSTANT)
      PRINT 100,AVE
100   FORMAT(5X,F8.2)
      DO 71 I=6,10
      J=I-5
71    HFC(I)=(AVE-HFC(J))**2
      ASUM=0.
      DO 72 I=6,10
72    ASUM=ASUM+HFC(I)
      DELS=ASUM/5.
      DEL=SQRTF(DELS)
      PRINT 73
73    FORMAT(18HSTANDARD DEVIATION)
      PRINT 100,DEL
      PRINT 444,BFZ,BFT,BFF
444   FORMAT(1X,3E12.5)
      RD=RD-1.
555   CONTINUE
      STOP
      END
£ENTRY
```

After this the data cards are placed.
The eigenvectors can be asked to be printed in case they are needed as in determining the orientation of magnetic susceptibility axes with respect to the crystallographic axes in the case of vanadyl-doped caesium sulphate

Experimental observations confirmed this to within 1°.

Temperature variation studies from 300 °K to 77 °K show that there is no abrupt change in the spectral patterns. The spectrum recorded at 77 °K with a small crystal in the low temperature tube is shown in Fig.(3.6). Within the temperature range of 77 °K to room temperature, (~297 °K), the overall spread of the spectrum gradually increases as we go from low temperature to high temperature. Fig.(3.7) shows the temperature variation of the parameters D and E within this range. It is seen that the change in E* is about 4% while in D* the change is 14%. This alters the ratio of D* to E* giving probably an indication of the overlap and covalency effects as suggested by Watkins[16]. The smooth variation of the parameters D and E suggests that structural changes involving first or second order phase transitions have probably not occured in this temperature range. Such changes are expected in Cs_2SO_4 doped with Mn^{2+} as this crystal is isomorphous with K_2SO_4 where a second order phase transition is indicated.[3]

The line widths at 77 °K for $+\frac{1}{2} \leftrightarrow -\frac{1}{2}$ transition are found to be the same as those of $\pm 5/2 \leftrightarrow \pm 3/2$ transitions (~9 oersted) indicating the crystals grown from slow evaporation of saturated solution do not develop

TABLE 3.7

The lines of $Mn^{2+}:Cs_2SO_4$ at 77 °K

H ∥ x-axis of the complex

(ALL VALUES IN oersted)

DPPH[a] Line	3316									
	-3/2 Observed	-5/2 calculated	-½ Observed	-3/2 calculated	-½ Observed	+½ calculated	+3/2 Observed	+½ Calculated	+5/2 Observed	+3/2 calculated
	1939	1928	2192	2181	2656	2645	3288	3296	4739	4745
	2024	2011	2274	2267	2745	2733	3387	3387	4822	4838
	2107	2096	2368	2355	2838	2823	3487	3480	4913	4934
	2192	2184	2459	2445	2932	2916	3585	3575	5012	5032
	2283	2275	2552	2538	3027	3012	3672	3673	5116	5133
	2380	2368	2645	2634	3125	3110	3756	3774	5229	5236

Standard deviation 13 [a]Diphenylpicrylhydrazyl

Input data (for second order perturbation equations 3.2(a)):

$A_x = -93$ $A_z = -93$; $A_y = -93$; $H_{ox} = 3304$ ($g_x = 2.0109$)

$D_x = 401$; $E_x = 470$;

$(b_4^o)_x = -20$; $(b_4^2)_x = 56$

(I of V^{51} = 7/2) the EPR spectrum shows a characteristic eight line hyperfine structure. The EPR spectrum of VO^{2+} when having an orthorhombic site symmetry can be described in a principal axis system by a spin-Hamiltonian type[10] :

$$\underline{H} = \beta(g_z H_z S_z + g_x H_x S_x + g_y H_y S_y) + A I_z S_z + B I_x S_x + C I_y S_y$$

a solution of which gives the magnetic field resonance values by[11]

$$H = H_o - Km - \frac{1}{2H_o}\left[a(15/4 - m^2) + bm^2 + cm\right] \quad .. \quad (4.1)$$

where

$$K^2g^2 = A^2g_z^2\cos^2\theta + D^2g^2\sin^2\theta$$

$$A^2 - D^2 = E$$

$$D^2g_\perp^2 = B^2g_x^2\cos^2\delta + C^2g_y^2\sin^2\delta$$

$$B^2 - C^2 = F$$

$$a = \left[A^2D^4 + B^2C^2K^2 - A^2E^2(\xi\, g_xg_yg_z/gg_\perp^2)^2\right]/2D^2K^2$$

$$b = \left[F^2(g_\perp g_z\cos\theta\sin\theta/g^2)^2 + E^2(\eta\, g_xg_y/g_\perp^2)^2\right]/K^2$$

$$c = E^2(\eta\, g_xg_y/g^2)^2/D^2$$

$$\xi = \cos\delta\sin\delta\cos\theta$$

$$\eta = \cos\delta\sin\delta\sin\theta$$

θ and δ being polar angles of the direction of the

is found to show the largest hyperfine structure spread, (lines marked a in Fig.(4.2), when H is along the c-axis of the crystal suggesting that the z-axis of the complex is along the c axis.It was also found that this spectrum has minimum hyperfine structure spread when H is along a-direction,(see lines marked b in Fig.(4.3) and those marked c in Fig.(4.4) respectively. This observation suggests that the x and y axes of the complex I are along the crystallographic b and c axes. The spectrum of complex II has been found to have a maximum spread when the magnetic field direction H makes an angle of 30° with c-axis in the bc-plane, (see lines marked d in Fig.4.5), and a minimum spread, (see lines marked e in Fig.4.6), at an angle of 90° in the same plane from the direction of maximum spread. These directions of maximum and minimum spectral spreads are very likely the z and x directions. The spectral lines corresponding to H $\|$ y axis of complex II are shown in Fig.(4.3) and are marked f. The y axis of this complex coincides with the crystallographic a-axis.

The angular variation of the spectrum corresponding to complex III has indicated that the maximum hyperfine structure spread of the spectrum comes up when H is nearly (but not exactly) parallel to the crystalline a-axis. After studying the angular variation of the EPR spectrum of this complex in the three crystallographic planes, the principal values of the g and A tensors

4.5 REFERENCES

1. A.V.Jagannadham and Putcha Venkateswarlu, Proc.Ind. Acad.Sciences, 69, 307(1969).
2. M.D.Sastry and P. Venkateswarlu, Mol.Phys. 13, 161(1967).
3. K.V.S.Rao and M.Dattatreya Saatry and Putcha Venkateswarlu, J.Chem.Phys. 49, 1714(1968).
4. R.H.Brocherts and C.Kikuchi, J.Chem.Phys., 40, 2270(1964).
5. A.Manoogian and J.A.Mackinnon, Can.J.Phys., 45, 2769(1967).
6. K.V.S.Rao and M Dattatreya Sastry and Putcha Venkateswarlu, J.Chem.Phys., 49, 4984(1968).
7. K.V.S.Rao and M.Dattatreya Sastry and P.Venkateswarlu, J.Chem.Phys., (to be published).
8. C.J.Ballhausen and H.B.Gray, Inorg.Chem. 1, 111(1962).
9. K.De Armond, B.B.Garrett, and H.S.Gutowsky, J.Chem. Phys., 42, 1019(1965).
10. B.Bleaney, Phil.Mag., 42, 447(1951).
11. G.H.Azarbayejani, Phys.Letters, 25A, 767(1967).
12. J.A.Weil and J.H.Anderson, J.Chem.Phys. 28, 864(1958).
13. J.E.Geusic and L.Carlton Brown, Phys.Rev., 112, 64(1958).
14. D.S.Schonland, Proc.Phys.Soc., 73, 788(1959).
15. A.Ogg, Phil.Mag., 5, 354(1928).
16. C.J.Ballhausen, INTRODUCTION TO LIGAND FIELD THEORY, McGraw-Hill Book Company Inc. New York, 1962.
17. C.K.Jorgensen, Acta.Chem.Scand. 11, 73, (1957).
18. C.Furlani, Ricerca Sci. 27, 1141, (1957).
19. D.S.McClure, ELECTRONIC SPECTRA OF MOLECULES AND IONS IN CRYSTALS, p132, Academic Press, New York, 1959.
20. S.D.Pande, "EPR of Eu^{2+}, Mn^{2+} and VO^{2+} in Single Crystals" Ph.D.Thesis, Indian Institute of Technology, Kanpur, 1969.
21. B.V.R.Chowdari and P.Venkateswarlu, Proc.Ind.Acad. Sci. 67, 105(1968).
22. B.V.R.Chowdari and P.Venkateswarlu, J.Chem.Phys., 48, 318(1968).

at the alkali site associated with a second neighbour alkali vacancy while that responsible for the spectrum III_4 is again a similar Mn^{2+} ion but associated probably with a fourth neighbour alkali vacancy. Both the complexes have their site symmetry axes along the <100> direction. It has been observed that spectrum II is more intense than spectrum III_4 which is again more intense than spectrum III_2. This observation indicates clearly that in Mn^{2+}:NaF, remote charge compensation is preferred to the local charge compensation.†

All the spectra II, III_2 and III_4 show superhyperfine structure. The spectra have been analysed using the expressions indicated earlier and the constants obtained are given in Table 5.4 where the data available from the earlier work are also included. The spectrum II is overlapped by the transition $M=\frac{1}{2} \leftrightarrow -\frac{1}{2}$ of the spectrum III_4 and also by that of the spectrum III_2. Its separate existence has been confirmed by taking the spectrum of a powdered sample as has been done by Veigele and Tantilla[14] in the case of Mn^{2+}:KF. Figure 5.1 shows the spectrum II as obtained from such a powdered or polycrystalline sample showing clearly the six hyperfine lines along with the superhyperfine structure.

---

†It may be mentioned that Hall et al[13] state that Mn^{2+} ions unassociated with vacancies, that is, at cubic sites, are not present at room temperature. The cubic spectrum is observed only beyond 300 °C, which rapidly revert to the preheated condition after cooling.

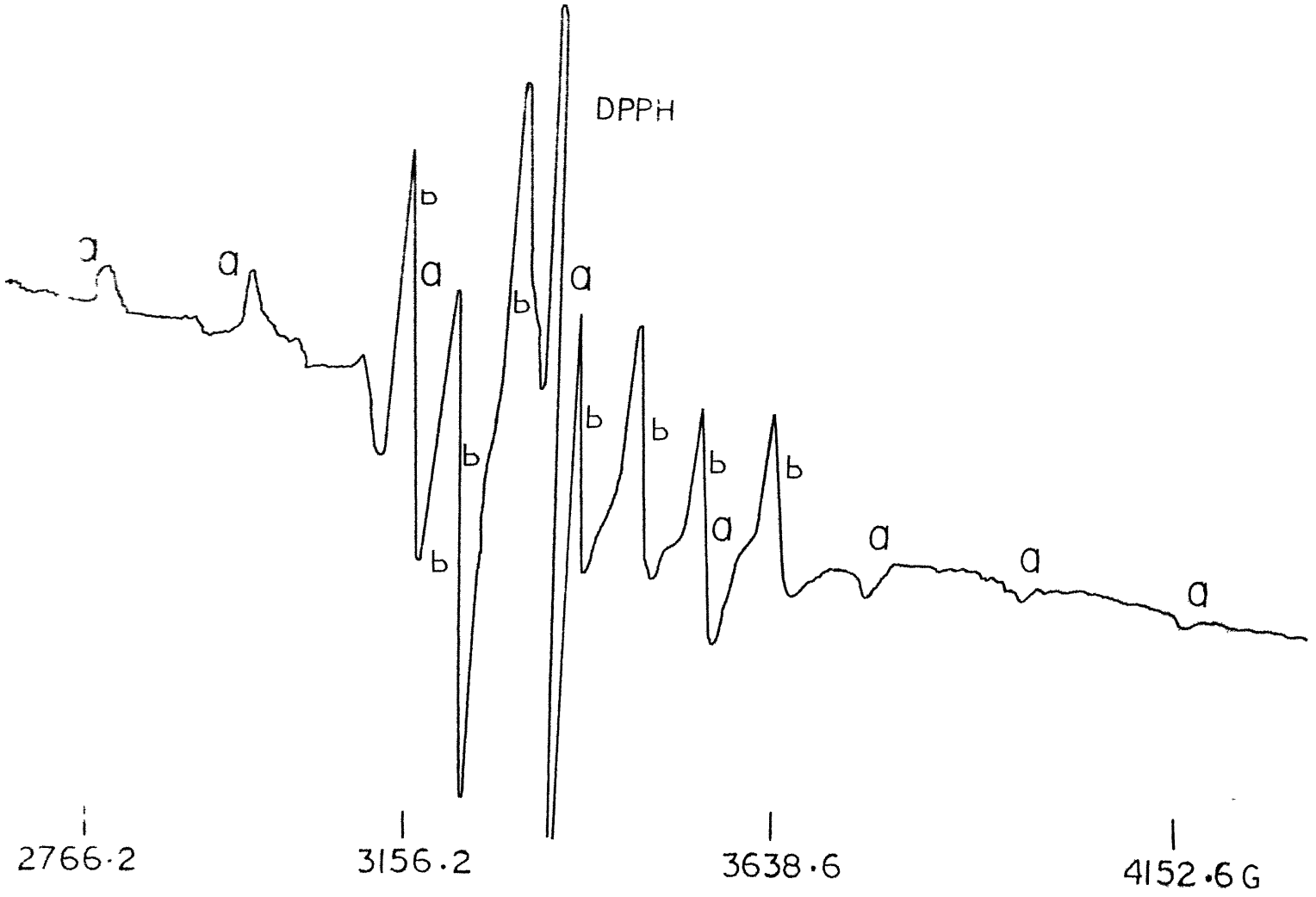

FIG.6·2 SPECTRUM II ELECTRON PARAMAGNETIC RESONANCE OF VO^{2+} IN NaCl AT LIQUID NITROGEN TEMPERATURE. LINES MARKED a ARE PARALLEL TRANSITIONS AND THOSE MARKED b ARE PERPENDICULAR TRANSITIONS. THE X-COORDINATE REPRESENTS MAGNETIC FIELD VALUES IN GAUSS.

6.6 REFERENCES

1. M.Dattatreya Sastry, and P. Venkateswarlu, Mol. Phys. 13,161(1967).
2. K.V.S.Rao, M.Dattatreya Sastry, and P.Venkateswarlu, J.Chem.Phys.49,1714(1968).
3. R.H.Borcherts and C.Kikuchi, J.Chem.Phys. 40,2270(1964).
4. A.Manoogian and J.A.MacKinnon,Can.J.Phys.45,2769 (1967).
5. K.V.S.Rao and M.Dattatreya Sastry and P.Venkateswarlu, J.Chem.Phys.49,4984(1968); J.Chem.Phys.(1969) to be published.
6. D.Kivelson,J.Chem.Phys.33,1094(1960).
7. R.H.Sands,Phys.Rev.99,1222(1955).
8. D.E.O'Reilly,J.Chem.Phys.29,1188(1958); J.Chem.Phys.30,591(1959).
9. A.Abragam, and M.H.L. Pryce, Proc.Roy.Soc.(London), A205,135(1951).
10. B.Bleaney,Phil.Mag.42,441(1951).
11. G.Hochstrasser, Phys.Chem.Glasses 7,178(1966).
12. R.Neiman, and D.Kivelson,J.Chem.Phys.35,156(1961).
13. H.M.McConnell, J.Chem.Phys.25,709(1956).
14. R.N.Rogers and G.E.Pake,J.Chem.Phys.33,1107(1960).
15. R.Wilson and D.Kivelson,J.Chem.Phys.44,154(1966).

APPENDIX B1

Computer programme used to find the spin-Hamiltonian parameters for $Mn^{++}:Cs_2SO_4$ system using equations 3.2

H(I) are the fine structure fields in gauss or oersted. FNOT,RD,RE,BFT are respectively H_o,D,E,b_4^0 and b_4^2

PPH is the DPPH field marker value while PH is the g-value of DPPH.

The program can be used to iterate for any number of times NUM. A least-square fit with the calculated field values HC(I) is incorporated.

```
C  C   PHR006 AVJ
       DIMENSION H(5),HC(5),DIF(5)
       READ 1234,NUM
1234   FORMAT(I3)
       DO 555 IND=1,NUM
       READ 1,(H(I),I=1,5)
1      FORMAT(1X,5F7.1)
       READ 1,FNOT,RD,RE,BFZ,BFT
       READ 4,PPH.PH
2      FORMAT(1X,5E12.5)
3      FORMAT(1X,3F7.1)
4      FORMAT(1X,2E12.5)
       PRINT 1234,IND
       PRINT 1,(H(I),I=1,5)
       PRINT 1,FNOT,RD,RE,BFZ,BFT
       PRINT 4,PPH,PH
       SE=RE**2
       HC(1)=FNOT-4.*RD+9.*SE/(H(1)+RD)-5.*SE/(H(1)+3.*RD)
            -4.*BFZ
       HC(2)=FNOT-9.*SE/(H(2)+RD)+9.*SE/(H(2)-RD)-5.*SE/(H(2
            )+3.*RD)+5.0*
      1BFZ-2.*RD
       HC(3)=FNOT-9.*SE/(H3)-RD)+5.*SE/(H(3)+3.*RD)+5.*SE/(H
            (3)--3.*RD)-9
      1.*SE/(H(3)+RD)
       HC(4)=FNOT+2.*RD+9.*SE/(H(4)+RD)-9.*SE/(H(4)-RD)-5.*
            SE/(H(4)-3.*RD
      1)-5.0*BFZ
       HC(5)=FNOT+4.*RD+9.*SE/(H(5)-RD)-5.*SE/H(5)-3.,RD)+
            4.*BFZ
       TEMP=1.5*RE*BFT/FNOT
       HC(1)=HC(1)+TEMP+TEMP
       HC(5)=HC(5)+TEMP+TEMP
       HC(2)=HC(2)+TEMP
       HC(4)=HC(4)+TEMP
       HC(3)=HC(3)-TEMP-TEMP-TEMP-TEMP
       DO 11 I=1,5
 11    DIF(I)=(H(I)-HC(I))**2
       SUM=0.
```